Growth of molybdenum disulphide on semiconductor substrates for heterojunction device applications

半導体基板上への二硫化モリブデンの合成とヘテロ接合デバイスへの応用

THESIS SUBMITTED BY

PRADEEP NIWAS DESAI

To the

Department of Physical Science and Engineering
Graduate School of Engineering
Nagoya Institute of Technology
Gokiso-cho, Showa-ku, Nagoya, Aichi, 466-8555 Japan

Under supervision of

(Dr./Prof.) Masaki Tanemura

In partial fulfilment of the requirements for the degree of

DOCTOR OF PHILOSOPHY

Nagoya Institute of Technology

September 2021

THIS THESIS IS DEDICATED TO

THE INDIVIDUALS AND AUTHORITIES, MENTIONED AND UNMENTIONED,

ENCOURAGING AND SUPPORTING ME IN MY PURSUIT OF DOCTORAL DEGREE

Declaration of Authorship

I, Pradeep Niwas Desai, declare that this thesis titled, 'Growth of molybdenum disulphide on semiconductor substrates for heterojunction device applications' and the work presented in it is my own.

Japanese titled 半導体基板上への二硫化モリブデンの合成とヘテロ接合デバイスへの応用:

Further, I confirm the following:

- This work was done wholly or mainly while in candidature for a research degree at this institute.
- None of any part/s of this thesis has previously been submitted for award of degree or any other qualifications at this institute or any other institution.
- None of the published work of others was consulted or reproduced without giving due credits.
- The sources are always given where I have quoted texts, figures, or tables from the works of others. Apart from such quotations, this thesis is entirely my own work.
- A methodical attempt has been made to acknowledge the inclusion of citations, results, observations, conclusions, opinions, and viewpoints of others.
- I have acknowledged all main sources of assistance.

Signature:

Date:

Thesis titled:

'Growth of molybdenum disulphide on semiconductor substrates for heterojunction device applications'

Abstract

The two-dimensional (2D) transition metal dichalcogenides (TMDCs) of layered materials have attracted significant interest for various applications in nanoelectronics and optoelectronics devices. In this thesis work, I have emphasized on the growth of TMDCs layers on Si, GaN semiconductor substrates by the chemical vapour deposition (CVD) technique. The heterostructures of MoS_2 with Si and GaN were analysed by device fabrication and their suitability for optoelectronics were explored.

Chapter 1 describes the background of TMDCs materials and their unique properties. Various synthesis methods of TMDCs layer and their characterizations process to identify layer structures, stability issues and current trend of device applications are discussed. Then, the challenges in synthesis of monolayer, few-layers of TMDCs and their continuous films were introduced.

In Chapter 2 deals with of the synthesis processes for the growth of molybdenum disulphide (MoS_2) layers and crystals were introduced. The CVD techniques used in these studies for the growth of MoS_2 layers were presented and discussed in detail. The physical and chemical characterisation methods of MoS_2 based 2D materials were introduced in this chapter. These characterisation techniques are used in ascertaining the chemical composition, structure and so on for the synthesised MoS_2.

Chapter 3 describes the fabrication of MoS_2 and p-type Si heterostructure using molybdenum oxide (MoO_3) as precursor. In this synthesis process, MoO_3 layer was

directly deposited on Si and sulphurization was performed in a CVD process. A heterojunction device fabricated for the deposited MoS_2 layers on the Si substrate showed a photovoltaic action and a photoresponsivity of 139 mA/W at 860 nm wavelength for a bias voltage of -5V. Then, I discuss about the effect of interface states in MoS_2/Si heterojunction and influence in photoresponsivity. The understanding of photocarriers behaviour in the fabricated MoS_2/Si heterojunction interface can be critical to develop high photoresponsive devices.

Chapter 4 deals with the feasibility of van der Waals (VdW) heteroepitaxy of MoS_2 layers on lattice matched GaN semiconductor. The uniform MoS_2 layers were directly grown on the n-type GaN wafer by sulphurisation process of MoO_3 thin layer using CVD process labelled II. Homogenous growth of the few-layers MoS_2 forming a continuous film was achieved, signifying the suitability of GaN semiconductor substrate. The fabricated MoS_2/GaN vertical heterojunction showed excellent rectifying diode characteristics with a photovoltaic action. Then, the band structure for the MoS_2/GaN heterojunction was investigated confirming a type II-based heterojunction. In addition, analyses of the growth of MoS_2 crystals on the lattice matched Ga-polar GaN wafer using ammonium tetrathiomolybdate (ATM) as a precursor in a CVD process, instead of using the molybdenum oxide-based precursors are demonstrated using CVD process labelled III. Unidirectional triangular MoS_2 crystals and continuous film were obtained on the free-standing Ga-polar GaN substrate in these studies. Then, a heterojunction device was fabricated for the synthesised MoS_2 layers on GaN substrate, obtaining better diode rectification behaviour compared to device fabricated using CVD process II.

Chapter 5 summarizes the whole thesis and future prospects.

Table of Contents

CHAPTER 1

1 Introduction to the research

1.1 Background of Layered Transition Metal Dichalcogenides

Transition Metal Dichalcogenides (TMDCs) are classes of materials with Transition metals M (Ti, Zr, Hf, V, Nb, Ta, Tc, Re, Pd, Pt, W or Mo atoms) in honeycomb structure with Chalcogen (Selenium, Tellurium or Sulphur) atoms in MX_2 type, visualised in **Figure 1.1**. These materials are subset of layered materials family. Approximately 60 TMDC compounds exists in this family. Two-third among them has chemical configuration where metal atom is covalently bonded with two Chalcogen atoms and the layers are held together by Van der Waals force. In other terms, the in-plane bonds are

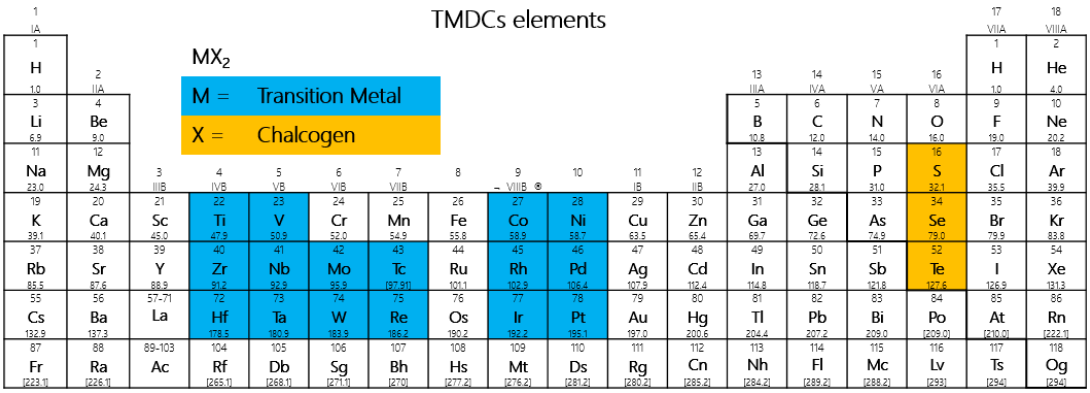

Figure 1.1: Periodic table highlighting combination elements of TMDCs

stronger than the out-plane bonds. The following can be visualized as depicted in **Figure 1.2** showing the structure of one of its constituent members, Molybdenum disulphide

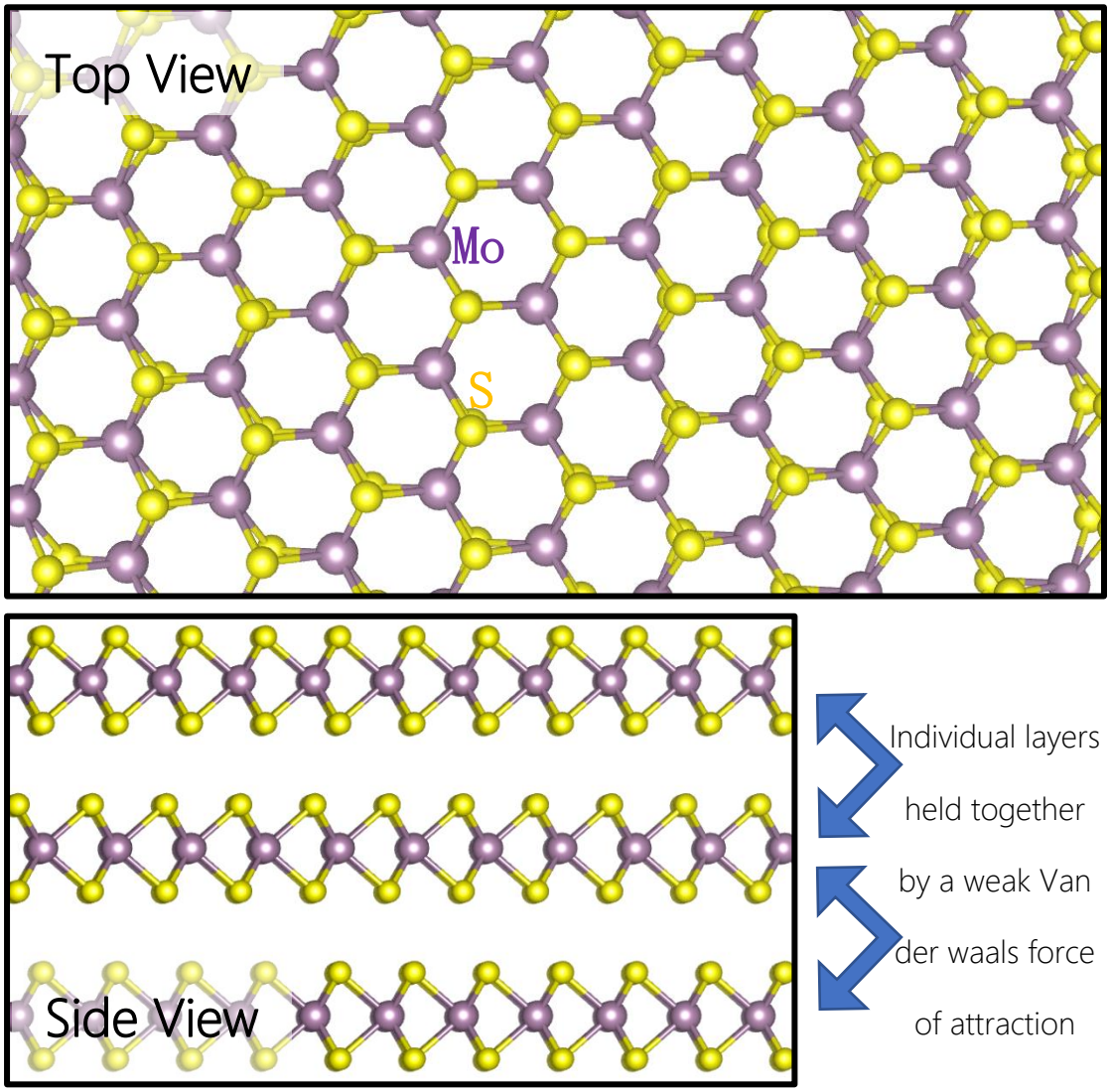

Figure 1.2: Molecular structure of MoS_2 (2H Phase) as depicted by Ball and stick diagram showing perspective top view and side view (Dickson et al. 1923)

(MoS_2). This class covers wide material property, which includes semiconductors such as MoS_2 and WS_2 (Tungsten disulphide), semimetals e.g., Tungsten ditelluride (WTe_2), Titanium diselenide ($TiSe_2$), metals such as Titanium disulphide (TiS_2), Vanadium

diselenide (VSe_2), superconductors (e.g., Tantalum disulphide TaS_2, Niobium diselenide $NbSe_2$) as well as insulators (e.g., Hafnium disulphide HfS_2). [1-11] Analogous to Graphene and Graphene like materials, these materials show exceptional optical and catalytic properties with semiconducting nature. This has been demonstrated in application consisting of transistor [9] as well as strong photoluminescence (PL). [12,13] The emergence of graphene as strongest, lightest, thinnest material with best heat and electrical conductivity showcased the capabilities of 2D materials related research. Although, much attention has been given to graphene, it has its notable limitations due to zero bandgap. [14,15] In this line, to find the alternative to the limitations of graphene, 2D materials with semiconducting properties has become focus of fundamental research and technological applications. Its strong photoluminescence, and catalytic properties has made 2D-TMDCs attractive candidates for applications in electronic, optoelectronic, sensing and catalysis. [16-21]

Since the first structural determination by Linus Pauling in 1923, and thereon subsequent discovery of more than 40 layered structures of TMDCs has been reported by late 1960s. As early as 1950s Robert Frindt reported first adhesive tape method for MoS_2 thin layer synthesis. Subsequently in various research were carried out and explored to synthesis monolayer MoS_2. Since the discovery of stable monolayer graphene, it guided the way for significant development in ultrathin film and monolayer TMDCs applications. Among these numerous TMDCs, MoS_2 holds wide research interests and is the focus of this thesis work.

1.2 Chemical Structure

TMDCs are arranged in various coordination phases with various structural arrangements. The prominent or the overall symmetry of TMDCs is hexagonal or rhombohedral and the consisting metal atoms have octahedral or trigonal prismatic coordination. The Trigonal prismatic i.e., 2H phase is most stable form of coordination sphere around the metal atom

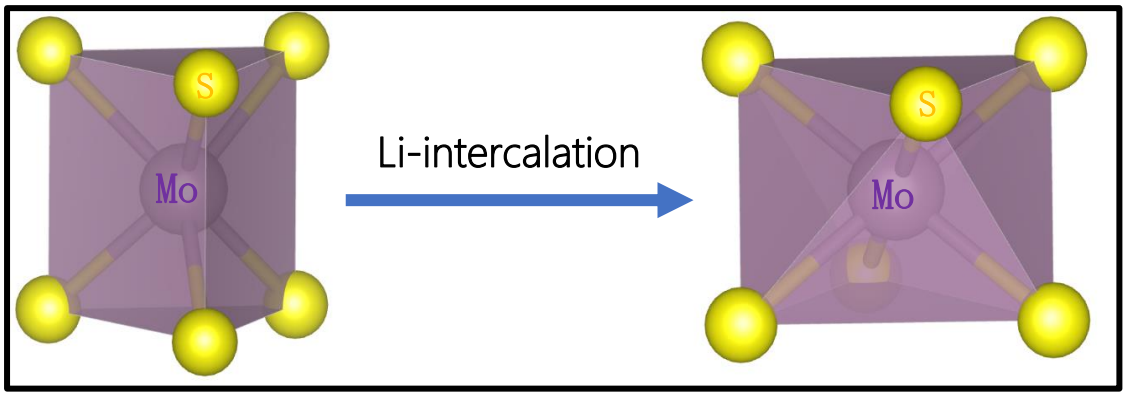

Figure 1.3: Atomic arrangement in 2H phase and 1T phase layered MoS_2

which has ABA stacking of atoms where chalcogen atoms occupy same position in different planes. The octahedral (1T) phase can be obtained by lithium intercalation of 2H phase. The resulting 1T metastable phase shows metallic characteristics which is unstable from than that of semiconducting 2H phase. Stacking order in octahedral phase show ABC stacking of corresponding atoms. The thermodynamic stability of these structures mainly depends on the combination of transition metals i.e. (group IV, V, VI, VII, IX or X) and chalcogen atoms (S, Se or Te). Also, honeycomb arrangements of the atoms give different edge structures depending on atomic arrangements in case of chemical vapour deposition (CVD) synthesized TMDCs. [22]

Table 1.1: Ionic radii in MoS_2 crystals, reported by Lucovsky et al.

Interlayer 'S-S'	'$2S^{2-}$'	Intralayer 'S-Mo'	'S^{2-}+Mo^{4+}'	'S^{2-}+Mo^{4+}' r^+/r^-

3.16 Å	3.68 Å	2.23 Å	2.44 Å	0.33 Å

Hexagonal MoS_2 belongs to the space group $D_{6h}(P6_3/mmc)$, contains two molecular units and total of six atoms within the primitive unit cell. [24] Lattice parameters are a,b = 3.162 Å, and c = 12.29 Å. Further ionic radii of MoS_2 are represented in **Table 1.1**. A group-theoretical analysis of the Γ point lattice modes for the 2H MoS_2 structure. The 6

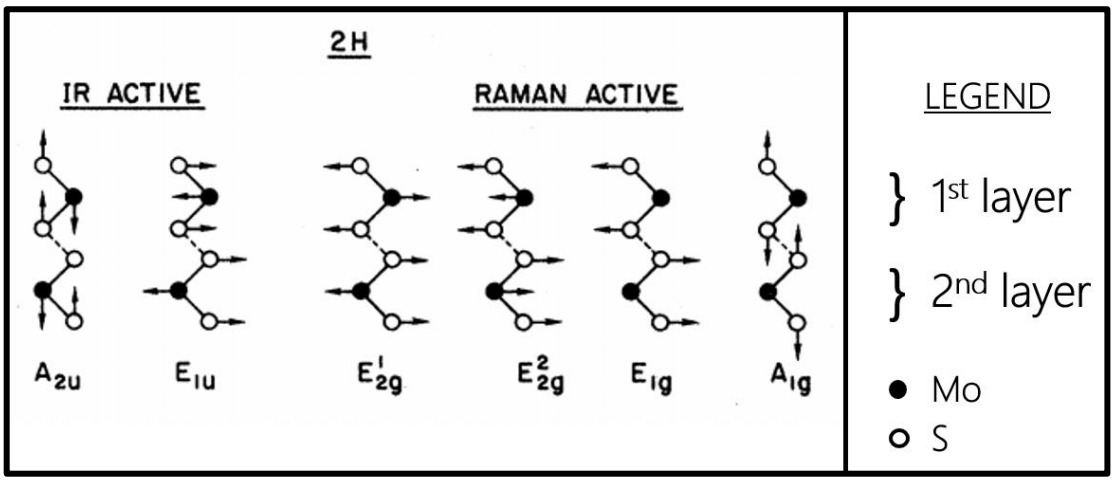

Figure 1.4: Displacement vectors for the infrared- and Raman-active modes in the 2H polytype as viewed along the [1000] direction. Among these, E_{2g}^1 and A_{1g} are dominant showing noticeable peaks in Raman spectrum. [Reprinted from Ref. 23 with permission from American Physics Society]

atoms per unit cell gives rise to 18 vibrational modes. Of these two are of our interests, namely E_{2g}^1 and A_{1g} for layered/bulk MoS_2. E_{2g}^1 has polarisation of vibration at basal plane with both Mo and S ions involved and is recorded at 383 ± 1 cm^{-1}. A_{1g} has polarisation of vibration at c-axis with S ions involved and recorded at 409 ± 1 cm^{-1}. [23] In **Figure 1.5** we can see the (a) Raman spectra of thin 1L to 6L and bulk MoS_2 films and in (b) Thickness-dependent Raman spectra for MoS_2. An interesting characteristic we observe is the red shift in E_{2g}^1 in-plane vibrations and blue shift in A_{1g} out-plane vibrations

as the MoS_2 layer thickness increases. For the material with 4 or more layer of MoS_2, the two vibrations modes converge with that of the bulk. Thus, the Raman study is used in detecting broadly the layer thickness.

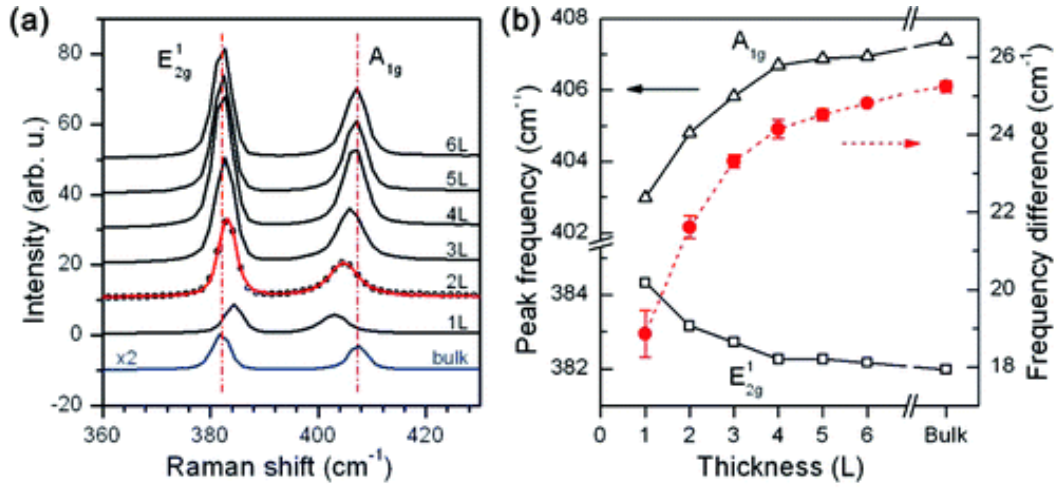

Figure 1.5: (a) Raman spectra of thin 1L to 6L and bulk MoS_2 films, and (b) Thickness-dependent Raman spectra for MoS_2, with peak frequency and frequency difference shown in vertical axis [Ref. 25. Copyright 2010 American Chemical Society, Reprinted with permission]

For single layer MoS_2 the frequency difference is 19 cm^{-1} and increases beyond 25 cm^{-1} for bulk layer as shown in **Figure 1.5** a,b.

1.3 Electronic band structure and optical properties

The Transition from bulk to monolayer for the TMDCs show interesting change in bandgap from indirect to direct bandgap, respectively. Here I have focused mainly on group VI transition metals Mo in combination with sulphur atoms i.e. MoS_2. These

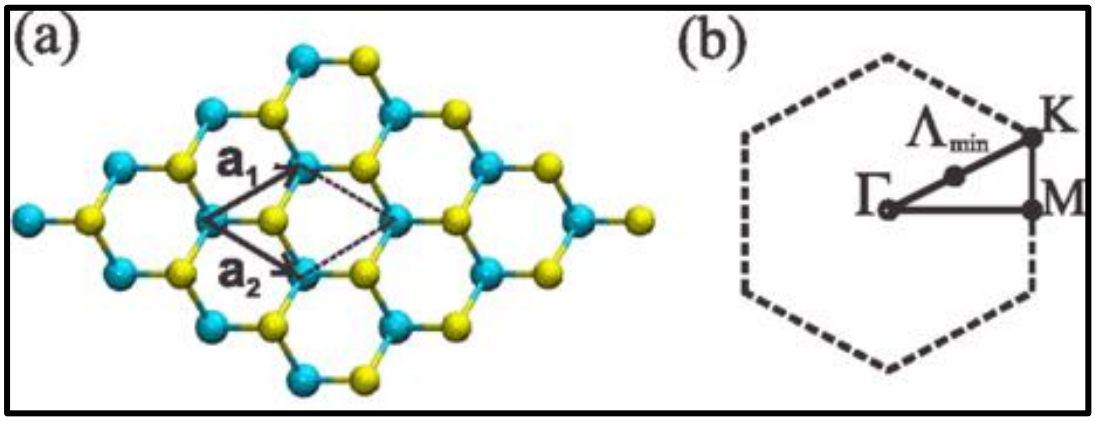

Figure 1.6: Top view of a monolayer of MoS_2. The lattice vectors (a_1 and a_2) that define the unit cell are indicated by vectors, and the outline of the unit cell is indicated by dashed lines. (b) The Brillouin zone, with the relevant high-symmetry k points indicated. [Reprinted from Ref. 30, with permission from American Physical Society]

structure shows semiconducting 2H stable phase which has been utilized for the fabrication of single layer field effect transistor (FET). [26] Interestingly, the conduction band and valance band positions change from bulk to few layers to monolayer due to change in electronic band structure as shown in **Figure 1.7** eventually, showing remarkable transformation from bulk indirect bandgap to monolayer direct bandgap.

The top of valance band and bottom of conduction band in the monolayer TMDCs are at the same K point of the wave vector axis, which is why they show strong photoluminescence in visible range of electromagnetic spectrum. Thus, these TMDCs are widely used as absorbing materials in solar cells as well as photovoltaics and applications

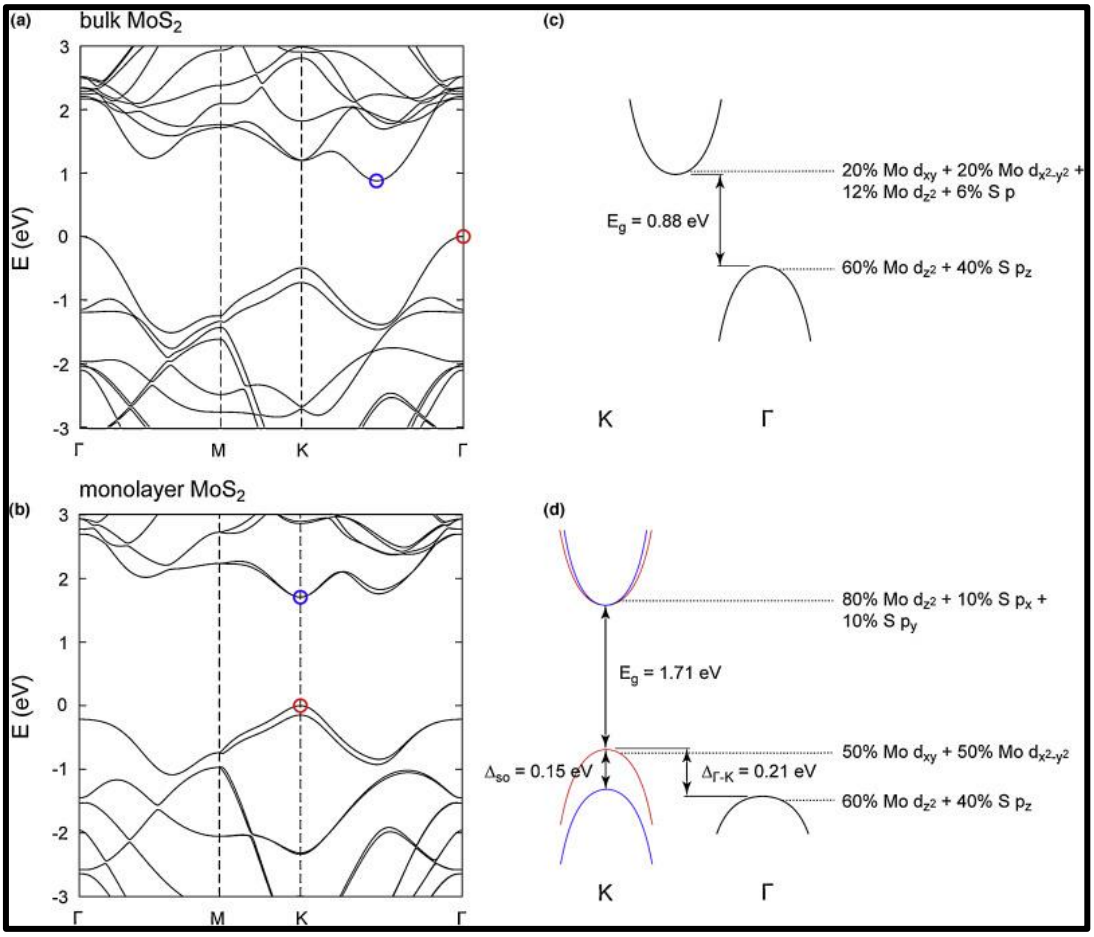

Figure 1.7: Electronic band structures of (a) bulk MoS_2 and (b) monolayer MoS_2 calculated from first principles using DFT within the GGA. Schematic drawings of low-energy bands in (c) bulk MoS_2 and (d) monolayer MoS_2 [reproduced from Ref 31 with an open access permission from Elsevier]

in various nano and optoelectronics. In practice these materials are used as channel materials for FET, in both top and back gated configuration with intrinsic mobility of 50 $cm^2/V.s$ and on/off ratio of more than 10^{10}. [27-29]

The electronic configuration of Molybdenum is represented as [Kr] $4d^5$ $5s^1$ and that of the Sulphur is [Ne] $3s^2$ $3p^4$. In band structures of **Figure 1.7** (a) bulk MoS_2 and (b)

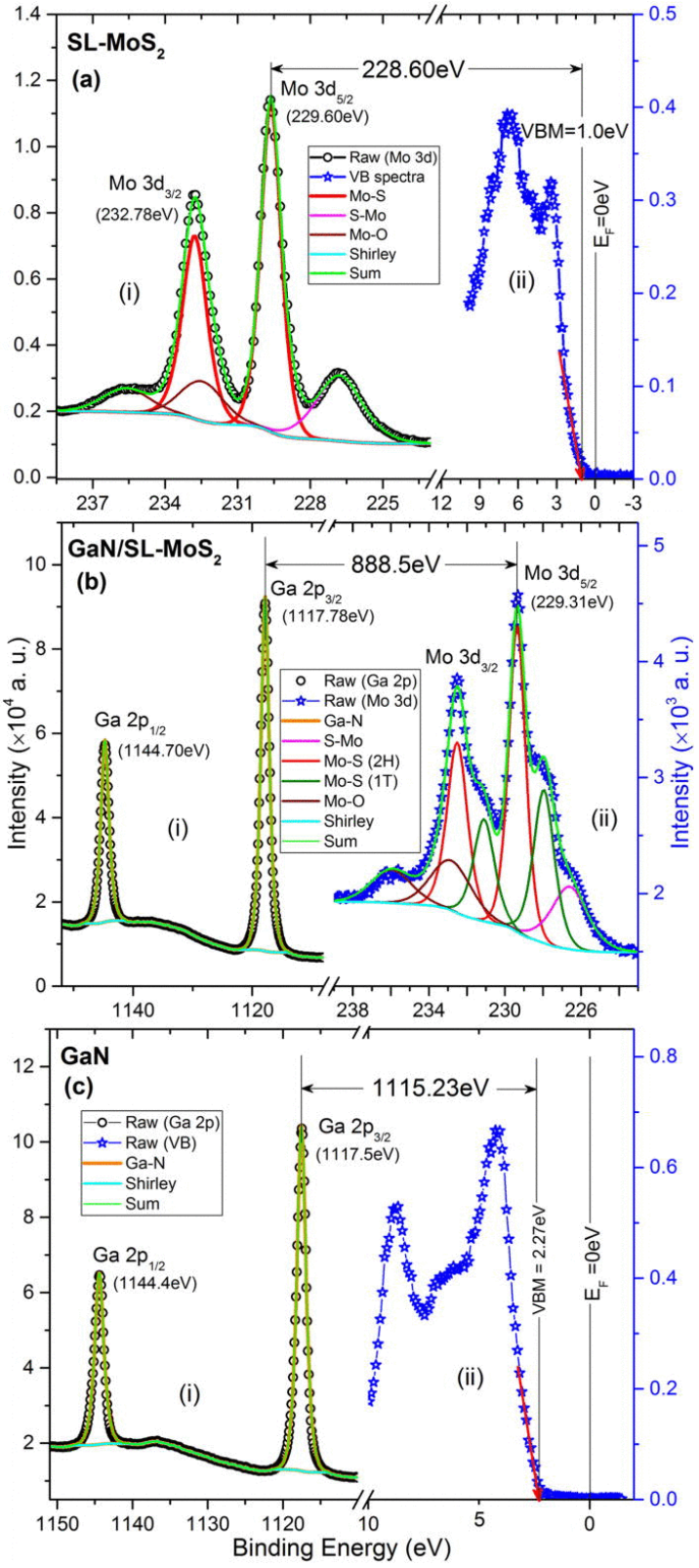

Figure 1.8: (a-i) and (a-ii) The Mo 3d core-level and valence band spectra of single-layer MoS_2. (b-i) and (b-ii) Ga 2p core-level and Mo 3d spectra of GaN/SL-MoS_2. (c-i) and (c-ii) Ga 2p core-level and valence band spectra acquired on GaN epilayer. The peak positions of core-levels are given in parentheses. [Reprinted from Ref. 32 with permission from AIP Publishing]

monolayer MoS_2 calculated from first principles using density functional theory (DFT) within the generalized gradient approximation (GGA) are shown. Here the Valence band maxima (VBM) and conduction band minima (CBM) are indicated by red and blue circles, respectively. Energies are given relative to the VBM. Schematic drawings of low-energy bands in (c) bulk MoS_2 and (d) monolayer MoS_2 showing the band gaps E_g as well as the valence band spin–orbit splitting Δ_{so} and the Γ valley band offset $\Delta_{\Gamma-K}$ for the case of monolayer MoS_2. The band structure parameters have been obtained at the DFT–GGA level of theory. The orbital composition of electronic states at band extrema is indicated.

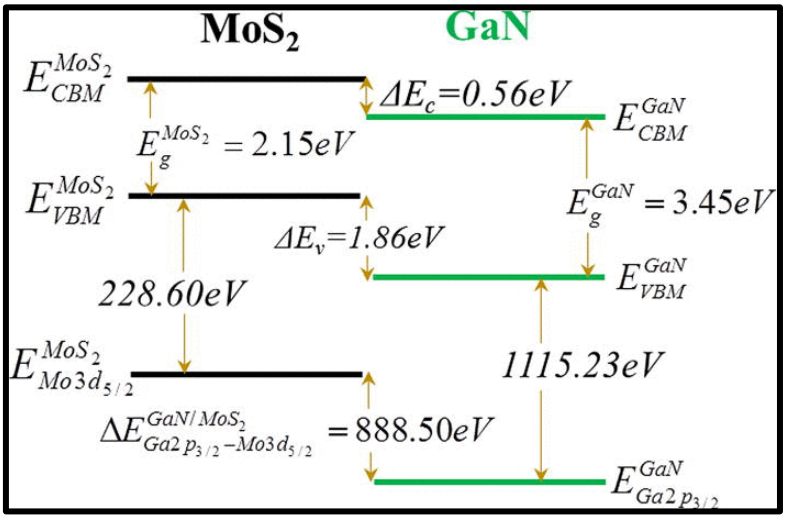

Figure 1.9: The schematic representation of type II band alignment at GaN/SL-MoS_2 heterojunction. [Reprinted from Ref. 32 with permission from AIP Publishing]

In **Figure 1.8**, Tangi et al. reports the VB spectrum of single layer MoS_2, in addition to Ga 2p and Mo 3d spectra of the heterojunction and Ga 2p of GaN. Absence of any other chemical state associated with Mo or S in Ga 2p core-level spectrum and Van der Waal epitaxy can be inferred by noticing the high intensity of Mo-S peak. In their study they report valence band offset (VBO) value of 1.86 ± 0.08 eV and conduction band offset (CBO) of 0.56 ± 0.1 eV. The determinations of these values highlight the importance of heterostructure based device application of MoS_2/GaN. Finally, a schematic of band

alignment diagram based on the heterojunction is depicted in their report as reprinted in **Figure 1.9** of type-II.

I carried the band offset study of few layer MoS_2 grow on free-standing GaN. Chapter 4 is dedicated to the study of the heterojunction between these materials and with band offset values as the key observations.

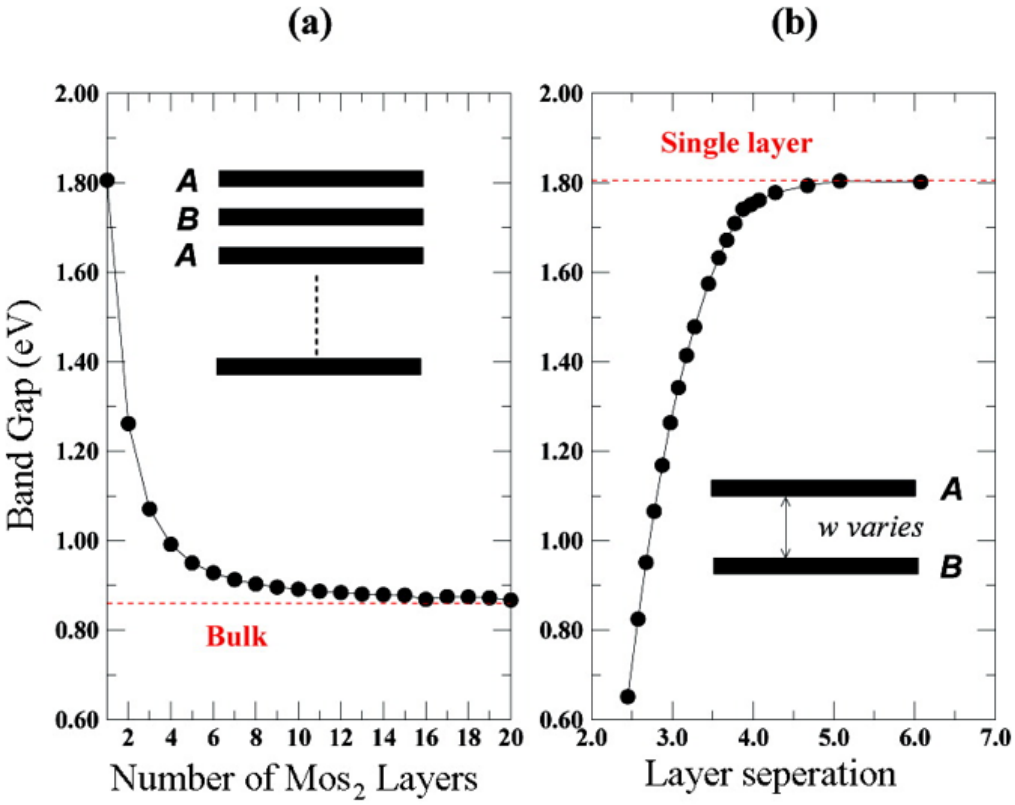

Figure 1.10: (a) Band gap in MoS_2 sheets with respect to number of layers (a) the number of sheets n and (b) separation distance w or z-axis distance between sheets. [Ref. 33. Copyright 2007 American Chemical Society, Reprinted with permission]

Band modulation in MoS_2 from bulk to mono layer is shown and best captured in **Figure 1.10**, as calculated by first principles calculations using DFT in the generalized gradient

approximation. We see a decrease of bandgap from 1.8 eV to 0.86 eV for transition from single to bulk layer in MoS_2.

1.4 MoS_2 and its material applications

The 2D TMDCs can be readily integrated to fabricate a heterostructure without constrains of lattice matching due to the dangling bond free lattice and strong Van der Waals interaction. Layered TMDCs have attracted significant attention for electronic and optoelectronic applications. [34,35] Being a direct bandgap semiconductor, MoS_2 demonstrates high optical absorption in visible range and as well as a large exciton binding energy. It has attracted significant interest in nanoelectronics, high-performance photodetectors and solar cell applications. [36-39]

Integration of the MoS_2 layers with three-dimensional (3D) bulk semiconductor (such as silicon, germanium, gallium nitride, etc.) has been also for fabrication of 2D/3D active heterojunction devices. [40-45] One of the important applications of TMDCs materials is for fabrication of photodiode, due to presence of a direct bandgap fast responsive (high speed) with excellent photosensitivity than that of Si device.

Field effect transistor (FET) fabricated with monolayer MoS_2 showed good room temperature mobility, and significant switching characteristics with on/off current ratio ~10^{10}. [39,40] Thus, utilization of these properties of MoS_2 has been explored in many studies.

In this prospect, I have explored the possibility of effective heterojunction fabrication of 2D MoS_2 with GaN and SiO_2/Si substrate. The fabrication of heterojunction with the CVD synthesized MoS_2 layers, their interfaces and device characteristics were analysed

in detail and included in this thesis. Kang et al. reported water reduction (H^+/H_2) and oxidation (H_2O/O_2) potentials from the simulation study for ML and bulk MoS_2. In **Figure 1.11**, the solid lines are obtained by Perdew-Burke-Ernzerhof (PBE), and dashed

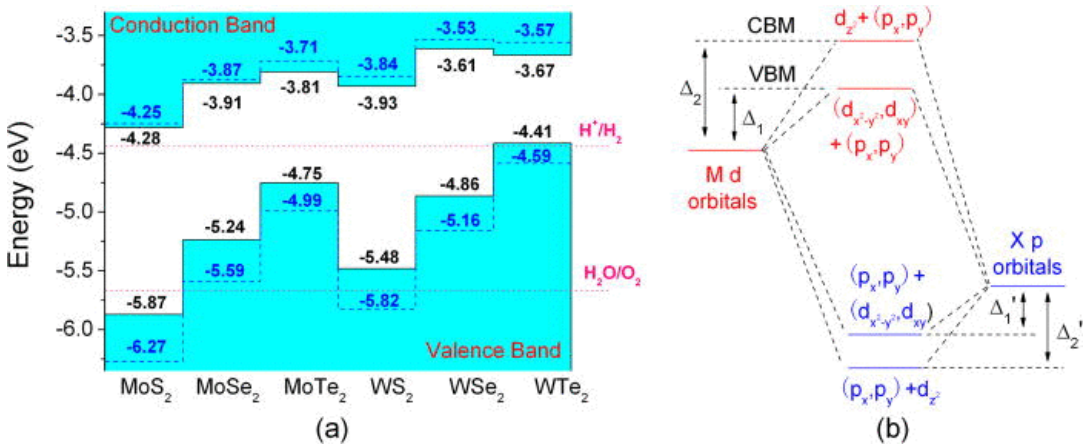

Figure 1.11: (a) Simulation calculated band alignment for MX_2 monolayers. The dotted lines indicate the water reduction (H^+/H_2) and oxidation (H_2O/O_2) potentials. The vacuum level is taken as zero reference. (b) Origin of CBM and VBM in MX_2 shown in schematic. [Reprinted from Ref. 48 with permission from AIP Publishing]

lines are obtained by Heyd-Scuseria-Ernzerhof (HSE06) hybrid functional. Their study indicates MoS_2 monolayer is a good candidate for photo-splitting of water.

In **Figure 1.12**, (a) absorption and (b) photoluminescence spectra of MoS_2 thin films with average thicknesses ranging from 1.3 to 7.6 nm are shown. An interesting observation of slight red shift in both the absorption resonance and photoluminescence energy is seen here. Mono layer MoS_2 shows the strong PL and its intensity decreases with number of stacked layers of MoS_2 of the material. Thus, it is worthwhile to note that transition from indirect to direct or in other words from bulk to monolayer, we can observe a noteworthy

enhancement in photoluminescence quantum yield. This makes it a better candidate for optoelectronic applications.

MoS_2 based vertical heterostructures devices has application as photodetectors with a better photoresponsivity and broad wavelength response. [49] Photoresponsivity from the

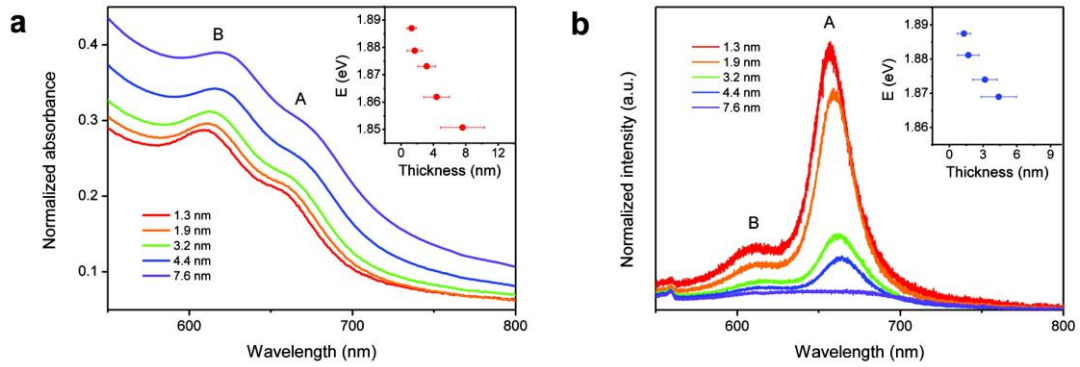

Figure 1.12: (a) Absorption and (b) photoluminescence spectra of MoS_2 thin films with average thicknesses ranging from 1.3 to 7.6 nm. Insets shows energy of the A exciton peak as a function of average film thickness [Ref. 50. Copyright 2011 American Chemical Society, Reprinted with permission]

monolayer MoS_2 based phototransistor can reach as high as 7.5 mA/W, which is found better than that of single layer graphene-based FET. [27] Due to the intrinsic property, fast carrier transfer of graphene and its zero bandgap there arise rapid electron-hole recombination. p-type Silicon-MoS_2 heterostructures shows intrinsic built-in electric field in p-n junction. Whereas n-type Silicon-MoS_2 heterostructures shows modulated barrier height at n-n junction as shown in **Figure 1.13**. In these both type of heterostructures we observe that the photogenerated excitons cannot be separated in forward bias condition due to relatively large barrier for electron and holes transfer but in reverse bias we observe

that the excitons in MoS_2 could be separated effectively at the interface as shown. This draws the explanation for occurrence of photocurrent at zero bias condition.

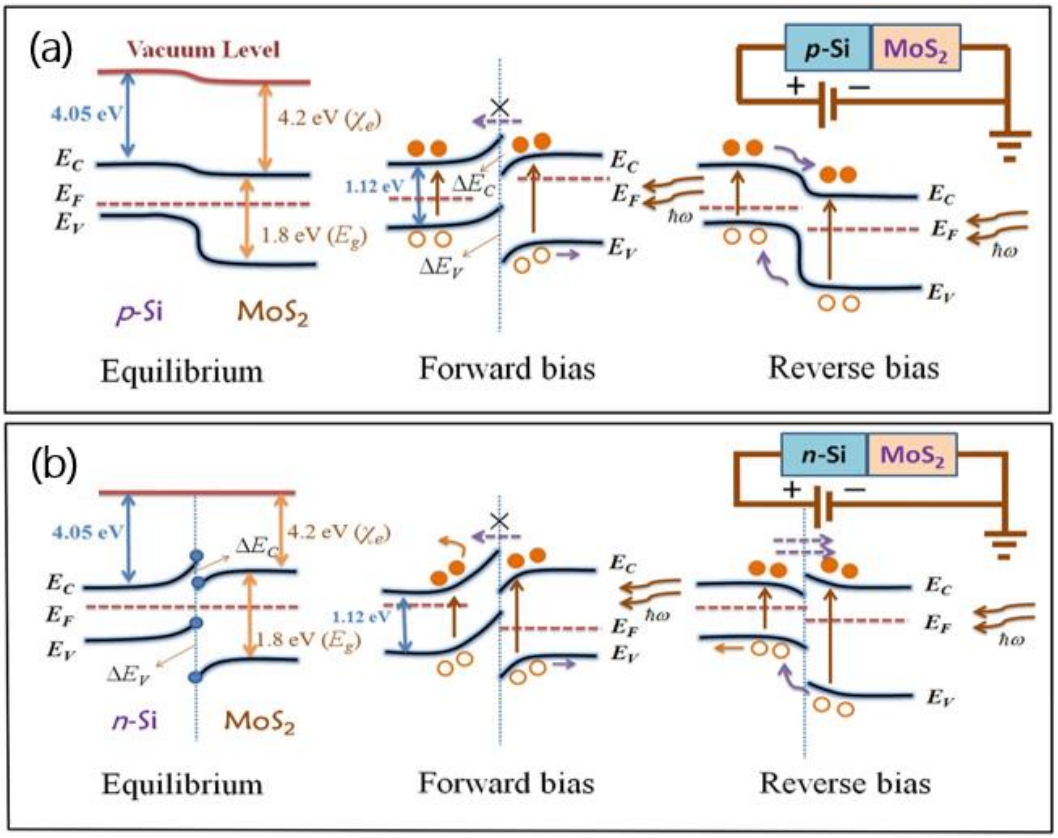

Figure 1.13: The band alignment between (a) p-Si and monolayer MoS_2, and (b) n-Si and monolayer MoS_2. [Reprinted from Ref 49 with permission from Springer Nature]

1.5 Growth substrate for MoS_2 crystal

The MoS_2 crystals and layers are grown on insulating as well as semiconducting substrates. The substrate selection has a crucial effect on the grain size, nucleation of crystal growth. The chemical vapour deposition method was used for the growth of MoS_2

on insulating and semiconducting substrates. Following, I highlight the heterostructure of MoS_2 with other substrates.

Lattice constant versus band gap diagram is shown in

Figure 1.14. Here we see the wide bandgap substrates such as GaN, SiC and Sapphire belonging in the UV region as well as n-type and p-type Silicon in infrared region. I also observe that lattice mismatch of MoS_2 is least GaN, which is ~ 0.8%. [51] In my study I have grown the MoS_2 crystals/layers on broad type of substrates.

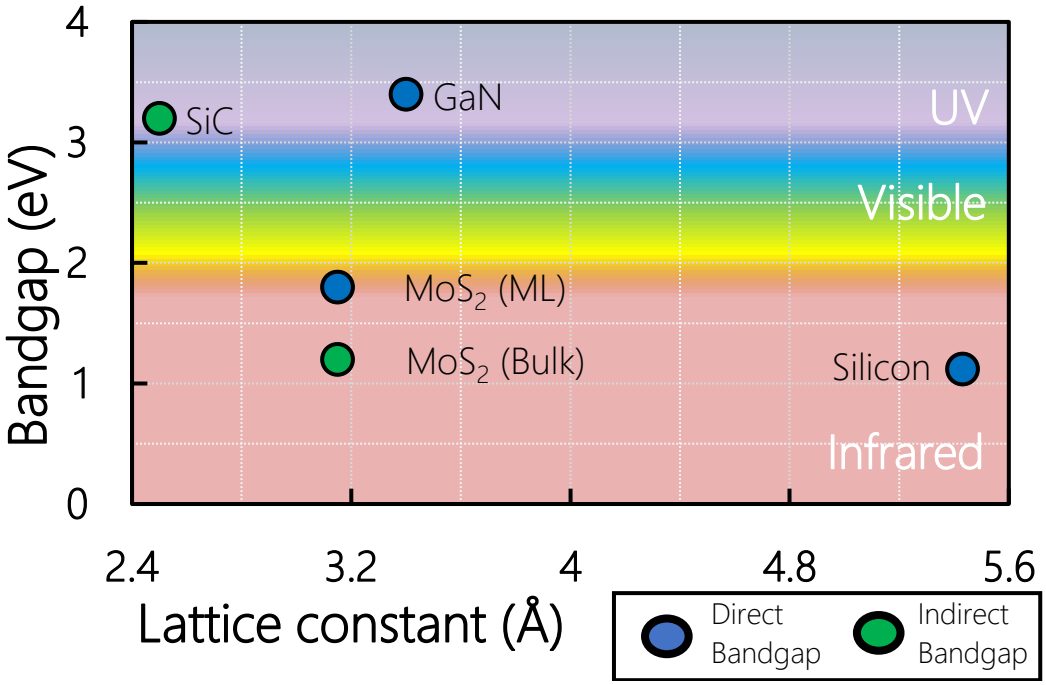

Figure 1.14: Lattice constant versus band gap diagram showing MoS_2 along with other semiconductors

1.5.1 On insulating substrate (SiO_2/Silicon and Sapphire)

Two insulating substrates were used namely, SiO_2/Silicon and Sapphire for MoS_2 crystals/layers growth. These substrates have a very large bandgap (~9 eV) and has a large lattice mismatch with that of MoS_2.

1.5.2 On p-type and n-type Silicon Semiconductor substrate

The resistivity of the p-type Si wafer was 10–20 Ω cm, which corresponded to the doping level of 1.340×10^{15} – 0.6637×10^{15} cm^{-3}. Prior to the thermal deposition, the substrates were cleaned using hydrofluoric acid to remove any oxide layer, then by acetone and iso-propyl alcohol for 10 min each by sonication. Using the chemical vapour deposition techniques, triangular crystals of domain sizes of 50 µm were synthesized without any orientations.

1.5.3 On Lattice matched GaN substrate

I used liquid phase grown germanium doped free-standing Ga-terminated GaN wafer with a doping level of $\leqq 1\times10^{18}$ cm^{-3}. The samples were cleaned using standard Piranha solution (H_2SO_4/H_2O_2 ~7/3) for 10 mins and then later with acetone and iso-propyl alcohol for 10 min each by sonication. Using the ammonia-based precursor in chemical vapour deposition techniques, triangular crystals of domain sizes of 1 µm were synthesized with two different types of orientation.

In fabrication of heterostructure semiconductors consideration is given to epitaxy nature of growth for it facilitates low defect interface and efficient vertical transport of charge carriers. Thus, designing energy-efficient, high-speed, high-power vertical devices. [52]

1.6 Heterostructure of MoS_2 with semiconducting substrate

In my study that is elaborated in subsequent chapter, I have studied the interface properties of MoS_2 with the semiconducting substrates. Heterojunction of MoS_2 layers and p-type Si yielded spectral photo response characteristics. These findings on the photocarriers behaviour in the fabricated MoS_2/Si heterojunction interface can be critical

to develop high photoresponsive heterojunction devices. Similarly, I demonstrated the growth of uniform few-layers MoS_2 film on free-standing GaN wafer using the sulphurisation process. A photovoltaic photoresponsivity was obtained in the MoS_2/GaN heterojunction with vertical current flow across the junction. Thus, demonstrating significance of developing MoS_2/GaN heterostructure-based photodiode and for other optoelectronics device application.

1.7 Overview of synthesis processes of MoS_2

Robert Frindt reported first adhesive tape method for MoS_2 thin layer synthesis in 1963 and subsequently in 1986 monolayer MoS_2 suspension was reported. Early part of 1990 saw significant development in carbon nanotubes and inorganic fullerenes followed by MoS_2 nanotubes and nested particles. [53-57]

Layered 2D TMDC nano-sheets are synthesized from either top-down route like mechanical exfoliation or bottom-up processes like CVD. To, study the 2D characteristics of these materials, it is imperative that synthesized structure must be few- and single-layer sheets, and uniform sample size is also highly desirable. To get proper sample size and uniform layer thickness CVD method is most suitable process for the synthesis of TMDCs. First CVD growth of TMDCs was demonstrated by Hofmann demonstrated MOCVD growth of MoS_2 on various substrates in 1988. [58] The precursors of Mo and W hexacarbonyls of the corresponding transition metals precursors were used with vaporized sulphur or hydrogen sulphide gas. However, the films are normally thick. For the synthesis of two-dimensional atomic layers or single layers, several techniques in CVD have been developed. Liu *et al*. reported a two-step thermolysis process [59], The

ammonium thiomolybdates [$(NH_4)_2MoS_4$] precursor was used with onto the substrates by dip-coating and annealed in Ar/H_2 environment at 500° C which was further converted to MoS_2 by annealing at sulphurisation at 1000° C using sulphur vapour along with Ar gas.

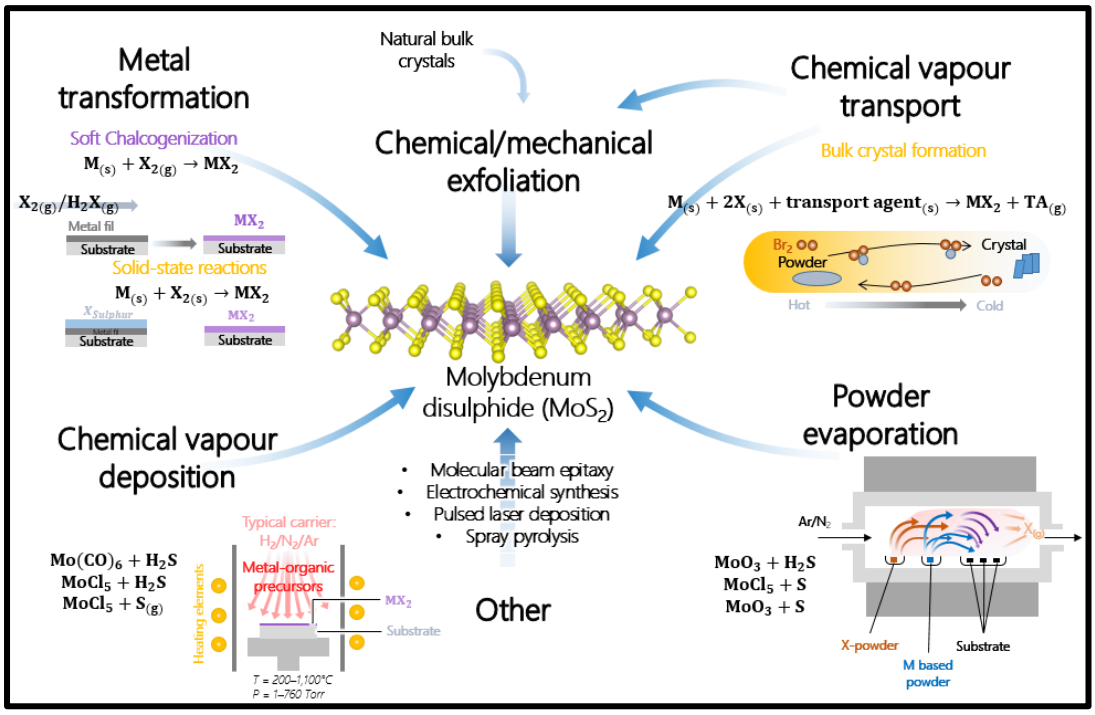

Figure 1.15: Summary of distinctive synthesis mechanism for development of MoS_2 like TMDCs. [Adapted from Ref. 64 with permission from Annual Reviews]

Three-layer MoS_2 was synthesized which was confirmed by high-resolution transmission electron microscopy (TEM) analysis which was transferred easily on another arbitrary substrate. The crystallinity of the crystals was significantly improved using sulphur vapours. Zhan *et al*. also reported CVD synthesis of MoS_2 by direct sulphurisation of Mo metal film to get large area, few layers film. [60] Electron beam deposited Mo on SiO_2 surface was used for CVD synthesis. The subsequent sulphurisation using sulphur vapour gives MoS_2 with thickness depending on deposited metal and area inside CVD furnace. Transition metal oxide precursor-based methods were reported by Lee *et al*. wherein, few-

layer MoS_2 was synthesized using CVD. [61] Synthesis of monolayer MoS_2 on graphene surface was reported by McCreary *et al*. [62] $MoCl_5$ precursor was used as the Mo source in the study. By changing the amount of precursor mono, bi and tri layer MoS_2 films were synthesized. The synthesis of TMDCs single crystal in CVD process is still a challenge till date, smaller domains of TMDCs are obtained compared to graphene crystals. However, some single crystal TMDCs were successfully synthesized in relatively large domain. The main challenge in synthesis of single crystal is reduction in nucleation density to reduce grain boundaries. Zhang *et al*. reported growth of single crystal monolayer TMDCs on single crystal sapphire substrate sulphur precursors by CVD growth. Also, monolayer TMDCs single crystal domains with size up to 370 µm was reported by Rong *et al*. in CVD growth. [63] This was achieved by controlling the supply of sulphur amount and time during the CVD process.

1.8 Motivation and objectives of current work

TMDCs are emerging new generation materials with interesting properties for various interesting catalytic, electronic, and optical applications. Also, the conductive properties of these TMDCs varies from insulating to superconducting. Contrary to graphene, they also show semiconducting nature with direct bandgap. Thus, they are widely explored for electronic applications which compensate the limitations faced by graphene. As, the bandgap of TMDCs such as MoS_2 is highly suitable for fabrication of field-effect transistors (FETs) they show great prospect for future electronic. Among the TMDCs, monolayer MoS_2 are particularly interesting for optoelectronic devices due to their direct bandgap (1.7eV-1.8 eV) in the visible wavelength range. Presently, synthesis of high

quality TMDCs layers and understanding their growth mechanism is of particular interest. Again, the atmospheric degradation of TMDCs layer is a hurdle for integration in device fabrication. Considering these facts, I have explored high quality TMDCs layer growth by CVD technique.

The objective of this thesis is to synthesize better quality and unique shape of TMDCs using CVD technique, studying the stability of the synthesized material for photoresponsive device application. The CVD synthesis process has significant advantage with better optical quality, large area uniform layer synthesis of MoS_2. Thus, I have used the CVD method to synthesize MoS_2 crystals and investigated its heterostructures, its properties and their applications. In CVD growth the reaction process of Mo precursors (in this experiments MoO_3) with sulphur is very critical to achieve high quality layer growth. Further adding to the study of synthesis of the TMDCs layer, optoelectronic device fabrication in conjunction with other semiconducting materials was investigated. Fabrication of heterostructures with a SiO_2/Si and GaN semiconductor for photoresponsive devices was explored. Thus, the research findings on synthesis and optoelectronic applications of MoS_2 layers were compiled systematically in this thesis.

1.9 Organization of the dissertation

This thesis contributes to the synthesis and application of CVD synthesized MoS_2 crystals and layer structures. Detailed characterization with fabrication of heterostructure with other layered materials was explored and reported.

In chapter 1 describes the general introduction of 2D-TMDCs.

In chapter 2 details of the two synthesis processes for the growth of MoS_2 layers and two for crystals using chemical vapour deposition (CVD) techniques are shown. The synthesized 2D materials are later characterized using various physical and chemical methods.

In Chapter 3 uniform few-layers MoS_2 film was synthesised on p-type Silicon wafer by sulphurisation process of MoO_3 thin layer. In this I study the influence of molybdenum sulphide and p-type silicon interface states on spectral photoresponse characteristics. A heterojunction device was fabricated for he synthesised MoS_2 layers on p- Silicon and device properties were investigated. The photovoltaic action and a photoresponsivity for the heterostructure were analysed and influence of trap states were confirmed.

In chapter 4 uniform few-layers MoS_2 film was synthesised on free-standing GaN wafer by sulphurisation process of MoO_3 thin layer, labelled CVD II. Photovoltaic photoresponsivity for the heterojunction with vertical current flow across the junction was studied. The XPS measurements were taken and were used in calculating band offset at the heterojunction of the two material. Finally, the process is explained using the band diagram. In addition to, growth of MoS_2 crystals on the lattice matched Ga-polar GaN wafer using ammonium tetrathiomolybdate (ATM) as a precursor in a chemical vapour deposition (CVD) process is presented using CVD III. A unidirectional triangular MoS_2 crystals and continuous film on free-standing Ga-polar GaN substrate are represented in this study. Suitability of bulk Ga-polar GaN wafer for MoS_2 crystals growth using the ammonia containing ATM precursor is addressed using this CVD process. The heterojunction fabricated by this process was analysed by a device fabrication in vertical configuration.

Chapter 5 summarizes the whole thesis and discusses about future prospects.

1.10 Bibliography

[1] Z. Zeng, C. Tan, X. Huang, S. Bao, and H. Zhang, "Growth of noble metal nanoparticles on single-layer TiS_2 and TaS_2 nanosheets for hydrogen evolution reaction," *Energy Environ. Sci.*, vol. 7, no. 2, pp. 797–803, Jan. 2014.

[2] F. Li, K. Tu, and Z. Chen, "Versatile electronic properties of VSe_2 bulk, few-layers, monolayer, nanoribbons, and nanotubes: A computational exploration," *J. Phys. Chem. C*, vol. 118, no. 36, pp. 21264–21274, Sep. 2014.

[3] L. Ma *et al.*, "A metallic mosaic phase and the origin of Mott-insulating state in 1T-TaS_2," *Nat. Commun.*, vol. 7, Mar. 2016.

[4] X. Xi *et al.*, "Strongly enhanced charge-density-wave order in monolayer $NbSe_2$," *Nat. Nanotechnol.*, vol. 10, no. 9, pp. 765–769, Sep. 2015.

[5] M. M. Ugeda *et al.*, "Characterization of collective ground states in single-layer $NbSe_2$," *Nat. Phys.*, vol. 12, no. 1, pp. 92–97, Jan. 2016.

[6] T. R. Chang *et al.*, "Prediction of an arc-tunable Weyl Fermion metallic state in $Mo_xW_{1-x}Te_2$," *Nat. Commun.*, vol. 7, no. 1, pp. 1–9, Feb. 2016.

[7] K. Sugawara *et al.*, "Unconventional charge-density-wave transition in monolayer 1T-$TiSe_2$," *ACS Nano*, vol. 10, no. 1, pp. 1341–1345, Jan. 2016.

[8] Y. I. Joe *et al.*, "Emergence of charge density wave domain walls above the superconducting dome in 1T-$TiSe_2$," *Nat. Phys.*, vol. 10, no. 6, pp. 421–425, Apr. 2014.

[9] B. Radisavljevic, A. Radenovic, J. Brivio, V. Giacometti, and A. Kis, "Single-layer MoS_2 transistors," *Nat. Nanotechnol.*, vol. 6, no. 3, pp. 147–150, Jan. 2011.

[10] W. Yang *et al.*, "Electrically Tunable Valley-Light Emitting Diode (vLED) Based on CVD-Grown Monolayer WS_2," *Nano Lett.*, vol. 16, no. 3, pp. 1560–1567, Mar. 2016.

[11] A. Thangaraja, S. M. Shinde, G. Kalita, and M. Tanemura, "An effective approach to synthesize monolayer tungsten disulphide crystals using tungsten halide precursor," *Appl. Phys. Lett.*, vol. 108, no. 5, p. 053104, Feb. 2016.

[12] A. Splendiani *et al.*, "Emerging photoluminescence in monolayer MoS_2," *Nano Lett.*, vol. 10, no. 4, pp. 1271–1275, Apr. 2010.

[13] K. F. Mak, C. Lee, J. Hone, J. Shan, and T. F. Heinz, "Atomically thin MoS_2: A new direct-gap semiconductor," *Phys. Rev. Lett.*, vol. 105, no. 13, p. 136805, Sep. 2010.

[14] A. K. Geim and I. V. Grigorieva, "Van der Waals heterostructures," *Nature*, vol. 499, no. 7459, pp. 419–425, 2013.

[15] A. H. Castro Neto, F. Guinea, N. M. R. Peres, K. S. Novoselov, and A. K. Geim, "The electronic properties of graphene," *Rev. Mod. Phys.*, vol. 81, no. 1, pp. 109–162, Jan. 2009.

[16] K. F. Mak, K. He, J. Shan, and T. F. Heinz, "Control of valley polarization in monolayer MoS_2 by optical helicity," *Nat. Nanotechnol.*, vol. 7, no. 8, pp. 494–498, Jun. 2012.

[17] Q. H. Wang, K. Kalantar-Zadeh, A. Kis, J. N. Coleman, and M. S. Strano, "Electronics and optoelectronics of two-dimensional transition metal dichalcogenides," *Nat. Nanotechnol.*, vol. 7, no. 11, pp. 699–712, Nov. 2012.

[18] O. Lopez-Sanchez, D. Lembke, M. Kayci, A. Radenovic, and A. Kis, "Ultrasensitive photodetectors based on monolayer MoS_2," *Nat. Nanotechnol.*, vol. 8, no. 7, pp. 497–501, 2013.

[19] A. Pospischil, M. M. Furchi, and T. Mueller, "Solar-energy conversion and light emission in an atomic monolayer p-n diode," *Nat. Nanotechnol.*, vol. 9, no. 4, pp. 257–261, 2014.

[20] J. Kibsgaard, Z. Chen, B. N. Reinecke, and T. F. Jaramillo, "Engineering the surface structure of MoS_2 to Â preferentially expose active edge sites for Â electrocatalysis," *Nat. Mater.*, vol. 11, no. 11, pp. 963–969, 2012.

[21] D. Voiry *et al.*, "Enhanced catalytic activity in strained chemically exfoliated WS_2 nanosheets for hydrogen evolution," *Nat. Mater.*, vol. 12, no. 9, pp. 850–855, Sep. 2013.

[22] S. Wang *et al.*, "Shape Evolution of Monolayer MoS_2 Crystals Grown by Chemical Vapor Deposition," *Chem. Mater.*, vol. 26, pp. 6371–6379, 2014.

[23] G. Lucovsky, R. M. White, J. A. Benda, and J. F. Revelli, "Infrared-reflectance spectra of layered group-IV and group-VI transition-metal dichalcogenides," *Phys. Rev. B*, vol. 7, no. 8, pp. 3859–3870, Apr. 1973.

[24] J. L. Verble and T. J. Wieting, "Lattice mode degeneracy in MoS_2 and other layer compounds," *Phys. Rev. Lett.*, vol. 25, no. 6, pp. 362–365, Aug. 1970.

[25] C. Lee, H. Yan, L. E. Brus, T. F. Heinz, J. Hone, and S. Ryu, "Anomalous lattice vibrations of single- and few-layer MoS_2," *ACS Nano*, vol. 4, no. 5, pp. 2695–2700, 2010.

[26] B. Radisavljevic, A. Radenovic, J. Brivio, V. Giacometti, and A. Kis, "Single-layer MoS_2 transistors," *Nat. Nanotechnol.*, vol. 6, no. 3, pp. 147–150, 2011.

[27] Z. Yin *et al.*, "Single-layer MoS_2 phototransistors," *ACS Nano*, vol. 6, no. 1, pp. 74–80, 2012.

[28] S. M. Shinde, G. Kalita, and M. Tanemura, “Fabrication of poly(methyl methacrylate)-MoS_2/graphene heterostructure for memory device application,” *J. Appl. Phys.*, vol. 116, no. 21, 2014.

[29] Y. Huang, J. Guo, Y. Kang, Y. Ai, and C. M. Li, “Two dimensional atomically thin MoS_2 nanosheets and their sensing applications,” *Nanoscale*, vol. 7, no. 46, pp. 19358–19376, 2015.

[30] J. E. Padilha, H. Peelaers, A. Janotti, and C. G. Van De Walle, “Nature and evolution of the band-edge states in MoS_2: From monolayer to bulk,” *Phys. Rev. B - Condens. Matter Mater. Phys.*, vol. 90, no. 20, p. 205420, Nov. 2014.

[31] O. V. Yazyev and A. Kis, “MoS_2 and semiconductors in the flatland,” in *Materials Today*, 2015, vol. 18, no. 1, pp. 20–30.

[32] M. Tangi *et al.*, “Determination of band offsets at GaN/single-layer MoS_2 heterojunction,” *Appl. Phys. Lett.*, vol. 109, no. 3, p. 032104, Jul. 2016.

[33] T. Li and G. Galli, “Electronic properties of MoS_2 nanoparticles,” *J. Phys. Chem. C*, vol. 111, no. 44, pp. 16192–16196, Nov. 2007.

[34] K. F. Mak, K. He, J. Shan, and T. F. Heinz, “Control of valley polarization in monolayer MoS_2 by optical helicity,” *Nat. Nanotechnol.*, vol. 7, no. 8, pp. 494–498, 2012.

[35] J. K. Ellis, M. J. Lucero, and G. E. Scuseria, “The indirect to direct band gap transition in multilayered MoS_2 as predicted by screened hybrid density functional theory,” *Appl. Phys. Lett.*, vol. 99, no. 26, p. 261908, Dec. 2011.

[36] R. Cheng *et al.*, “Electroluminescence and photocurrent generation from atomically sharp WSe_2/MoS_2 heterojunction p-n diodes,” *Nano Lett.*, vol. 14, no. 10, pp. 5590–5597, 2014.

[37] S. Krishnamoorthy *et al.*, “High current density 2D/3D MoS_2/GaN Esaki tunnel diodes,” *Appl. Phys. Lett.*, vol. 109, no. 18, p. 183505, Oct. 2016.

[38] K. Zhang *et al.*, “Large scale 2D/3D hybrids based on gallium nitride and transition metal dichalcogenides,” *Nanoscale*, vol. 10, no. 1, pp. 336–341, Dec. 2018.

[39] D. Ruzmetov *et al.*, “Van der Waals interfaces in epitaxial vertical metal/2D/3D semiconductor heterojunctions of monolayer MoS_2 and GaN,” *2D Mater.*, vol. 5, no. 4, p. 045016, Aug. 2018.

[40] M. L. Tsai *et al.*, “Monolayer MoS_2 heterojunction solar cells,” *ACS Nano*, vol. 8, no. 8, pp. 8317–8322, 2014.

[41] D. Mahalu, M. Peisach, W. Jaegermann, A. Wold, and R. Tenne, “Controlled photocorrosion of tungsten diselenide: influence of molecular oxygen,” *J. Phys. Chem.*, vol. 94, no. 21, pp. 8012–8013, Oct. 1990.

[42] Y. Yoon, K. Ganapathi, and S. Salahuddin, "How Good Can Monolayer MoS_2 Transistors Be?," *Nano Lett.*, vol. 11, no. 9, pp. 3768–3773, Sep. 2011.

[43] R. Ganatra and Q. Zhang, "Few-Layer MoS_2 : A Promising Layered Semiconductor," *ACS Nano*, vol. 8, no. 5, pp. 4074–4099, May 2014.

[44] S. Qiao *et al.*, "A vertically layered MoS_2 /Si heterojunction for an ultrahigh and ultrafast photoresponse photodetector," *J. Mater. Chem. C*, vol. 6, no. 13, pp. 3233–3239, Mar. 2018.

[45] L. Wang *et al.*, "MoS_2/Si Heterojunction with Vertically Standing Layered Structure for Ultrafast, High-Detectivity, Self-Driven Visible-Near Infrared Photodetectors," *Adv. Funct. Mater.*, vol. 25, no. 19, pp. 2910–2919, May 2015.

[46] O. Lopez-Sanchez, D. Lembke, M. Kayci, A. Radenovic, and A. Kis, "Ultrasensitive photodetectors based on monolayer MoS_2," *Nat. Nanotechnol.*, vol. 8, no. 7, pp. 497–501, Jul. 2013.

[47] X. Hong *et al.*, "Ultrafast charge transfer in atomically thin MoS_2/WS_2 heterostructures," *Nat. Nanotechnol.*, vol. 9, no. 9, pp. 682–686, Sep. 2014.

[48] J. Kang, S. Tongay, J. Zhou, J. Li, and J. Wu, "Band offsets and heterostructures of two-dimensional semiconductors," *Appl. Phys. Lett.*, vol. 102, no. 1, 2013.

[49] Y. Li, C. Y. Xu, J. Y. Wang, and L. Zhen, "Photodiode-like behavior and excellent photoresponse of vertical Si/monolayer MoS_2 heterostructures," *Sci. Rep.*, vol. 4, no. 1, pp. 1–8, Nov. 2014.

[50] G. Eda, H. Yamaguchi, D. Voiry, T. Fujita, M. Chen, and M. Chhowalla, "Photoluminescence from chemically exfoliated MoS_2," *Nano Lett.*, vol. 11, no. 12, pp. 5111–5116, Dec. 2011.

[51] P. Gupta *et al.*, "Layered transition metal dichalcogenides: promising near-lattice-matched substrates for GaN growth," *Sci. Rep.*, vol. 6, no. 1, pp. 1–8, Jul. 2016.

[52] D. Ruzmetov *et al.*, "Vertical 2D/3D Semiconductor Heterostructures Based on Epitaxial Molybdenum Disulfide and Gallium Nitride," *ACS Nano*, vol. 10, no. 3, pp. 3580–3588, Mar. 2016, doi: 10.1021/acsnano.5b08008.

[53] Y. Rong *et al.*, "Controlling sulphur precursor addition for large single crystal domains of WS_2," *Nanoscale*, vol. 6, no. 20, pp. 12096–12103, 2014.

[54] I. Bilgin *et al.*, "Chemical Vapor Deposition Synthesized Atomically Thin Molybdenum Disulfide with Optoelectronic-Grade Crystalline Quality," *ACS Nano*, vol. 9, no. 9, pp. 8822–8832, Sep. 2015.

[55] G. Ye *et al.*, "Defects Engineered Monolayer MoS_2 for Improved Hydrogen Evolution Reaction," *Nano Lett.*, vol. 16, no. 2, pp. 1097–1103, 2016.

[56] H. Li *et al.*, "Fabrication of single- and multilayer MoS_2 film-based field-effect transistors for sensing NO at room temperature," *Small*, vol. 8, no. 1, pp. 63–67, 2012.

[57] D. Kong, J. J. Cha, H. Wang, H. R. Lee, and Y. Cui, "First-row transition metal dichalcogenide catalysts for hydrogen evolution reaction," *Energy Environ. Sci.*, vol. 6, no. 12, p. 3553, 2013.

[58] W. K. Hofmann, "Thin films of molybdenum and tungsten disulphides by metal organic chemical vapour deposition," *J. Mater. Sci.*, vol. 23, no. 11, pp. 3981–3986, Nov. 1988.

[59] K. K. Liu *et al.*, "Growth of large-area and highly crystalline MoS_2 thin layers on insulating substrates," *Nano Lett.*, vol. 12, no. 3, pp. 1538–1544, 2012.

[60] Y. Zhan, Z. Liu, S. Najmaei, P. M. Ajayan, and J. Lou, "Large-area vapor-phase growth and characterization of MoS_2 atomic layers on a SiO_2 substrate," *Small*, vol. 8, no. 7, pp. 966–971, 2012.

[61] Y.-H. Lee *et al.*, "Synthesis of Large-Area MoS_2 Atomic Layers with Chemical Vapor Deposition," *Adv. Mater.*, vol. 24, no. 17, pp. 2320–2325, 2012.

[62] K. M. McCreary *et al.*, "Large-area synthesis of continuous and uniform MoS_2 monolayer films on graphene," *Adv. Funct. Mater.*, vol. 24, no. 41, pp. 6449–6454, 2014.

[63] Y. Zhang *et al.*, "Controlled Growth of High-Quality Monolayer WS_2 Layers on Sapphire and Imaging Its Grain Boundary," *ACS Nano*, vol. 7, no. 10, pp. 8963–8971, 2013.

[64] S. Das, J. A. Robinson, M. Dubey, H. Terrones, and M. Terrones, "Beyond Graphene: Progress in Novel Two-Dimensional Materials and van der Waals Solids," *Annu. Rev. Mater. Res.*, vol. 45, pp. 1–27, 2015.

CHAPTER 2

2 Growth mechanism of MoS_2 and its characterization methodology

2.1 Background of the study

To get proper sample size and uniform layer thickness CVD method is most suitable process for the synthesis of TMDCs.

A general outline to the synthesis of MoS_2 is stated in section 1.7 of previous Chapter.

First CVD growth of TMDCs was demonstrated by Hofmann demonstrated MOCVD growth of MoS_2 on various substrates in 1988. The synthesis of TMDCs single crystal in CVD process is still a challenge till date, smaller domains of TMDCs are obtained compared to graphene crystals. MoO_3 with 99.9% purity and Sulphur with 98.0% were used as source materials. High purity gases (99.9999%) such as Ar, H_2, and Ar+H_2 gas mixture were used as carrier, without affecting the surface of the substrate under study, during my several laboratory experiments and will be mentioned in the relevant CVD processes in the text. In this study, crystal size of up to 50 µm monolayer TMDCs was obtained, also few layer MoS_2 of varying thicknesses.

Table 2.1 outlines the synthesis processes that is described in this chapter. Process no. I was deployed to synthesize crystals of MoS_2 on various substrates. This process is divided into two techniques, first in which MoO_3 powder is kept in furnace with substrate kept at

a particular distance, vertically and horizontally. Growth of crystals on these substrates which are kept are varying distance are studied. In second technique, MoO_3 is thermally deposited on various substrates. This is the source of precursor and has uniform vapour concentration of the precursor available for the crystal formation.

Further, process no. II was deployed for growth of MoS_2 layers with varying length on different substrates under study. In this process various growth parameters are considered for growth of few layers with varying thickness or number of stacking layer of MoS_2.

Lastly, process III is a two-stage thermolysis method of ammonia-based precursor. In this mechanism the precursor was spin-coated on various substrates under study and later subjected to the thermolysis process in quartz tube H_2 environment.

The growth parameters are studied for each process and are optimised for the desired characteristics of MoS_2. Various characterisations are carried out and studied to ascertain their efficacy.

Table 2.1: Highlights of the synthesis processes

CVD methods		**Expected output**	**Precursor**
Process I	Technique 1	Triangular Crystals	MoO_3 powder
	Technique 2		Thermally deposited MoO_3 on substrates
Process II		Few layer	Thermally deposited MoO_3 on substrates
Process III		Individual & conjoint crystal	Spin-coated Ammonia tetrathiomolybdate on substrates

2.2 Instruments used for characterisation

Optical microscopy analysis was performed using the digital optical microscope VHX-500 in reflectance mode with a Moticam 2000 2.0M pixel camera.

Raman spectroscopy is extensively used for identification on many 2D materials as it gives fingerprint scattering for every material. Raman spectroscopy is a relatively easy, non-destructive, non-contacting, and quick measurement method to probe the inelastic scattering of light from a sample surface at room temperature at ambient pressure. The wavelength of the bands is affected by the energy of the laser, and the following wavelengths are given for a laser excitation energy of 532.08 nm, in which an NRS-3300 laser Raman spectrometer was used to obtain the Raman spectra. Raman spectrum for MoS_2 shows typically two signature peaks at specific wavenumbers corresponding to in-plan vibration of metal and chalcogen atoms (E_{2g}) and out of plan vibration of sulphur atoms (A_{1g}).

X-ray Photoelectron Spectroscopy (XPS) is a surface analysis with a typical depth of 5-10 nm, used to determine the quantitative atomic composition, chemical and electronic states of elements in the sample. The process works by irradiating a sample with monochromatic X-rays, typically mono-energetic Al Kα X-rays, resulting in the emission of photoelectrons from the surface of the sample. An electron energy analyser is used to measure the kinetic energy of the emitted photoelectrons over a range of electron kinetic energies. The emitted atoms cause peaks to appear in the spectrum from characteristic energies of electrons. From the binding energy and intensity of a photoelectron peak, the elemental identity, chemical state, and quantity of a detected element can be determined.

XPS analysis was performed by VersaProbe using monochromated Al Kα excitation source (1486.6 eV).

Field emission scanning electron microscopy (FE-SEM) images were taken with JEOL JSM 5600 with an accelerating voltage of 20 kV. FE-SEM is a technique used in investigation of the surface of the material and their electronic properties. With electron beams surface of materials are probed. The reflected electrons contain various information such as morphology, chemical composition etc, which are reproduced as SEM images.

Atomic force microscopy (AFM) images were taken with a JSPM-5200 scanning probe microscope. The least count AFM measurement were nearly 0.1 nm. AFM measurements is a high-resolution type of microscopy with resolution which is designed to trace out the topography of the surface. The tip of the cantilever 'touches' the samples with a repulsion force which pushes it upward. During the scanning of the topography by the cantilever a laser is monitored reflected from the tipoff the cantilever. A photodiode detects this movement thus the variations in the height profile. Finally, a surface of any material can be produced as a reproduction of variation of voltage. This method is used for measurement of the step height at the edge of the deposited MoS_2 layer on the substrates.

Photoluminescence (PL) characterization was carried out with a confocal scanning (NX-3DFLIM-N03, Tokyo Instruments, Japan) equipped with a Nd:YVO_4 diode laser.

Current density-voltage (J-V) characteristic measurements were performed at room temperature using two probes system and a Keithley 2401 SourceMeter. Quantum efficiency (QE) measurement was done using a SM-250 hyper monochromatic light system.

2.3 Synthesis mechanism - CVD process I

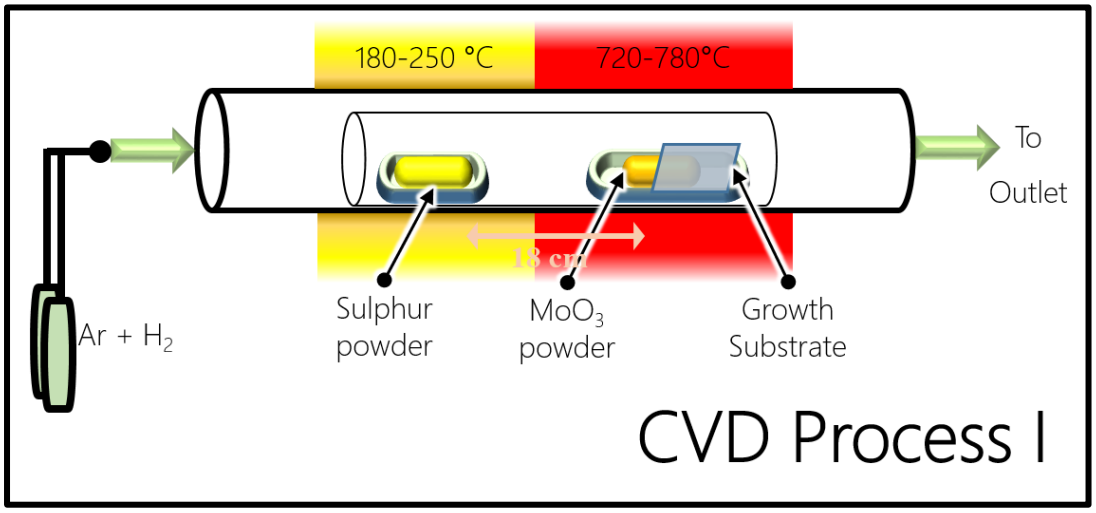

Figure 2.1: Schematic diagram of CVD process I deployed in synthesizing MoS_2 crystals

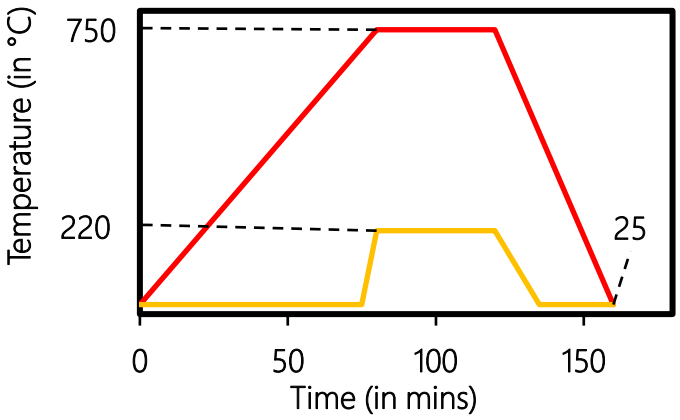

Figure 2.2: Temperature profile of furnaces in CVD process I

In this thesis, I report synthesis of the unique ribbon shaped 2D-MoS_2 structure in modified CVD method. As depicted in **Figure 2.1**, I deployed various CVD techniques for optimizing the growth. I also successfully synthesised millimetre scale monolayer MoS_2 as well as crystals with the size of up to 100 µm. These MoS_2 crystals were characterised by Optical, Raman and PL analysis.

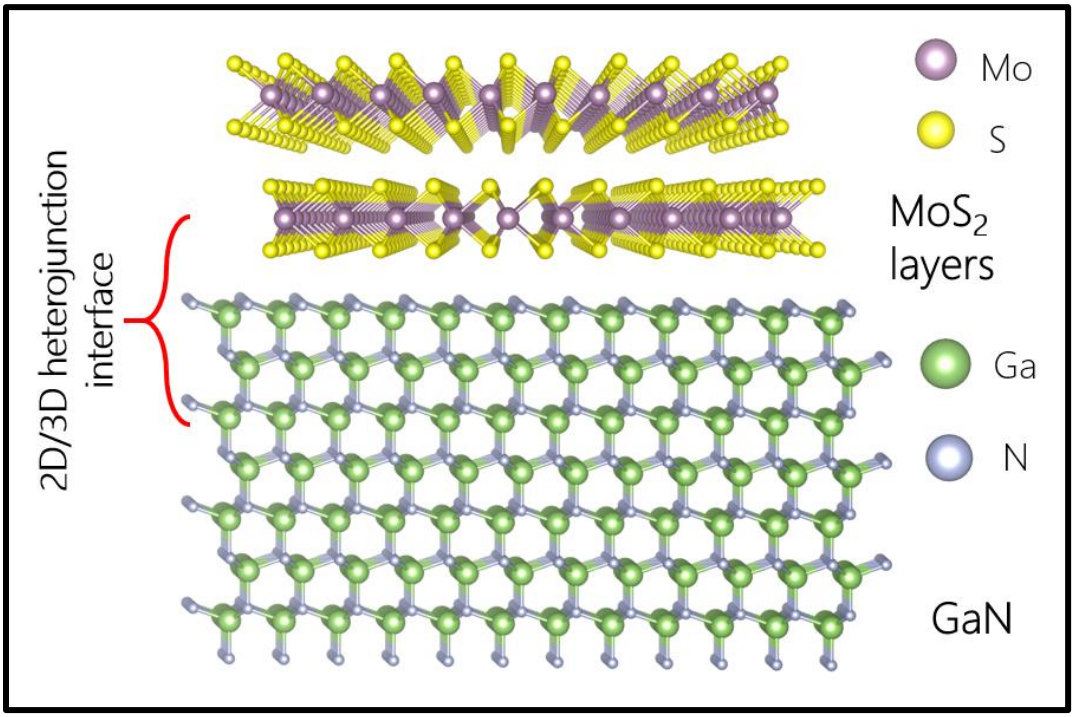

Figure 2.3: Ball and stick diagram of MoS_2 and GaN in CVD II

2.3.1 Results from CVD process I (technique 1)

As depicted in the **Figure 2.4**, placement of the precursor and growth substrates are shown.

Here, the Sulphur containing ceramic boat is placed in the middle of Low temperature

furnace (LTF). In a second ceramic boat MoO_3 powder is kept, which is in the middle of

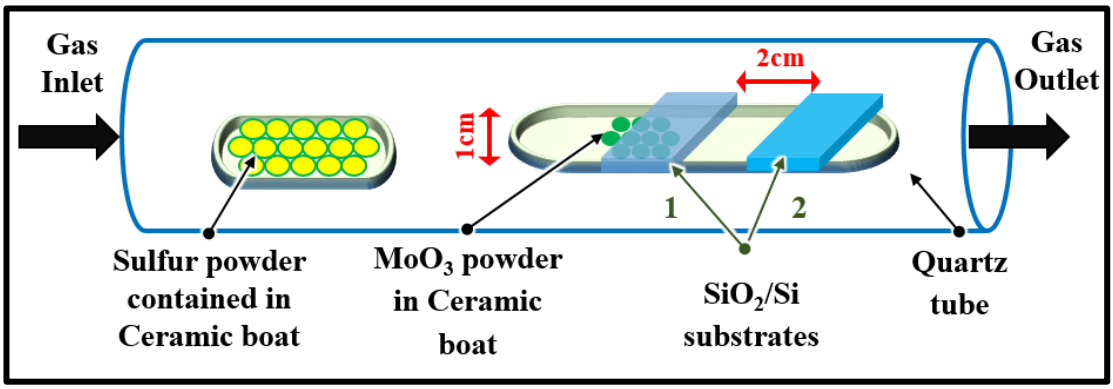

Figure 2.4: Schematic diagram of the CVD technique 1, showing the placement of precursor and the growth substrates

the high temperature furnace (HTF). The distance between the Sulphur and the MoO_3 precursor is 18 cm. Two growth SiO_2/Silicon substrate are kept facing down. The substrate no. 1 is kept over the precursor as shown. The vertical distance between the precursor and the substrates is approximately 1 cm and the distance between the two substrate is 2 cm.

Figure 2.5 shows the optical images of the MoS_2 crystals grown by using the CVD process I and technique 1 i.e., the Sulphurisation of MoO_3. Crystals of domain sizes of maximum 50 µm were synthesized by this technique. The crystals grown on substrate no 1 are clustered together compared to that of the substrate no 2.

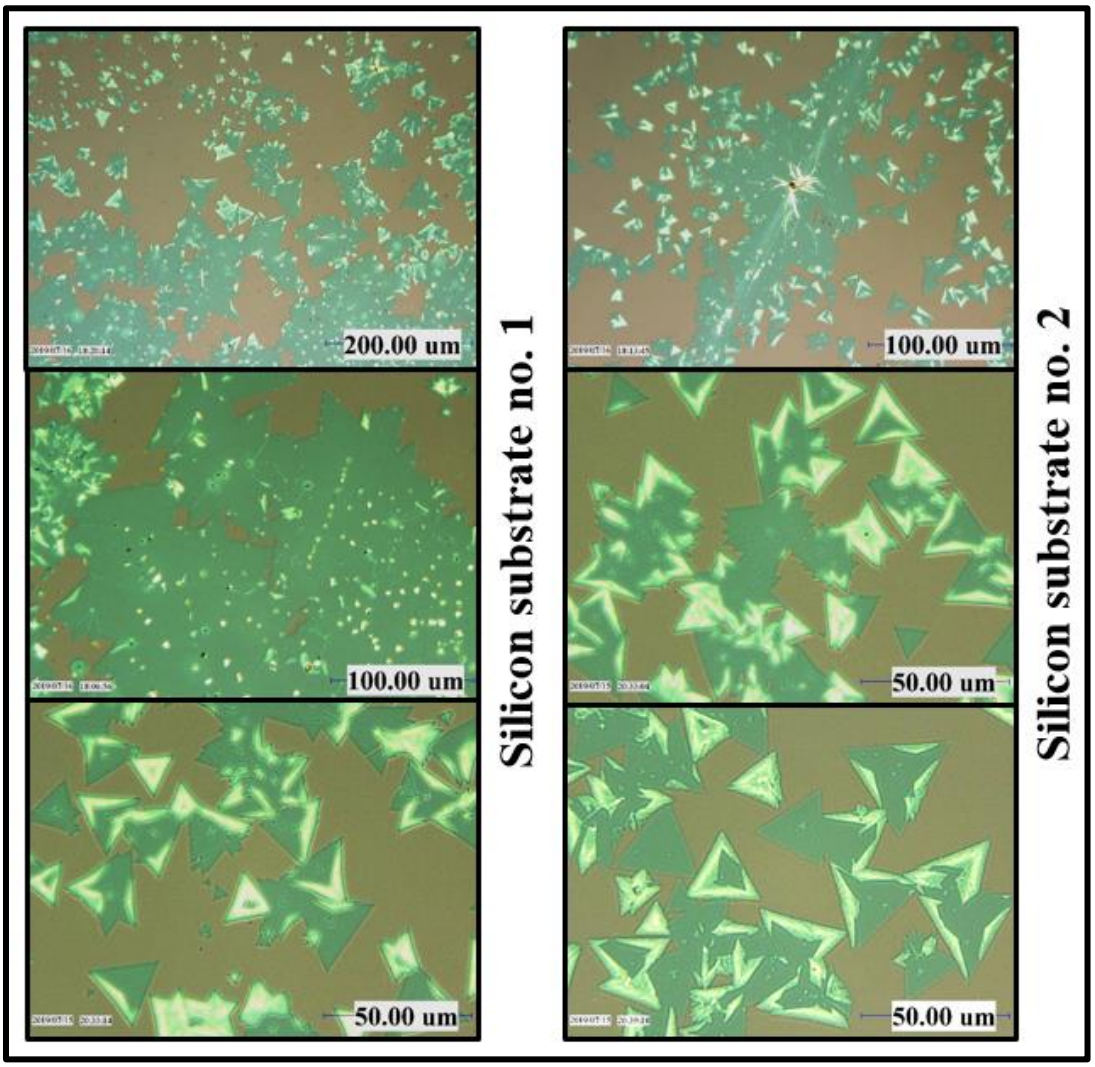

Figure 2.5: Optical images of MoS_2 crystals grown on SiO_2/Si substrates

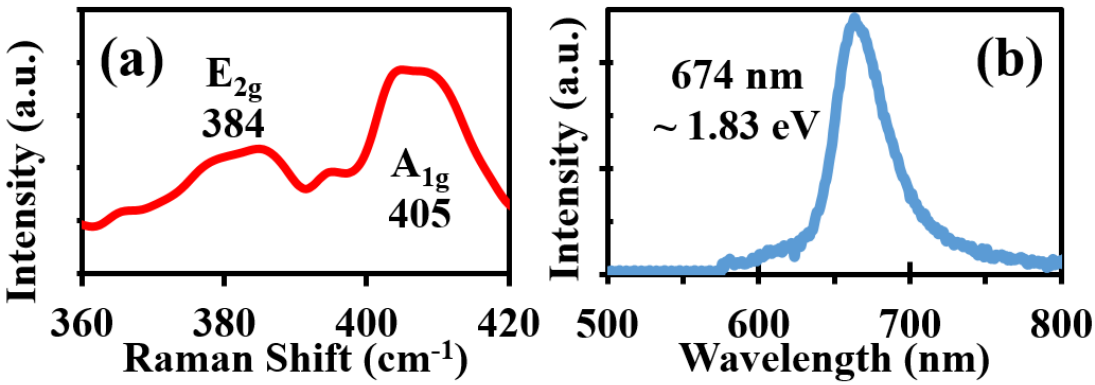

Figure 2.6: Raman and PL spectra of MoS_2 crystals grown on SiO_2/Si substrates using CVD technique 1

Figure 2.6 shows the Raman and the PL spectra of the MoS_2 crystals grown using the technique 2. Raman mode vibrations of Mo and S atoms E_{2g}-384 cm^{-1} and A_{1g}-405 cm^{-1} can be observed from the spectrum in **Figure 2.6** a. The difference between the Raman frequencies of E_{2g} and A_{1g} was found to be Δk- 21 cm^{-1} which represents mono layer growth of MoS_2. As seen in **Figure 2.6** b, MoS_2 gives strong PL signals at 674 nm. The optical quality and bandgap can be confirmed by the PL study.

2.3.2 Results from CVD process I (technique 2)

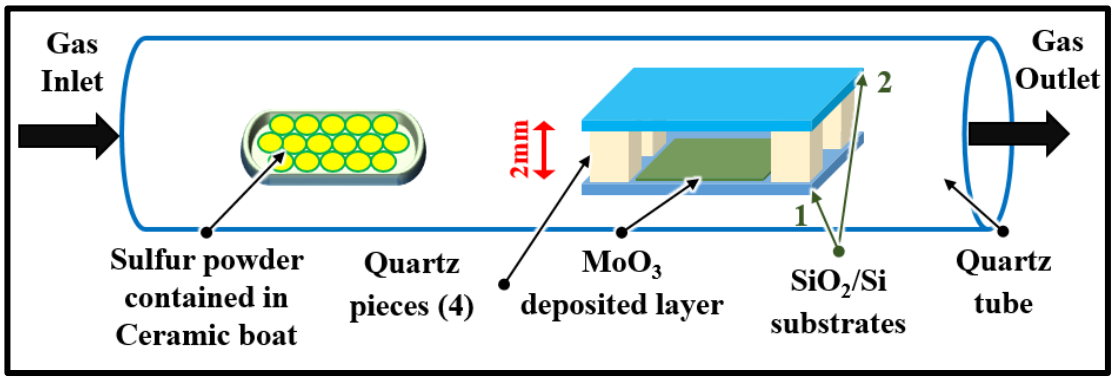

Figure 2.7: Schematic diagram of the CVD technique 2, showing the placement of precursor and the growth substrates

As depicted in the **Figure 2.7**, placement of the precursor and growth substrates are shown. Here, the Sulphur containing ceramic boat is placed in the middle of LTF. In a second ceramic boat thermally deposited MoO_3 on SiO_2/Silicon substrate is kept, which is in the middle of the HTF. On top of this substrate another substrate facing each other is placed. Quartz pieces are kept in between these two substrates so that the distance of nearly 2 mm is maintained. Thus, allowing the carrier gases and Sulphur fumes to flow between the substrates. The distance between the Sulphur and the MoO_3 precursor is 18 cm.

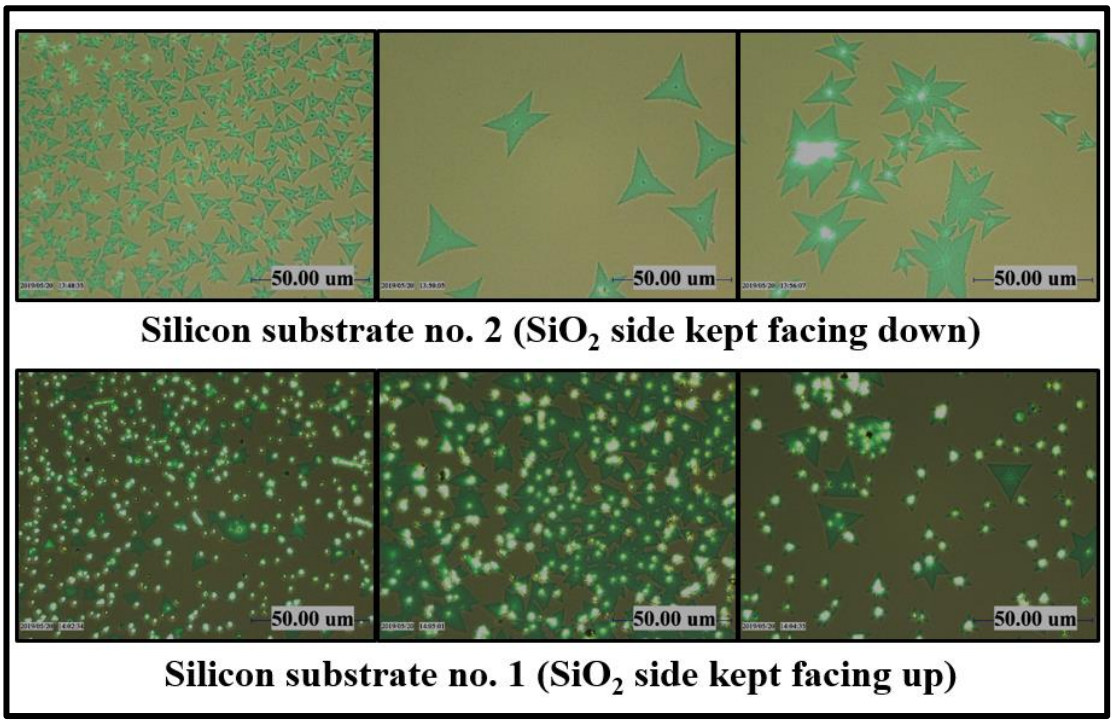

Figure 2.8: Optical images of MoS_2 crystals grown on SiO_2/Si substrates using CVD process I technique 2

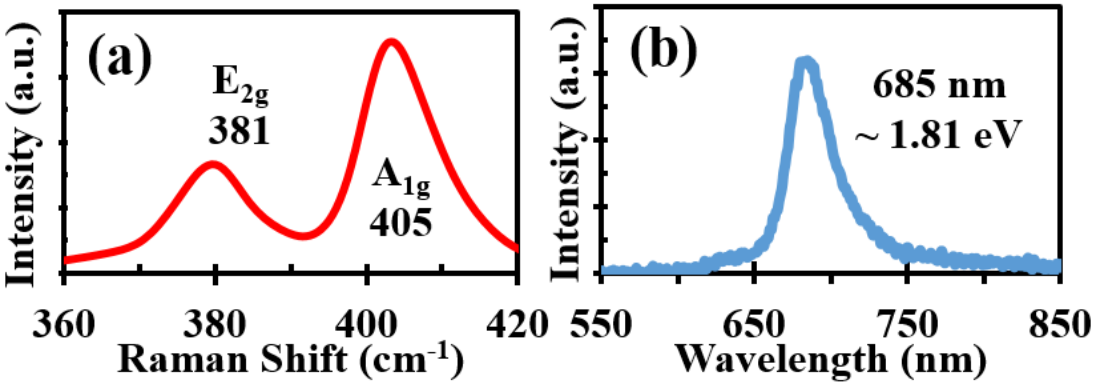

Figure 2.9: Raman and PL spectra of MoS_2 crystals grown on SiO_2/Si substrates using CVD process I technique 2

Figure 2.8 shows the optical images of the MoS_2 crystals grown by using the CVD process I, i.e. the Sulphurisation of MoO_3, and technique 2. Crystals of domain sizes of maximum 30 µm were synthesized by this technique. The crystals grown on substrate no 1 are clustered together compared to that of the substrate no 2. **Figure 2.9** shows the

Raman and the PL spectra of the MoS_2 crystals grown using the technique 2. Raman mode vibrations of Mo and S atoms E_{2g} - 381 cm^{-1} and A_{1g} - 405 cm^{-1} can be observed from the spectrum in **Figure 2.9** a. The difference between the Raman frequencies of E_{2g} and A_{1g} was found to be Δk - 24 cm^{-1} which represents few layers growth of MoS_2. As seen in **Figure 2.9** b, MoS_2 gives strong PL signals at 685 nm. The optical quality and bandgap can be confirmed by the PL study.

2.3.3 Characterization results of synthesised MoS_2 crystals

Domain size and shapes of synthesized materials with size more than 10 µm can be clearly seen, with lesser size crystals SEM analysis was performed. The synthesis of these materials was conducted on SiO_2/Si, GaN, Sapphire substrate.

Figure 2.10 shows optical images of CVD synthesized MoS_2 on SiO_2/Si substrate. The merging of MoS_2 crystals to form the layer is represented in Figure 2.10 (a) represents

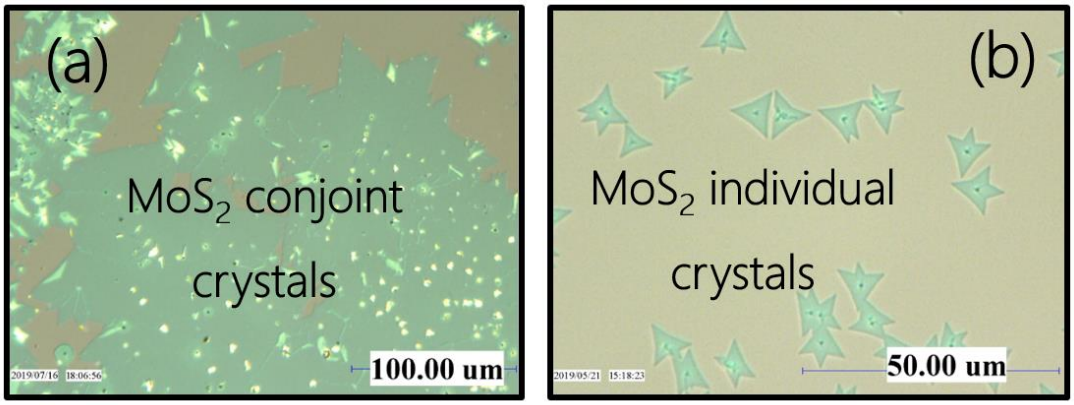

Figure 2.10: Optical images of CVD synthesized (a) MoS_2 layer formed by merging of crystals (b) MoS_2 crystals.

synthesized MoS_2 crystals whereas Figure 2.10 (b) shows ribbon structures.

High resolution topographical analysis is performed with the scanning probe with resolution up to fractions of nano-meters. The AFM study indicated uniformity of the

layers MoS_2 crystals. The atomic arrangement in 2D structure for these crystals shows theoretical values of 0.64 and 0.69 nm for single layer MoS_2, respectively.

Figure 2.11 shows MoS_2 crystal on SiO_2/Si substrate with thickness of 1.4 nm which are in close agreement with the theoretical values for bilayer. [11] Further, smooth layer surface was observed with clean crystals without any visible defects.

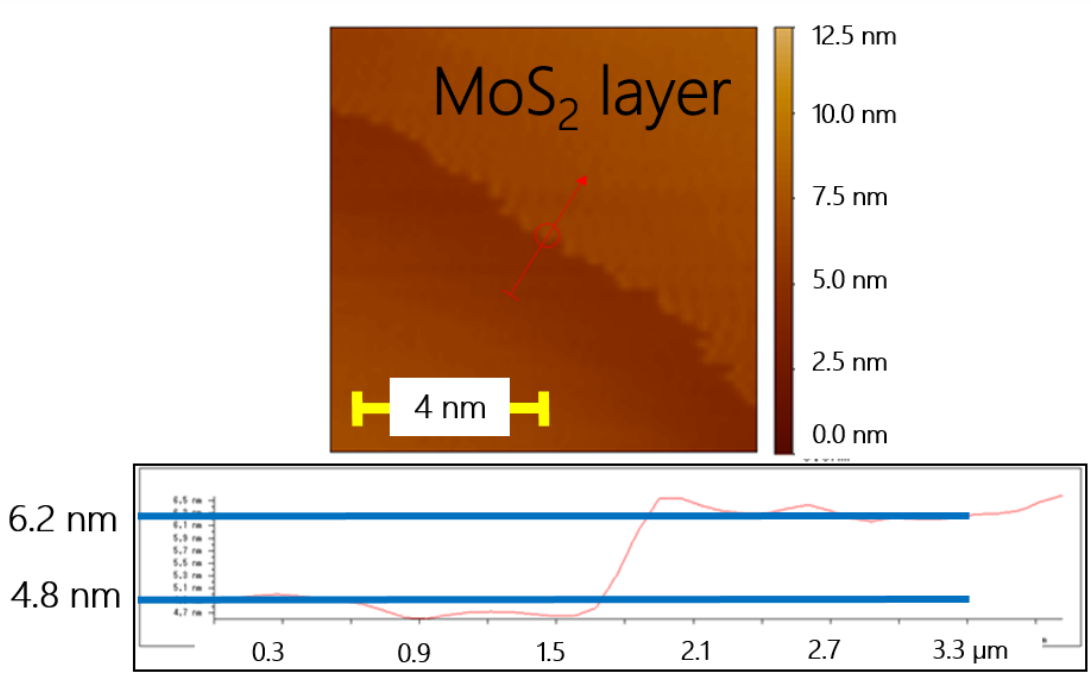

Figure 2.11: AFM images of monolayer MoS_2 crystals synthesized by CVD process I technique 2

FE-SEM studies were performed with JEOL JSM-7800F using lower electron detector (LED) with an accelerating voltage of 5 kV.

FE-SEM analysis provides with a better resolution of smaller crystals as well as provides information on uniformity of the crystal or layer structure. The SEM images of MoS_2 crystals are visible in **Figure 2.12** a-c. Here we can see triangular and dendritic type of crystals. In **Figure 2.12** d, we can see deposition of MoS_2 continuous layer alongside the triangular crystal growth.

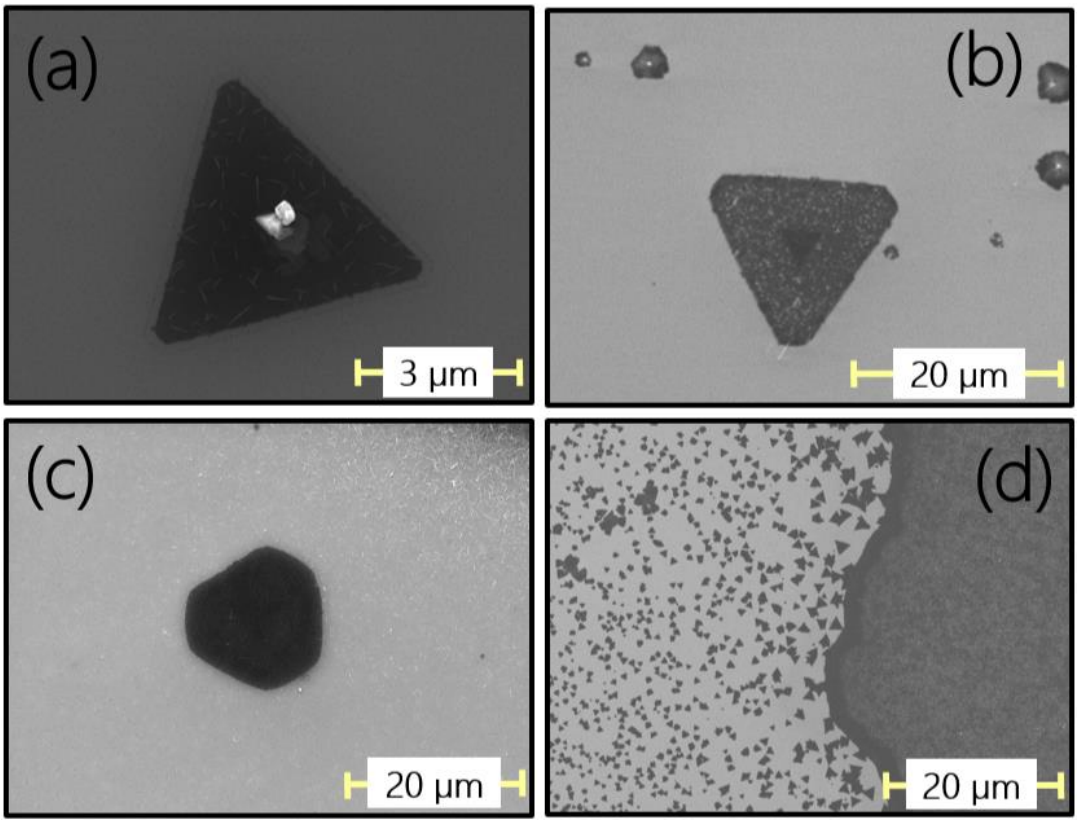

Figure 2.12: SEM images of MoS_2 crystals in (a Triangular), (b) Truncated, (c) Hexagonal shape crystals, and (d) MoS_2 layer using CVD process I

In the direct bandgap semiconductors such as MoS_2, the energy gap between the valance and conduction band is such that the absorption of light in visible region is observed. In monolayer, MoS_2 gives strong PL signals at 684 nm. The optical quality and bandgap can be confirmed by the PL study.

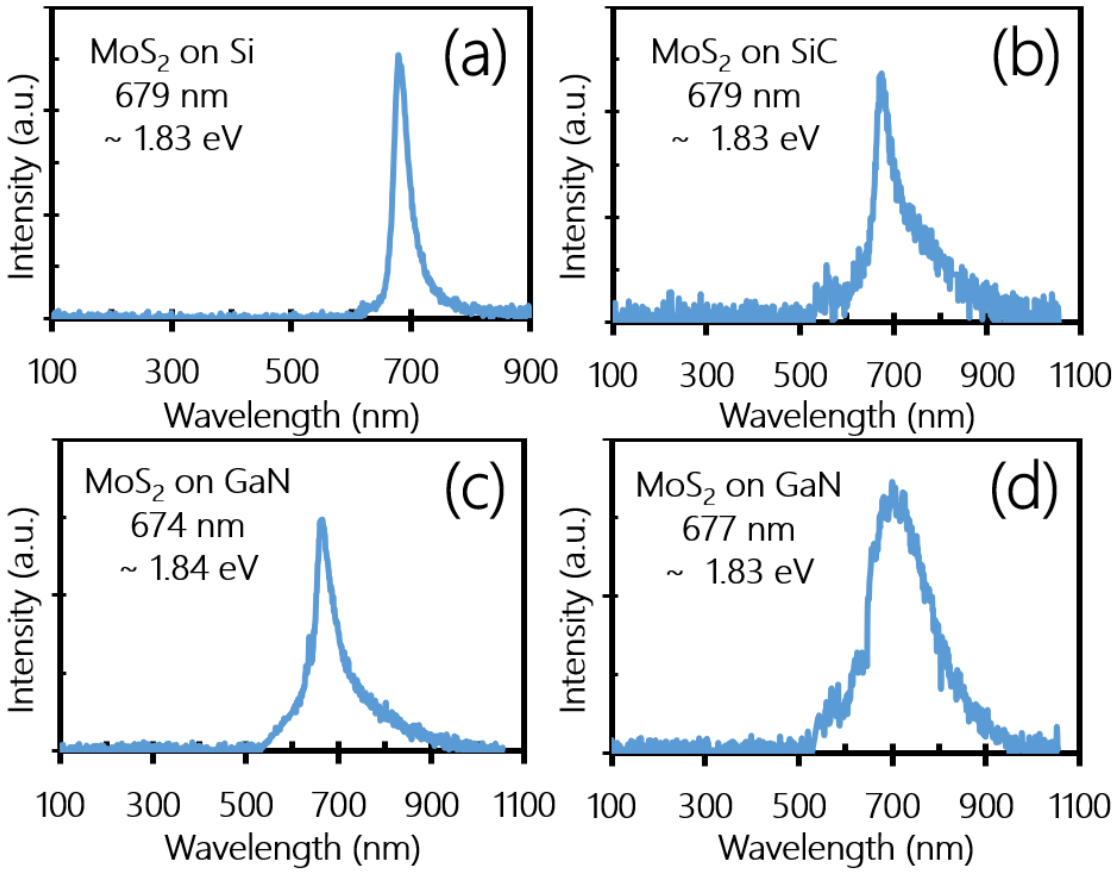

Figure 2.13: Photoluminescence spectra for MoS_2 on (a) SiO_2/Silicon, (b) SiC, (c) Ga-polar GaN and (d) N-polar GaN substrates CVD process I technique 2

Figure 2.13 shows PL signals for MoS_2 at excitation wavelength of 679 nm, 679 nm, 674 nm, and 677 nm for SiO_2/Silicon, SiC, Ga-polar GaN and N-polar GaN substrates, respectively. Sharp peaks with full width half maximum (FWHM) of around 40 shows synthesis of good optical quality MoS_2 layer. [2,12]

2.4 Synthesis mechanism - CVD process II

2.4.1 Characterization results of synthesised MoS_2 layer

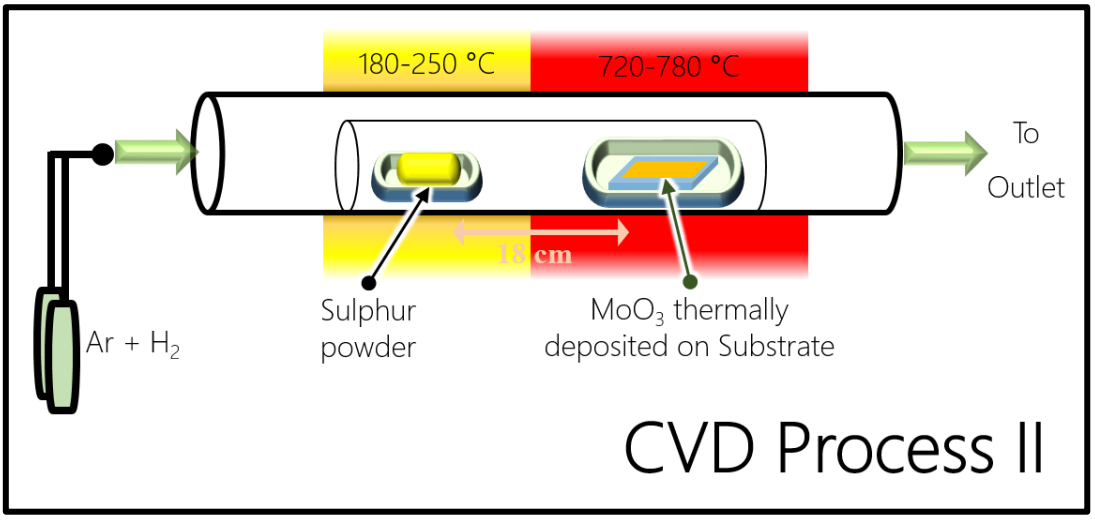

Figure 2.14: Schematic diagram of CVD process II, by sulphurisation of thermally deposited MoO_3 substrate, deployed in synthesizing MoS_2 few layers

Multiple analysis technique has been utilized for characterization of synthesized MoS_2 layered materials. Qualitative confirmation for the TMDCs is mainly done by Raman study. Raman peak positions and mapping images are widely used for determining the quality of synthesized TMDCs. Other techniques such as Optical and FE-SEM were used to confirm the size and the crystals structure on SiO_2/Si substrate, which provide excellent contrast between the two. The layer nature of the TMDCs are confirmed by AFM analysis by thickness measurement. One of the exciting properties of layered TMDCs is improved

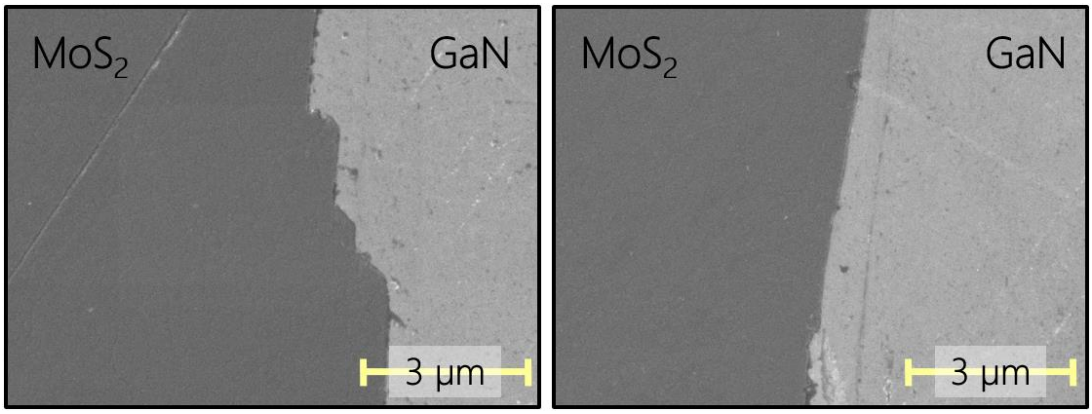

Figure 2.15: SEM images showing MoS_2 layers synthesised on GaN substrate by CVD process II

PL from bulk to monolayer due to transformation to direct bandgap. Thus, PL signal intensity and full width half maximum (FWHM) provides further confirms the optical quality of MoS_2 layers. XPS also called as electron spectroscopy for chemical analysis (ESCA) spectra determines the chemical nature of these materials with peak area analysis confirming the relative composition of metal and chalcogen.

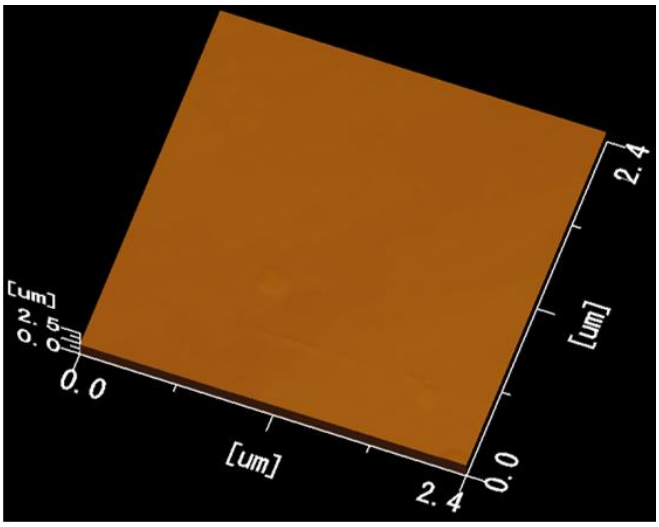

Figure 2.16: AFM image of surface (2.42×2.53 µm) of MoS_2 synthesized on GaN. With Mean height 1.11 µm and RMS 0.018 µm

Figure 2.15 shows SEM images and **Figure 2.16** shows the AFM topographical image of the few layers of MoS_2 which is synthesised using CVD process II.

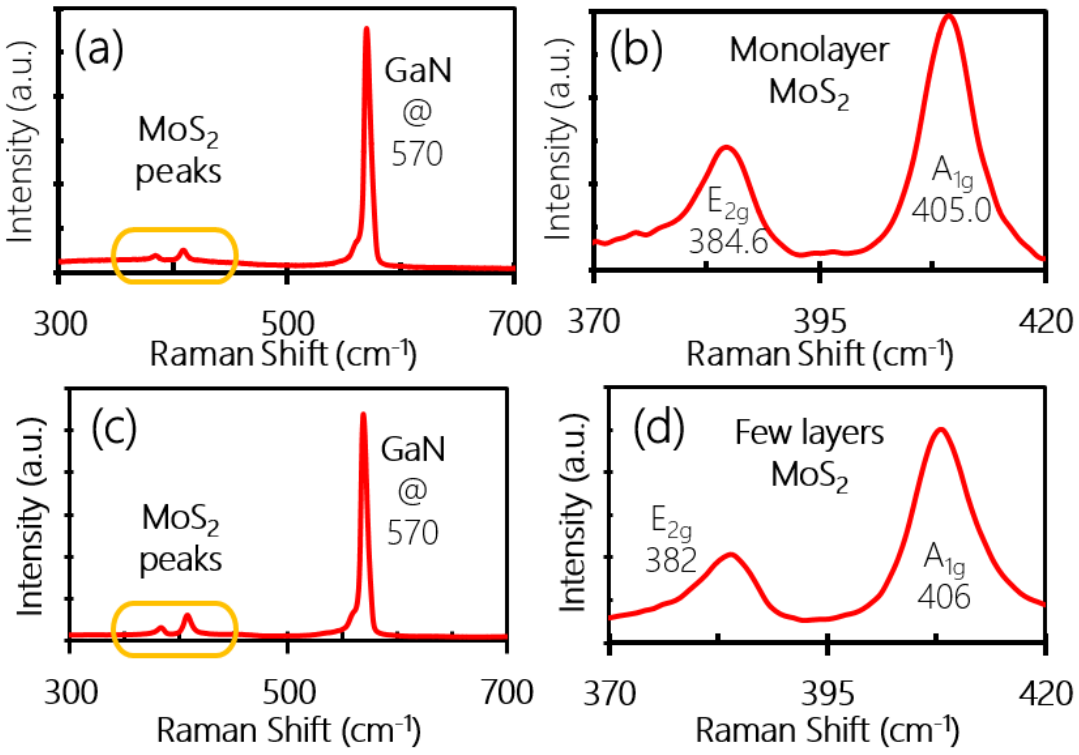

Figure 2.17: Raman Spectrums for (a) 2D MoS_2 growth on GaN substrate, (b) Corresponding MoS_2 peaks, (c) Few layer MoS_2 growth on GaN substrate and (d) Corresponding MoS_2 peaks, by CVD process II

Figure 2.17 represents typical Raman spectrums for layered MoS_2 grown on GaN substrate. Characteristic Raman intensities corresponding to in plane Raman mode vibrations of Mo and S atoms E_{2g}-384.6 cm^{-1} and A_{1g}-405.0 cm^{-1} can be observed from the spectrum in **Figure 2.17** b. The difference between the Raman frequencies of E_{2g} and A_{1g} was found to be Δk - 20.4 cm^{-1} which is characteristic for 2D MoS_2. Raman mode vibrations of Mo and S atoms E_{2g}-382 cm^{-1} and A_{1g}-406 cm^{-1} can be observed from the spectrum in **Figure 2.17** c. The difference between the Raman frequencies of E_{2g} and A_{1g} was found to be Δk - 24 cm^{-1} which represents few layers growth of MoS_2. [9,10]

Typical XPS spectrum for CVD synthesized MoS_2 is represented in Figure 2.18. Figure 2.18 (a) and Figure 2.18 (b) represents the XPS core-level spectrum with chemical state

doublet Mo 3d peaks ($Mo3d_{5/2}$ and $Mo3d_{3/2}$) at 230 and 233 eV and S 2p peaks ($S2p_{3/2}$ and $S2p_{1/2}$) at 162 and 164 eV, respectively. [12-14]

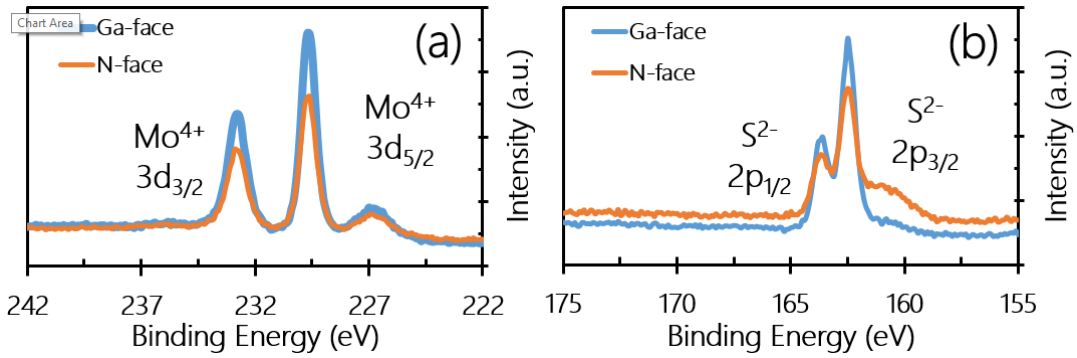

Figure 2.18: XPS spectra for (a) MoS_2-Mo 3d transition (b) MoS_2-S 2p transition

2.5 Synthesis mechanism - CVD process III

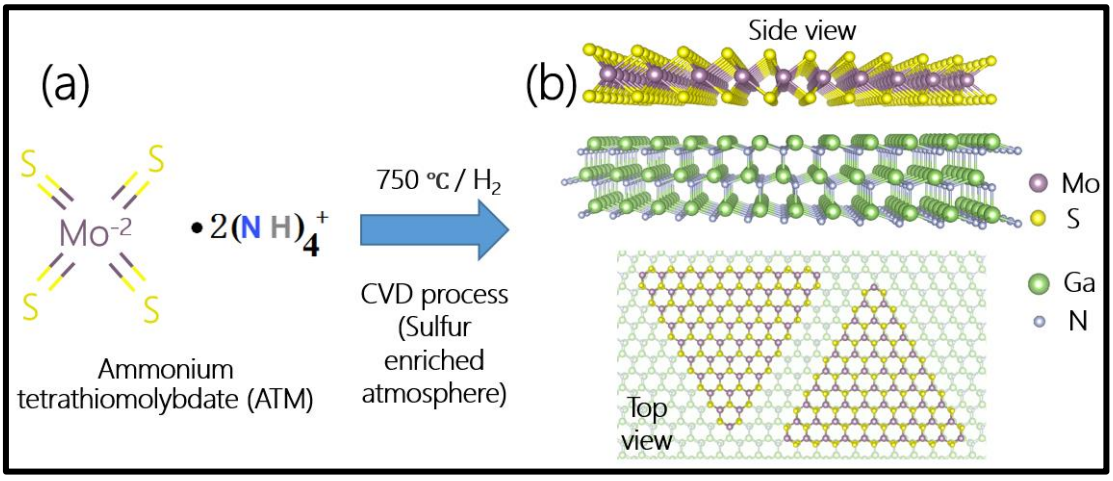

Figure 2.19: (a) Schematic of ATM precursor and reaction process for MoS_2 crystals growth on GaN substrate (b) Side and cross view of MoS_2 monolayer crystals on lattice matched GaN substrate

A two stage thermolysis process of ammonium tetrathiomolybdate (ATM) [$(NH_4)_2MoS_4$] precursor was used to synthesis MoS_2 crystals and layers on Silicon and GaN substrate.

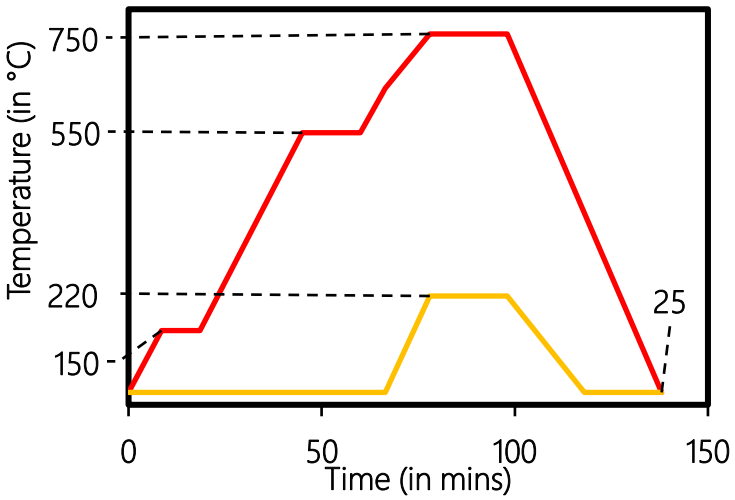

Figure 2.20: Temperature profile of furnace and Sulphur in CVD process III

In **Figure 2.21** we see the schematic of the synthesis process. First the ammonia precursor was spin coated on to the substrate and later it was subjected to thermolysis process in CVD process III. The concentration of ATM precursor was optimised to 1mg per 1 ml of DMF solution. In **Figure 2.20** we see the temperature profile of the furnace and the sulphur containing ceramic boat. The substrate spin coated was initially raised to a temperature of 150 °C for 10 minutes to aid in removing moisture.

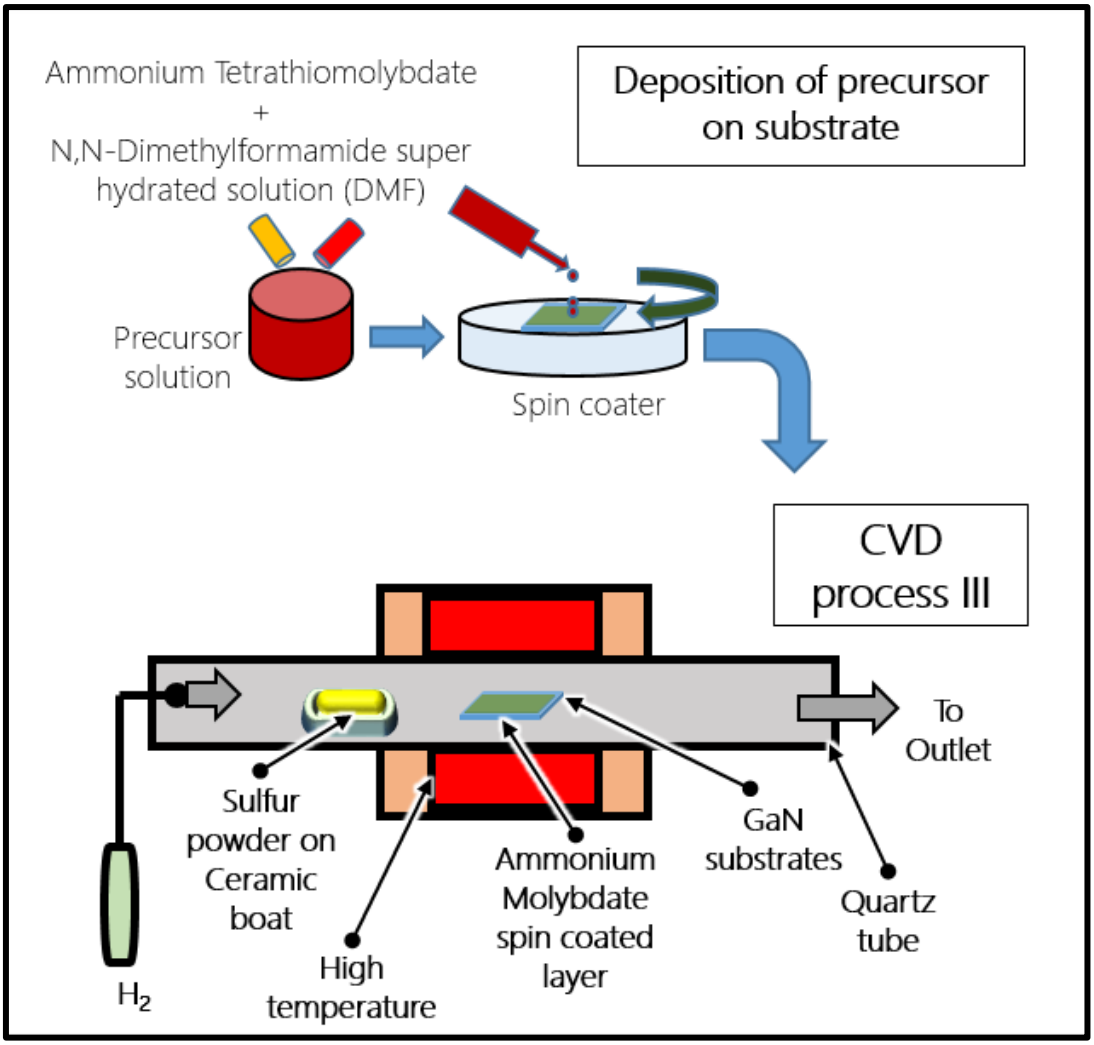

Figure 2.21: Schematic diagram of synthesis by spin coating and later by CVD process III, by two-stage thermolysis process of ammonium tetrathiomolybdate precursor deployed in synthesizing MoS_2 crystals

Further at temperature of 550 °C 15 minutes and later 750 °C 20 minutes for thermolysis to MoS_2 under sulphur rich conditions.

2.5.1 Characterisation results of synthesised MoS_2

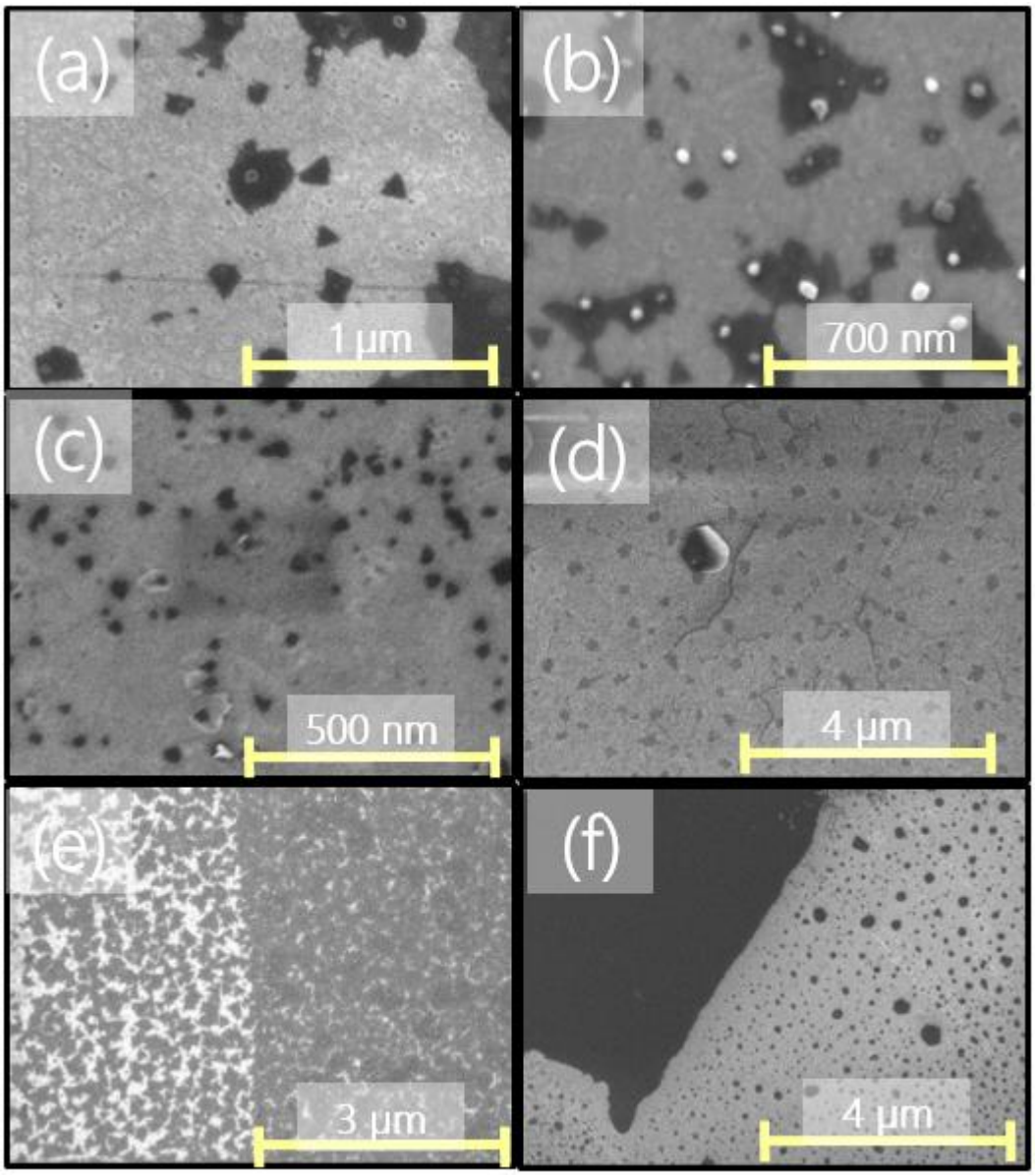

Figure 2.22: SEM images of MoS_2 synthesised on (a), (b) SiC, (c) p-type Silicon, (d) n-type Silicon, (e) free standing Ga-polar GaN and (f) free standing N-polar GaN substrates, using CVD process III

In **Figure 2.22**, we see the SEM images of MoS_2 synthesised using the CVD process III, in which thermolysis of ammonia-based precursor is carried out. Here we can observe the triangular crystal formations on selective substrates. Except the n-type Silicon and N-polar GaN substrates where the MoS_2 forms as a patched layer, we can locate the

triangular shapes of MoS_2 crystals with different domain sizes. The domain size ranges at approximately 0.5 µm. Using this technique for deposition of MoS_2 on SiC substrate, an overall triangular symmetry can be seen in the SEM images which are not oriented epitaxially.

2.6 Observations

The three CVD processes demonstrated in this chapter were extensively followed to carry out various studies in relation to MoS_2 growth and fabrication on appropriate substrates. The various experimental parameters were optimized to obtain the desired characteristic MoS_2, in terms of layer thickness for few-layer growth and crystal sizes and morphology for triangular crystal growths.

Table 2.2: Key observational results of various synthesis processes

CVD methods [Growth substrates]		**Results**	**Key growth parameter that were optimised**	**Synthesis deployed for further research in [and main result]**
Process I [SiO_2/Si, p/n type Silicon]	Technique 1	50 µm crystals	Vertical & horizontal distance between precursor and substrate	-

	Technique 2	30 µm crystals	Timing match of Sulphur vapour formation and attainment of High temperature in HTF	
Process II [p-type Silicon, GaN]		Few to bulk layers	Concentration of MoO_3 precursor used & time of growth in thermal evaporation	Chapter 3 [Spectral response]; Chapter 4 [Band offset]
Process III [SiC, Ga/N polar GaN, p/n type Silicon]		Individual & conjoint crystal of 1µm size	Concentration of ammonia-based precursor in DMF solution, Rotation speed of spin coating	Chapter 4 [Crystal synthesis, Diode rectification]

2.7 Bibliography

[1] Y. Rong *et al.*, "Controlling sulphur precursor addition for large single crystal domains of WS_2," *Nanoscale*, vol. 6, no. 20, pp. 12096–12103, 2014.

[2] I. Bilgin *et al.*, "Chemical Vapor Deposition Synthesized Atomically Thin Molybdenum Disulfide with Optoelectronic-Grade Crystalline Quality," *ACS Nano*, vol. 9, no. 9, pp. 8822–8832, Sep. 2015.

[3] G. Ye *et al.*, "Defects Engineered Monolayer MoS_2 for Improved Hydrogen Evolution Reaction," *Nano Lett.*, vol. 16, no. 2, pp. 1097–1103, 2016.

[4] H. Li *et al.*, "Fabrication of single- and multilayer MoS_2 film-based field-effect transistors for sensing NO at room temperature," *Small*, vol. 8, no. 1, pp. 63–67, 2012.

[5] D. Kong, J. J. Cha, H. Wang, H. R. Lee, and Y. Cui, “First-row transition metal dichalcogenide catalysts for hydrogen evolution reaction,” *Energy Environ. Sci.*, vol. 6, no. 12, p. 3553, 2013.

[6] W. K. Hofmann, “Thin films of molybdenum and tungsten disulphides by metal organic chemical vapour deposition,” *J. Mater. Sci.*, vol. 23, no. 11, pp. 3981–3986, Nov. 1988.

[7] K. K. Liu *et al.*, “Growth of large-area and highly crystalline MoS_2 thin layers on insulating substrates,” *Nano Lett.*, vol. 12, no. 3, pp. 1538–1544, 2012.

[8] Y. Zhan, Z. Liu, S. Najmaei, P. M. Ajayan, and J. Lou, “Large-area vapor-phase growth and characterization of MoS_2 atomic layers on a SiO_2 substrate,” *Small*, vol. 8, no. 7, pp. 966–971, 2012.

[9] Y.-H. Lee *et al.*, “Synthesis of Large-Area MoS_2 Atomic Layers with Chemical Vapor Deposition,” *Adv. Mater.*, vol. 24, no. 17, pp. 2320–2325, 2012.

[10] K. M. McCreary *et al.*, “Large-area synthesis of continuous and uniform MoS_2 monolayer films on graphene,” *Adv. Funct. Mater.*, vol. 24, no. 41, pp. 6449–6454, 2014.

[11] Y. Zhang *et al.*, “Controlled Growth of High-Quality Monolayer WS_2 Layers on Sapphire and Imaging Its Grain Boundary,” *ACS Nano*, vol. 7, no. 10, pp. 8963–8971, 2013.

[10] Y. Gao *et al.*, “Large-area synthesis of high-quality and uniform monolayer WS_2 on reusable Au foils,” *Nat. Commun.*, vol. 6, p. 8569, 2015.

[11] D. J. Trainer *et al.*, “Inter-Layer Coupling Induced Valence Band Edge Shift in Mono- to Few-Layer MoS_2,” *Sci. Rep.*, vol. 7, no. 1, p. 40559, Dec. 2017.

[12] S. M. Shinde *et al.*, “Stacking-controllable interlayer coupling and symmetric configuration of multilayered MoS_2,” *NPG Asia Mater.*, vol. 10, no. 2, p. e468, Feb. 2018.

[13] D. K. Nandi *et al.*, “Highly Uniform Atomic Layer-Deposited MoS_2@3D-Ni-Foam: A Novel Approach to Prepare an Electrode for Supercapacitors,” *ACS Appl. Mater. Interfaces*, vol. 9, no. 46, pp. 40252–40264, Nov. 2017.

[14] H. Zhu, X. Qin, L. Cheng, A. Azcatl, J. Kim, and R. M. Wallace, “Remote Plasma Oxidation and Atomic Layer Etching of MoS_2,” *ACS Appl. Mater. Interfaces*, vol. 8, no. 29, pp. 19119–19126, Jul. 2016.

CHAPTER 3

3 Study of influence of MoS_2-Silicon heterostructure interface states on spectral photoresponse

3.1 Background of the study

Fabrication of heterojunction with TMDCs layers and convention bulk semiconductors are of great interest for optoelectronics device applications. Here, I demonstrate the influence of interface in a MoS_2 and p-type Si heterostructure on bias dependent photoresponse. The heterostructure of MoS_2 layers deposited on the p-type Si wafer exhibited a photovoltaic action and a photoresponsivity of 139 mA/W at 860 nm wavelength for a bias voltage of -5V. It was observed that due to an effective field effect across the heterojunction the spectral photoresponse of the device improved substantially with an applied bias voltage than that of a photovoltaic mode. Further, I observed at the bias voltage that the increase in photoresponsivity at a higher wavelength (>600 nm) was significant than that at a lower wavelength (<500 nm). This phenomenon can be attributed to the surface recombination of photocarriers for higher energy photons in presence of interface states at the MoS_2/Si heterojunction. Thus, understanding the behaviour of

photocarriers in the fabricated MoS_2/Si heterojunction interface can be critical to develop high photoresponsive heterojunction devices.

Transition metal dichalcogenides (TMDCs) layered materials with intriguing optoelectrical properties has attracted significant interest for various device application. [1-6] Considering the bandgap of two dimensional (2D) TMDCs layered materials in the range of 1.7eV-2.2 eV is of significant interest to integrate with other semiconductors to develop VdW heterostructures. [7-13] The structure of monolayer TMDCs is composed of central metal atom covalently bonded to two chalcogen atoms above and below forming three layered structure. The individual TMDCs layers are held together by Van der Waals forces, similar to graphene and various other layered materials. [1,7] In TMDCs, depending on the central metal atom and surrounding chalcogen it shows p-type (WS_2) or n-type (MoS_2) semiconducting properties in addition to metallic, superconducting as well as insulating properties. [13-15] To develop an efficient VdW heterojunction device, the p-type as well as n-type TMDCs were integrated with other bulk semiconductors, such as Si, GaN. [12,16-19] It was experimentally observed that by combining TMDCs layer with Si and other conventional semiconductors, ultra-fast charge transfer occurred at the interface of atomic layers, and therefore bringing new possibilities of its device application. [20]

TMDC layers have been deposited on the Si surface by various approaches to develop a heterojunction device for applications such as in solar cells and photodiode. [20-23] The ongoing research interests in MoS_2 layered material based photoresponsive device owes to some of its properties such as its high optical absorption in visible spectrum, faster photoresponse, self-driven photodetection and its relative ease of fabrication. [20-24] Thus, the combination of n-type MoS_2 with p-type Si is of significant interest to fabricate

a VdW heterojunction device and harnessing both their device applicability. [25-27] Salahuddin et al. has reported the fabrication of heterojunction photodetectors with mechanically exfoliated MoS_2 flake on amorphous Si. [20] Monolayer MoS_2 deposition has been demonstrated by CVD method on p-type Si thereby aiding in development of heterojunction solar cells. [28] Further, two stage process of sulphurisation of metal and metal oxide films deposited on Si substrate has been performed to synthesis MoS_2 layers. [29,30] It has been also demonstrated that vertically standing MoS_2 layered structure can be deposited with a scalable sputtering method directly on Si substrate forming the heterojunction-type photodetectors. [21] Understanding the photoresponsive behaviour in the interface between the MoS_2 and p-type Si heterojunction is crucial in this prospect. Here in my study, I observed the photovoltaic effect and bias dependent photoresponse for a MoS_2/Si device, where photoresponse properties of the devices are influenced by the presence of interface states. In what follows, the details of the MoS_2/Si

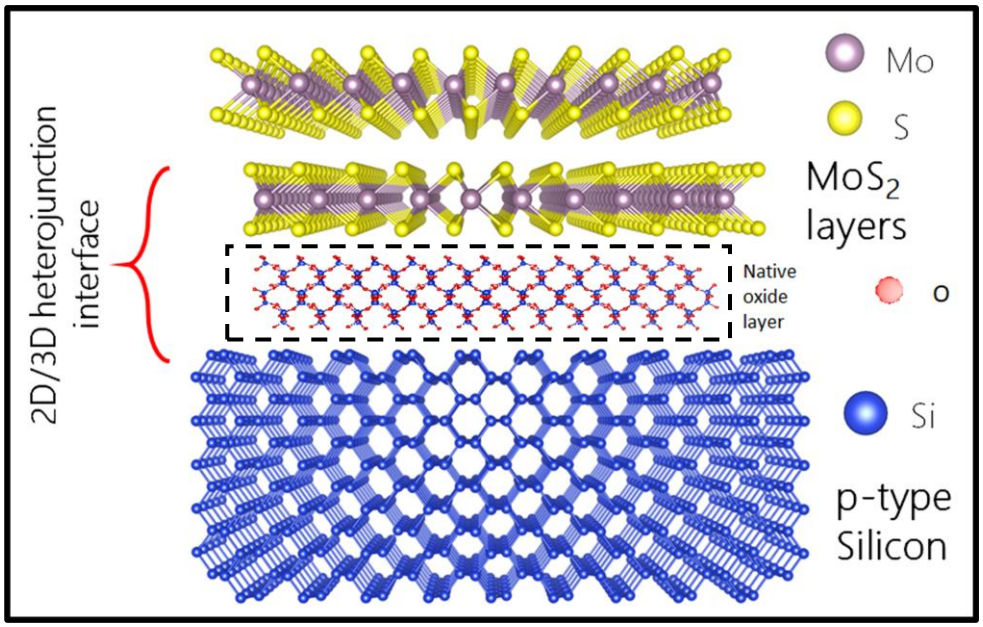

Figure 3.1: Ball and stick diagram depicting the heterojunction interface between MoS_2 few-layers and Silicon substrate

photoresponsive device characteristics and spectral photoresponse behaviour were explained.

In the **Figure 3.1**, the ball and stick diagram of MoS_2 layer atop of Si substrate is shown. Here we see, each molybdenum (Mo) atoms are surrounded by six sulphur (S) atom forming a trigonal prismatic coordination sphere. The bulk MoS_2 consist of several layers like graphite, where the S-Mo-S configuration forms a monolayer. Whereas the Si bulk single crystal has a diamond structure with one Si atom has four nearest neighbours connected by a covalent bond and does not naturally form any 2D structures as that of graphite. Recently, template-based growth of Si monolayer, known as silicene has been demonstrated on various substrates. [31] The layered structure of MoS_2 has ignited lot of interest to develop MoS_2-Si based VdW heterojunction.

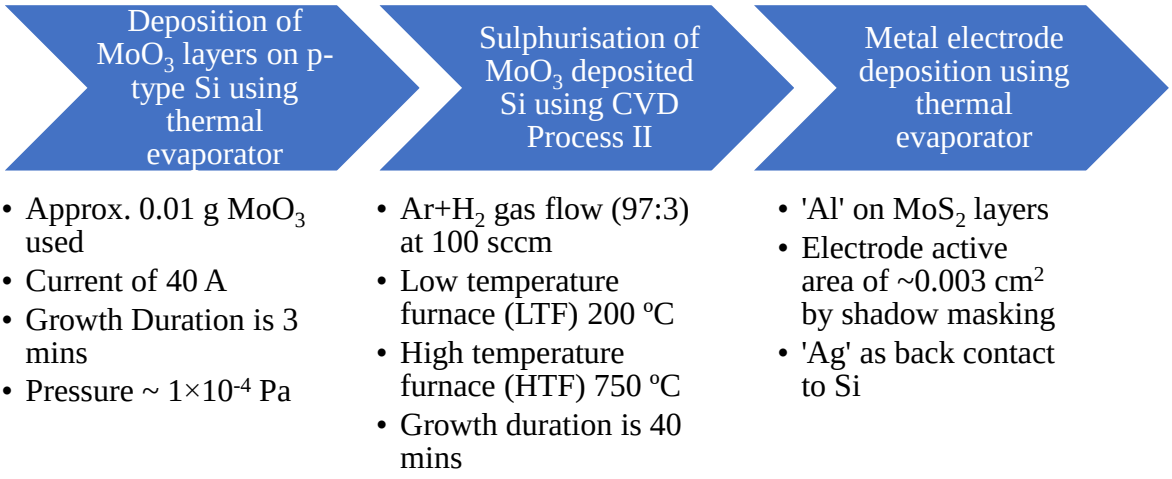

Diagram 3.1: Flow diagram of experimental procedure for the synthesis of MoS_2 on p-type Si substrate and device fabrication (CVD details in section 2.4)

3.2 Synthesis process for MoS_2 layer on Si

For developing p-n heterojunction with MoS_2, p-type Si wafer was used. The resistivity of the p-type Si wafer used is in the range of 10-20 Ω.cm, which corresponds to doping level of 1.340×10^{15}~0.6637×10^{15} cm^{-3}**.** The substrate was cleaned using hydrofluoric acid to remove any oxide layer, then by acetone and iso-propyl alcohol for 15 min each by sonification, done prior to the thermal deposition process. I performed the synthesis of MoS_2 layer on p-type Si in two stages. Firstly, using the thermal evaporating technique, molybdenum oxide (MoO_3) (approximately 0.1g) was physically deposited onto the surface of p-type Si substrate. The duration of evaporation was kept at 3 minutes and at 40 A of current under ~10^{-4} Pa of vacuum condition. A thin layer of MoO_3 was thus obtained on the Si substrate. Following the above process, MoS_2 layer was thus synthesized by sulphurisation process at a higher temperature and in an inert atmosphere ($Ar+H_2$). The sulphurisation process was carried in a quartz tube and in Ar and H_2 gas mixture (97:3 ratio respectively) at 100 sccm of maintained gas flow. The low temperature furnace (LTF) is was kept at 200 ºC for sulphur to evaporate and the high temperature furnace (HTF) was kept at 750 ºC for the evaporated sulphur to react with MoO_3. A growth period of 40 minutes was established in this process, during which sulphur produced in LTF reacts with the MoO_3 to form MoS_2 layer on the p-Si substrate. Further to fabricate the heterojunction device, metal electrodes were deposited on the synthesized MoS_2 layer and p-Si substrate. Prior to the thermal deposition of the metals, a shadow mask was placed above the substrate and MoS_2 layer so that a portion was exposed for the deposition. Aluminium (Al) electrodes on MoS_2 layer having an area of ~0.09 cm^2 and Silver (Ag) electrodes as back contact to p-type Si were deposited by thermal evaporation process.

Fabricated sample was characterized by Optical microscopy, Raman spectroscopy, Scanning electron microscopy (SEM), X-ray Photoelectron spectroscopy (XPS), Atomic force microscopy (AFM).

3.3 Characterization of synthesized MoS_2 layer on Si

In **Figure 3.3**, I show the optical microscope image of the MoS_2 layer and Si heterostructure synthesized at 750 °C. The image shows a uniform film formation of MoS_2 layer on the p-type Si substrate. Further, I carried out Raman spectroscopic analysis of the synthesized layer. **Figure 3.2** shows a Raman spectrum for the MoS_2/Si heterostructure. E_{2g} and A_{1g} peaks corresponding to MoS_2 layer were observed at 384 and 408 cm^{-1}, respectively, along with the Si peak at 520 cm^{-1}. **Figure 3.4** shows the AFM image at the interface of MoS_2 layer and Si substrate. The AFM image also confirmed the flake like structure of the MoS_2 on

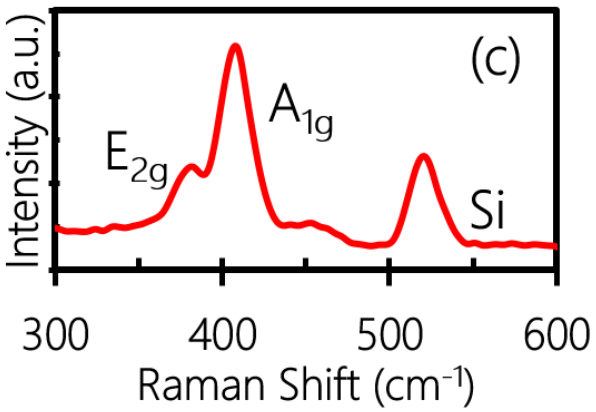

Figure 3.2: Raman spectra of MoS_2/Si heterostructure

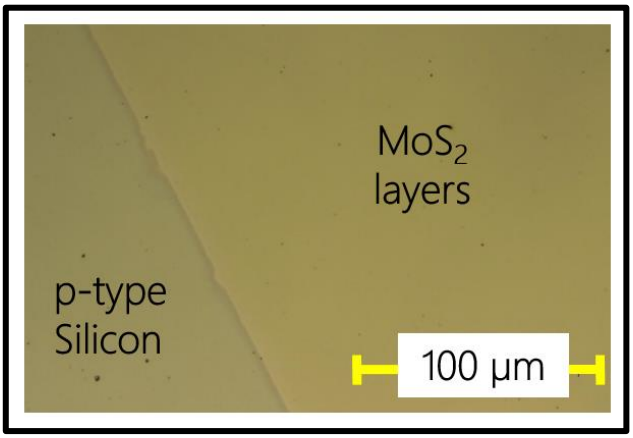

Figure 3.3: Optical image of MoS_2 layers atop p-type Si

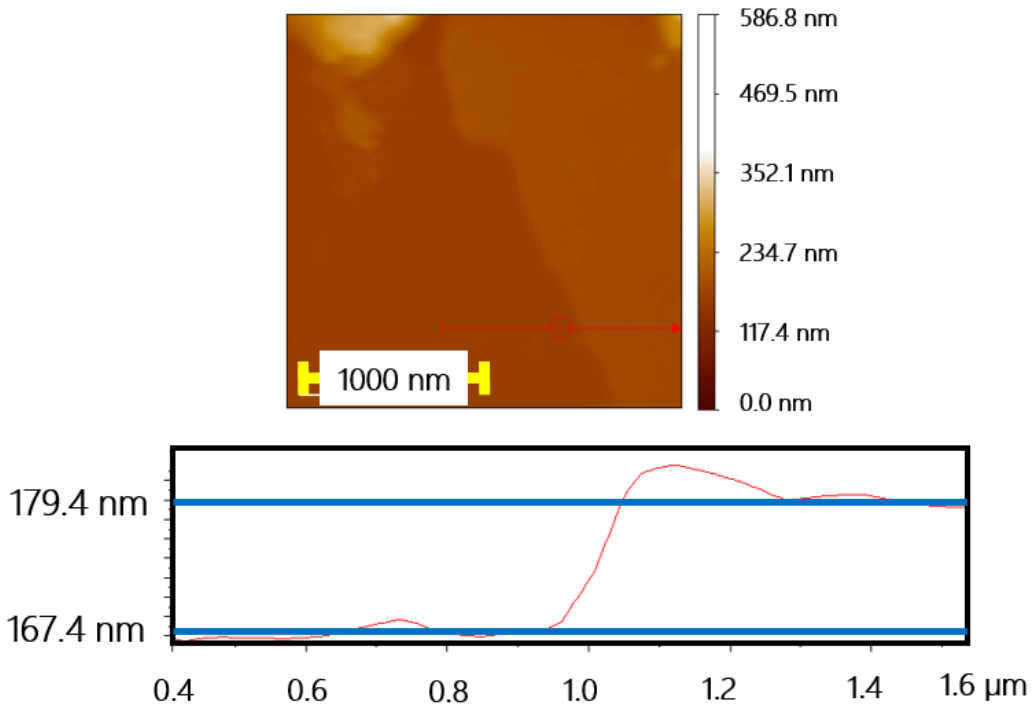

Figure 3.4: AFM image and line profile taken at MoS_2-Si heterostructure interface

the p-type Si. The line profile depicted in **Figure 3.4** estimates the thickness of deposited MoS_2 layer as 14 nm, signifying the formation of few-layers structure. Thus, a continuous film of few-layers MoS_2 was directly obtained at a comparatively tolerable substrate temperature for the Si. Many other TMDCs required much higher growth temperature (~1000 °C), which have adverse effect on the Si substrate. Now, I explore the interface characteristics of the as-synthesized MoS_2 layers on the p-type Si to understand the photocarriers behaviour.

Figure 3.5 (a) shows the survey spectrum for as-synthesized MoS_2 on the Si substrate. The survey spectrum clearly shows the Mo3d and S2p peaks for the MoS_2 layers, while C1s and O1s peaks were observed due to the surface chemical absorption. In the survey spectrum the Si2p peak was not quite visible due to relative higher thickness of the MoS_2 layer. Hence, the individual Si2p peak was analysed for more than 10 XPS cycles. The

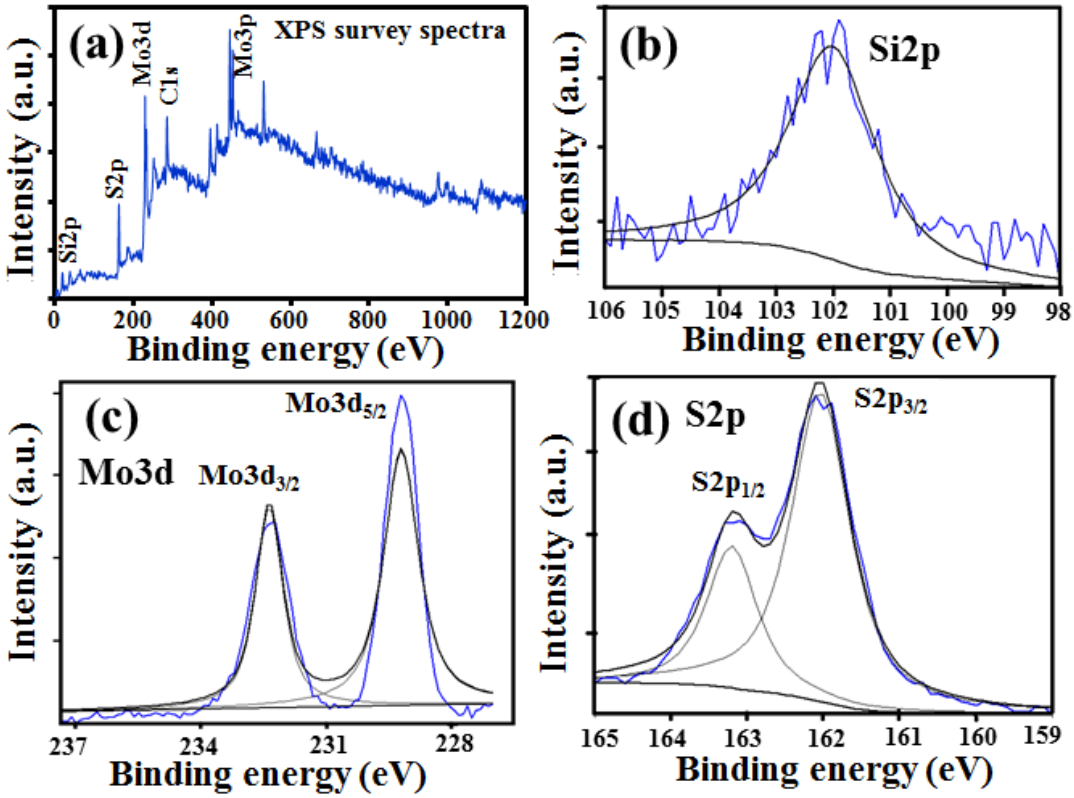

Figure 3.5: XPS. (a) Survey spectra heterostructure (b) Si2p – 102 eV (c) S2p ($2p_{3/2}$ – 162 eV and $2p_{1/2}$ – 164 eV) for as-synthesized MoS_2-Si (d) Mo3d ($3d_{5/2}$ – 229 eV and $3d_{3/2}$ – 233 eV)

Si2p peak was detected with a peak centre at 102.3 eV as shown in **Figure 3.5** (b). The deconvoluted S2p doublet peaks for MoS_2 layer was confirmed with $2p_{3/2}$ and $2p_{1/2}$ peaks at 162 and 164 eV, respectively, as shown in **Figure 3.5** (c). Similarly, **Figure 3.5** (d) shows the deconvoluted doublet Mo3d peaks with peak centres at 229 and 233 eV for $Mo3d_{5/2}$ and $Mo3d_{3/2}$, respectively. The XPS analysis also confirmed the formation of a thin heterostructure of the synthesized MoS_2 film on p-type Si, with chemical structure as reported in previous studies. [32] Stoichiometry analysis of the MoS_2 layers was also performed from the XPS spectra, however a noticeable S vacancy was not possible to determine from the deconvoluted spectra. Previous studies showed the presence of S

vacancy in the chemically synthesized MoS_2 layers, which can significantly influence the interface of heterojunction devices. [33,34] One of the main reasons of the interface states in the fabricated MoS_2/Si heterojunction can be presence of S vacancies with the chemical growth process.

3.4 Device fabrication and performance

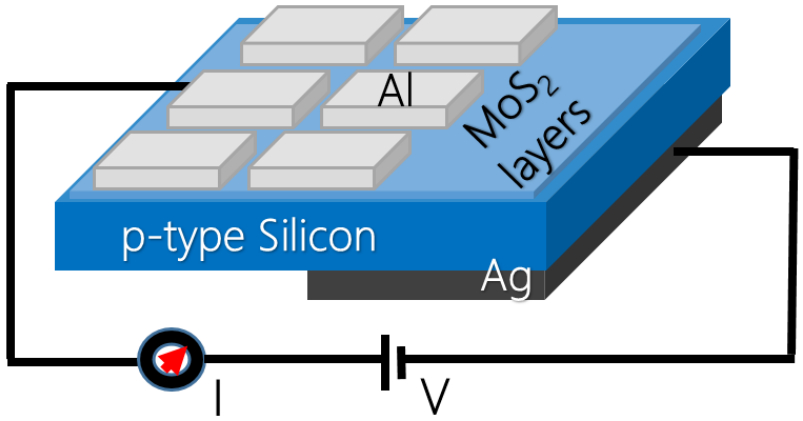

Figure 3.6: (a) Schematics of the fabricated MoS_2/Si heterostructure device

The heterojunction device was investigated by fabricating a two-terminal diode structure under dark and monochromatic light.

Figure 3.6 shows the schematic of the fabricated MoS_2/Si heterostructure device with respective metal electrodes. J-V characteristics of fabricated Al/MoS_2/Si/Ag device were investigated to confirm the formation of a heterostructure diode. **Figure 3.7** (a) shows the J-V characteristic of the fabricated device without light illumination for an applied bias range of -5 to +5V. A good rectifying diode characteristic was observed with a turn on voltage around 1V. **Figure 3.7** (b) shows a log plot of the J-V curve. Rectification ratio of approximately 10^3 was estimated with low leakage current. The ideality factor is found to be 3.7, which is slightly higher than that of conventional p-n junction diode. **Figure**

3.7 (c) shows the J-V characteristics of the device under dark (blue line) and illumination

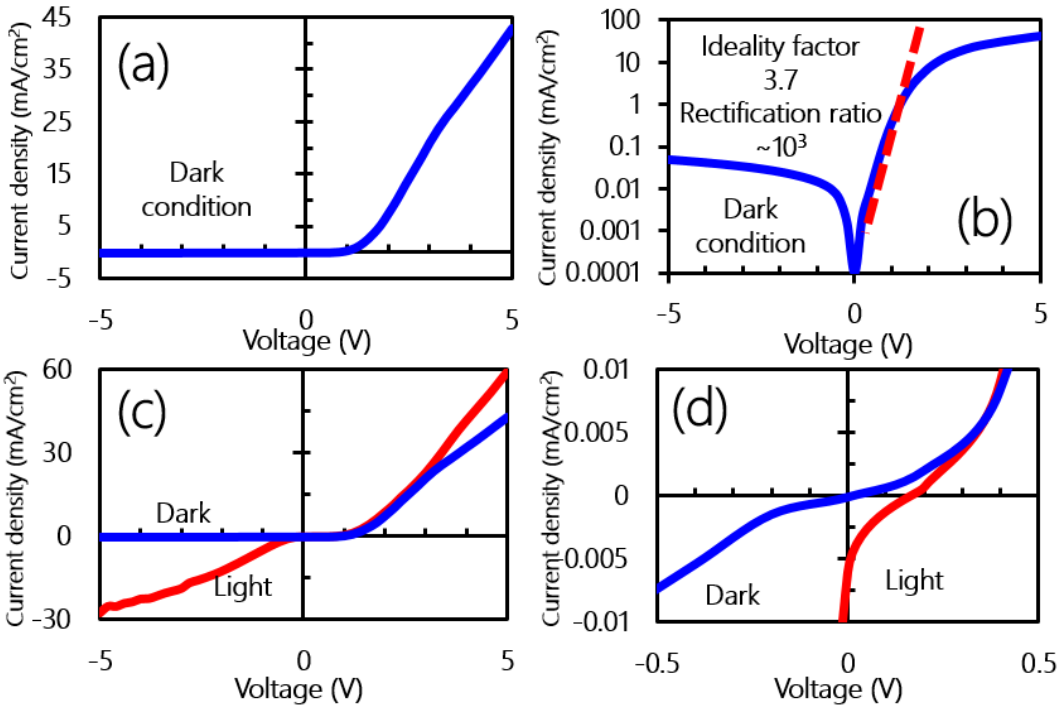

Figure 3.7: (a) J-V characteristics without light illumination (b) Log plot J-V characteristics without light illumination (c) J-V characteristics without (blue line) and with (red line) light illumination (d) J-V characteristics showing photovoltaic action at the lower bias voltage with light illumination

of monochromatic light (red line). The J-V curve shows excellent photoresponse with light to dark ratio of 5×10^2 at the bias voltage of -5V. **Figure 3.7** (d) shows J-V characteristics at lower bias voltage range (±0.5V). A photovoltaic action was also observed with the illumination of light. The electrical characteristic behaviour in dark and photovoltaic action is similar with previous reported results by Li et al. [22] The photovoltaic action and photoresponse at the bias voltage were further analysis with the spectral response characteristics.

3.5 Spectral response of the heterojunction

Figure 3.9 (a-b) shows the spectral response of fabricated device under a bias voltage of 0 and -5 V, respectively. The 0V bias voltage corresponds to the photovoltaic mode as observed from the J-V characteristics. The device showed better spectral response above

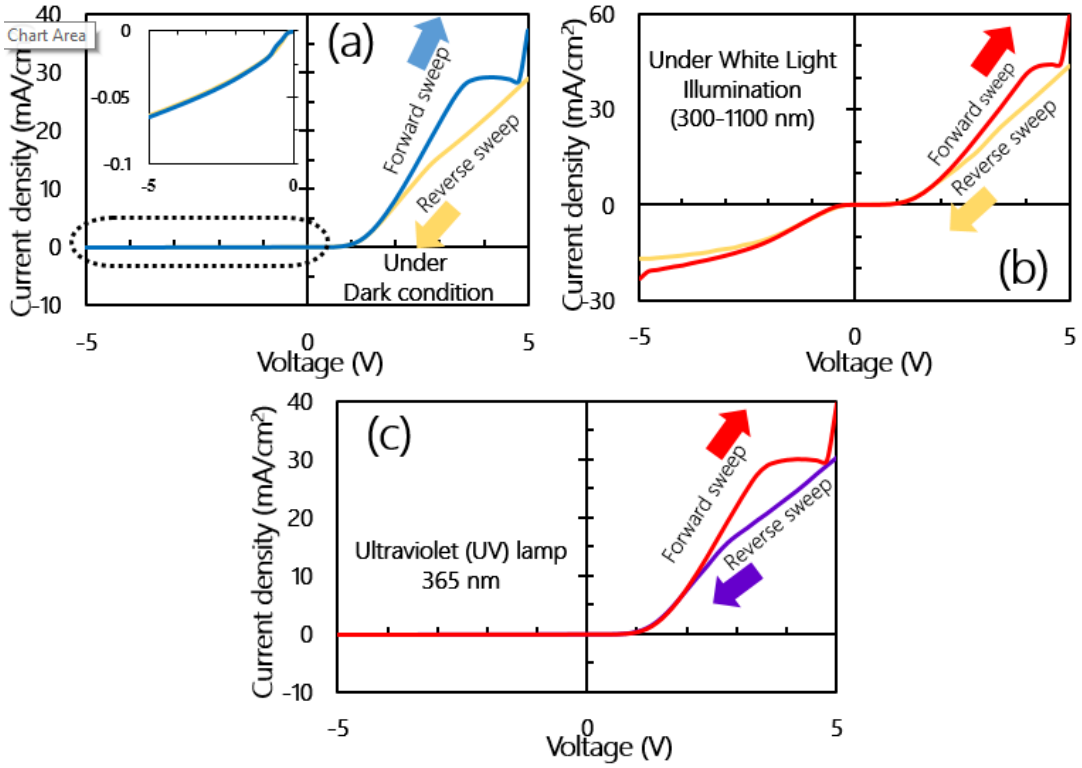

Figure 3.8: (a) Forward and reverse sweep J-V characteristics without light illumination. Forward and reverse sweep J-V characteristics with (b) monochromatic light illumination (300-1100 nm) of 100 mW/cm^2 (c) ultraviolet light (365 nm) of 614 μW/cm^2

600 nm wavelength. The overall spectral response (mA/W) was low in the photovoltaic mode. A significant enhancement (around 6000 times at 860 nm) in spectral response (mA/W) is observed predominantly above 600 nm wavelength with an applying bias voltage of -5V, which is due an effective field effect across the heterojunction. The bias

will attract photo-generated carriers from the Si substrate, contributing to a high photocurrent. However, the enhancement in responsivity below 500 nm wavelength is relatively low (around 155 times at 365 nm). In the **Figure 3.9** (c) shows the change in photoresponse (mA/W) for 0 and -5V at 365 (ultraviolet), 550 (green) and 860 nm (near infrared) wavelength. It is clearly observed that the relative increase in photoresponse for higher wavelength is much pronounced than that of shorter wavelength with the applied bias voltage (-5V). This suggest excited photocarriers recombination at the MoS_2/Si interface for shorter wavelength (<500 nm). The bias voltage dependent photocarriers generation and photoresponse at various wavelength can be an interesting fact to understand the interface of MoS_2/Si heterostructure.

Electrical hysterics in the MoS_2/Si heterojunction device was investigated with the forward and reverse sweep of J-V characteristics analysis. **Figure 3.8** (a) shows the J-V characteristic for dark condition. Electrical hysteresis is observed towards the higher forward bias voltage, indicating the charge trapping effect at the MoS_2/Si interface. However, electrical hysteresis was not observed in the reverse saturation current as shown in the inset of **Figure 3.8** (a). **Figure 3.8**(b) shows the forward and reverse sweep J-V characteristic for monochromic light illumination of 100 mW/cm^2. Prominent electrical hysteresis is observed at the higher forward bias voltage similar with the dark condition. For the illumination condition, hysteresis was also observed for the reverse saturation current with an increase in current due to the generated photocarriers. Similarly, the device was tested under illumination of 365 nm wavelength as shown in **Figure 3.8** (c). The hysteresis at the higher bias voltage is prominent in this measurement under the UV light. This suggests charge trapping/de-trapping effect of electrons at the MoS_2/Si interface due to which the hysteresis appeared in dark and light illumination conditions.

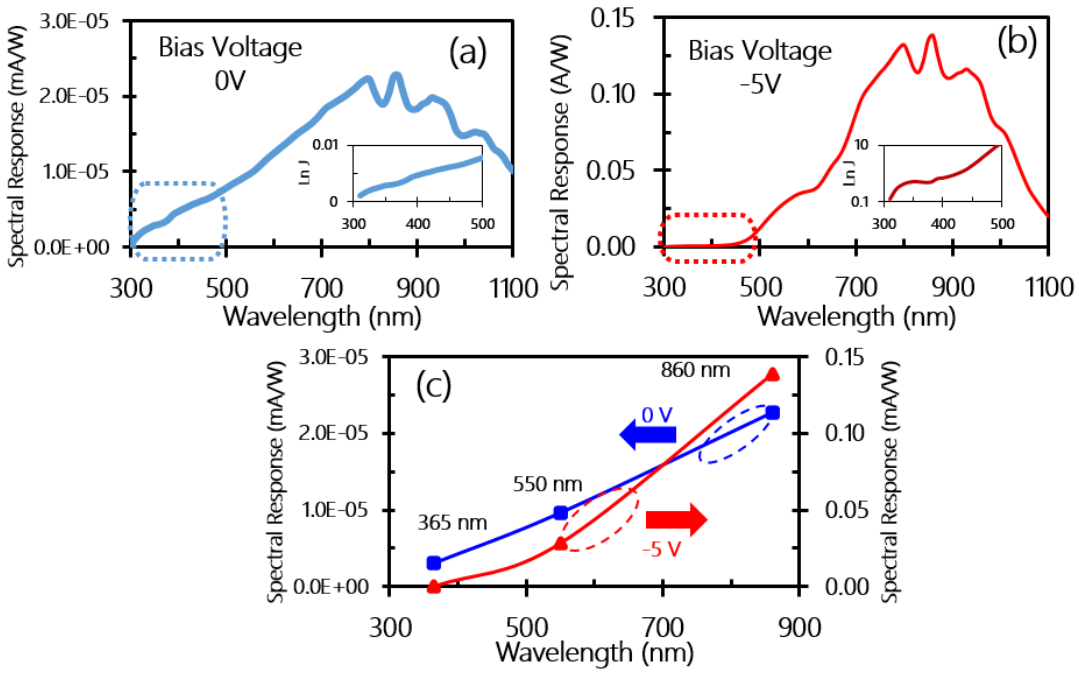

Figure 3.9: Spectral response of fabricated Al/MoS_2/Si/Ag heterojunction device for (a) 0V and (b) -5V bias voltage, (c) change in photoresponse (mA/W) for 0 and -5V at 365 (ultraviolet), 550 (green) and 860 nm (near infrared) wavelength

This explains the anomalous behaviour of photoresponse at the lower wavelength (>500 nm) for the applied bias voltage of 0 and -5V. The surface recombination of higher energetic photons at the MoS_2/Si interface is much higher due to which an inhomogeneous enhancement in photoresponse was obtained with the field effect at the applied bias voltage (-5V). The presence of interface states was further analysed by exploring the structure of Mo and S atoms for the synthesized few-layers MoS_2 on p-type Si surface.

3.6 Energy band diagram

Figure 3.10 (a) shows an energy band diagram for the p-type Si and n-type MoS_2 layers.

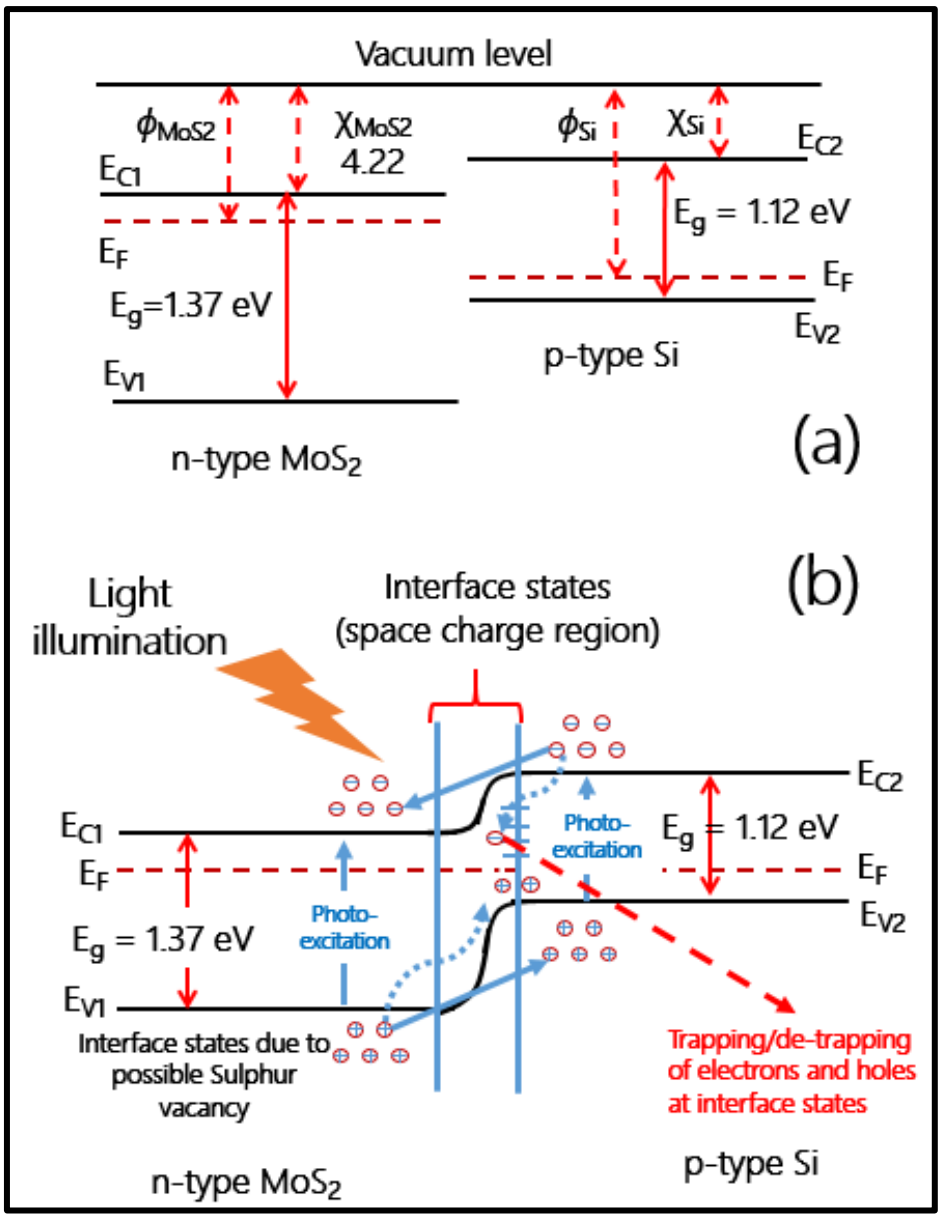

Figure 3.10: (a) Energy band diagram before contact of MoS_2 layers with p-type Si (b) Equilibrium band diagram of MoS_2/Si heterostructure with interface states at the junction presenting the trapping and detrapping process

The respective electron affinity and fermi energy of the two materials were represented before the formation of a heterojunction. **Figure 3.10** (b) shows the energy band diagram

of the MoS_2/Si heterojunction for equilibrium condition. Efficient exciton dissociation and charge transfer occurred with the light illumination in presence of a large build-in-field at the MoS_2/Si heterojunction interface. The effective field effect due to the bias voltage drives the photo-generated carriers toward the electrodes, achieving a significant enhancement in photocurrent. However, as obtained from the photoresponse and J-V characteristics presence of interface states are observed, which significantly influence the spectral photoresponse characteristics. It can be estimated that trapping and detrapping occurred at the interface states of the MoS_2/Si heterojunction with the current flow across the junction. Under illumination condition, the photo-generated electrons and holes also can trapped/de-trapped and thereby influencing the photovoltaic action and photoresponse characteristics under the bias condition. It has been observed that there are S vacancies in the most of chemically synthesized MoS_2 layers, due to which there can be appearance of interface states at the MoS_2/Si interface. [33,34] The other factor, such as, high growth temperature of MoS_2 layers can also adversely affect the p-Si surface and thereby influencing the heterojunction device properties.

Thus, these understanding in the fabricated MoS_2/Si heterojunction can be significant for further enhancement of spectral photoresponse characteristics for the TMDCs layer and Si based photoresponsive device for practical applications.

3.7 Conclusions and key findings of the study

In conclusions, I have demonstrated the fabrication of the heterojunction of MoS_2 layers and p-type Si and their spectral photoresponse characteristics. The fabricated MoS_2/Si

heterojunction device showed good rectification characteristics with a rectification ratio of 10^3 and low reverse saturation current at the bias voltage of ±5V. The MoS_2 layers deposited on the p-type Si wafer showed a photovoltaic action and a photoresponsivity of 139 mA/W in a bias voltage of -5V. The spectral photoresponse (mA/W) of the device was enhanced with applied bias voltage than that of photovoltaic mode. The increase in photoresponsivity at a higher wavelength (>600 nm) is significant than that of lower wavelength (<500 nm) at the bias voltage of -5V. This can be explained with high energetic photocarriers surface recombination in presence of interface states at the MoS_2/Si heterojunction. The occurrence of interface states can be related to the sulphur vacancies in chemically synthesized MoS_2 layers as well as adverse effect of high growth temperature on the Si surface. These findings on the photocarriers behaviour in the fabricated MoS_2/Si heterojunction interface can be critical to develop high photoresponsive heterojunction devices.

3.8 Bibliography

[1] K. F. Mak, C. Lee, J. Hone, J. Shan, and T. F. Heinz, "Atomically thin MoS_2: A new direct-gap semiconductor," *Phys. Rev. Lett.*, vol. 105, no. 13, 2010.

[2] A. Splendiani *et al.*, "Emerging photoluminescence in monolayer MoS_2," *Nano Lett.*, vol. 10, no. 4, pp. 1271–1275, Apr. 2010.

[3] B. Radisavljevic, A. Radenovic, J. Brivio, V. Giacometti, and A. Kis, "Single-layer MoS_2 transistors," *Nat. Nanotechnol.*, vol. 6, no. 3, pp. 147–150, Jan. 2011.

[4] O. Lopez-Sanchez, D. Lembke, M. Kayci, A. Radenovic, and A. Kis, "Ultrasensitive photodetectors based on monolayer MoS_2," *Nat. Nanotechnol.*, vol. 8, no. 7, pp. 497–501, Jun. 2013.

[5] Q. H. Wang, K. Kalantar-Zadeh, A. Kis, J. N. Coleman, and M. S. Strano, "Electronics and optoelectronics of two-dimensional transition metal dichalcogenides," *Nature Nanotechnology*, vol. 7, no. 11. Nature Publishing Group, pp. 699–712, 06-Nov-2012.

[6] W. Yang *et al.*, "Electrically Tunable Valley-Light Emitting Diode (vLED) Based on CVD-Grown Monolayer WS_2," *Nano Lett.*, vol. 16, no. 3, pp. 1560–1567, Mar. 2016.

[7] K. S. Novoselov, A. Mishchenko, A. Carvalho, and A. H. Castro Neto, "2D materials and van der Waals heterostructures," *Science*, vol. 353, no. 6298. American Association for the Advancement of Science, 29-Jul-2016.

[8] H. Fang *et al.*, "Strong interlayer coupling in van der Waals heterostructures built from single-layer chalcogenides," *Proc. Natl. Acad. Sci. U. S. A.*, vol. 111, no. 17, pp. 6198–6202, Apr. 2014.

[9] X. Duan *et al.*, "Lateral epitaxial growth of two-dimensional layered semiconductor heterojunctions," *Nat. Nanotechnol.*, vol. 9, no. 12, pp. 1024–1030, Jan. 2014.

[10] G. Gao *et al.*, "Artificially stacked atomic layers: Toward new van der waals solids," *Nano Lett.*, vol. 12, no. 7, pp. 3518–3525, Jul. 2012.

[11] M. M. Furchi, A. Pospischil, F. Libisch, J. Burgdörfer, and T. Mueller, "Photovoltaic effect in an electrically tunable Van der Waals heterojunction," *Nano Lett.*, vol. 14, no. 8, pp. 4785–4791, Aug. 2014.

[12] S. K. Pradhan, B. Xiao, and A. K. Pradhan, "Enhanced photo-response in p-Si/MoS_2 heterojunction-based solar cells," *Sol. Energy Mater. Sol. Cells*, vol. 144, pp. 117–127, Jan. 2016.

[13] A. Pospischil, M. M. Furchi, and T. Mueller, "Solar-energy conversion and light emission in an atomic monolayer p-n diode," *Nat. Nanotechnol.*, vol. 9, no. 4, pp. 257–261, Mar. 2014.

[14] M. Y. Li *et al.*, "Epitaxial growth of a monolayer WSe_2-MoS_2 lateral p-n junction with an atomically sharp interface," *Science (80).*, vol. 349, no. 6247, pp. 524–528, Jul. 2015.

[15] R. Cheng *et al.*, "Electroluminescence and photocurrent generation from atomically sharp WSe_2/MoS_2 heterojunction p-n diodes," *Nano Lett.*, vol. 14, no. 10, pp. 5590–5597, Oct. 2014.

[16] Z. Zhang, Q. Qian, B. Li, and K. J. Chen, "Interface Engineering of Monolayer MoS_2/GaN Hybrid Heterostructure: Modified Band Alignment for Photocatalytic Water Splitting Application by Nitridation Treatment," *ACS Appl. Mater. Interfaces*, vol. 10, no. 20, pp. 17419–17426, May 2018.

[17] C. Y. Huang *et al.*, "Hybrid 2D/3D MoS_2/GaN heterostructures for dual functional photoresponse," *Appl. Phys. Lett.*, vol. 112, no. 23, p. 233106, Jun. 2018.

[18] S. Qiao *et al.*, "Large Lateral Photovoltage Observed in MoS_2 Thickness-Modulated ITO/MoS_2/p-Si Heterojunctions," *ACS Appl. Mater. Interfaces*, vol. 9, no. 21, pp. 18377–18387, May 2017.

[19] M. A. Hossain, B. A. Merzougui, F. H. Alharbi, and N. Tabet, "Electrochemical deposition of bulk MoS_2 thin films for photovoltaic applications," *Sol. Energy Mater. Sol. Cells*, vol. 186, pp. 165–174, Nov. 2018.

[20] M. R. Esmaeili-Rad and S. Salahuddin, "High performance molybdenum disulfide amorphous silicon heterojunction photodetector," *Sci. Rep.*, vol. 3, no. 1, pp. 1–6, Aug. 2013, doi: 10.1038/srep02345.

[21] L. Wang *et al.*, "MoS_2/Si heterojunction with vertically standing layered structure for ultrafast, high-detectivity, self-driven visible-near infrared photodetectors," *Adv. Funct. Mater.*, vol. 25, no. 19, pp. 2910–2919, May 2015.

[22] Y. Li, C. Y. Xu, J. Y. Wang, and L. Zhen, "Photodiode-like behavior and excellent photoresponse of vertical Si/monolayer MoS_2 heterostructures," *Sci. Rep.*, vol. 4, no. 1, pp. 1–8, Nov. 2014.

[23] L. Hao *et al.*, "Electrical and photovoltaic characteristics of MoS_2/Si p-n junctions," *J. Appl. Phys.*, vol. 117, no. 11, p. 114502, Mar. 2015.

[24] A. Molle, A. Lamperti, D. Rotta, M. Fanciulli, E. Cinquanta, and C. Grazianetti, "Electron Confinement at the Si/MoS_2 Heterosheet Interface," *Adv. Mater. Interfaces*, vol. 3, no. 10, p. 1500619, May 2016.

[25] L. Z. Hao *et al.*, "High-performance n-MoS_2/i-SiO_2/p-Si heterojunction solar cells," *Nanoscale*, vol. 7, no. 18, pp. 8304–8308, May 2015.

[26] S. Qiao *et al.*, "A vertically layered MoS_2/Si heterojunction for an ultrahigh and ultrafast photoresponse photodetector," *J. Mater. Chem. C*, vol. 6, no. 13, pp. 3233–3239, Mar. 2018.

[27] X. Liu *et al.*, "High Response, Self-Powered Photodetector Based on the Monolayer MoS_2/P-Si Heterojunction with Asymmetric Electrodes," *Langmuir*, vol. 34, no. 47, pp. 14151–14157, Nov. 2018.

[28] M. L. Tsai *et al.*, "Monolayer MoS_2 heterojunction solar cells," *ACS Nano*, vol. 8, no. 8, pp. 8317–8322, 2014.

[29] V. Dhyani and S. Das, "High-Speed Scalable Silicon-MoS_2 P-N Heterojunction Photodetectors," *Sci. Rep.*, vol. 7, no. 1, pp. 1–9, Mar. 2017.

[30] V. Dhyani, P. Dwivedi, S. Dhanekar, and S. Das, "High performance broadband photodetector based on MoS_2/porous silicon heterojunction," *Appl. Phys. Lett.*, vol. 111, no. 19, p. 191107, Nov. 2017.

[31] J. Zhao *et al.*, “Rise of silicene: A competitive 2D material,” *Progress in Materials Science*, vol. 83. Elsevier Ltd, pp. 24–151, 01-Oct-2016.

[32] S. M. Shinde, G. Kalita, and M. Tanemura, “Fabrication of poly(methyl methacrylate)-MoS_2/graphene heterostructure for memory device application,” *J. Appl. Phys.*, vol. 116, no. 21, p. 214306, Dec. 2014.

[33] D. Liu, Y. Guo, L. Fang, and J. Robertson, “Sulfur vacancies in monolayer MoS_2 and its electrical contacts,” *Appl. Phys. Lett.*, vol. 103, no. 18, p. 183113, Oct. 2013.

[34] D. M. Sim *et al.*, “Controlled Doping of Vacancy-Containing Few-Layer MoS_2 via Highly Stable Thiol-Based Molecular Chemisorption,” *ACS Nano*, vol. 9, no. 12, pp. 12115–12123, Oct. 2015.

CHAPTER 4

4 Study of semiconducting properties of MoS_2 layers on GaN

4.1 Background of the study

The GaN is an important group-III nitride semiconductors in present optoelectronics and high-power/high-temperature device technologies. [1-5] The in-plane lattice mismatch of GaN and MoS_2 is nearly 0.8% at room temperature and it further reduces at growth temperature. Considering which both the materials can be used as substrate for growth on one another to develop a novel heterostructures. [6-10] In the layered heterostructures, without dangling bonds at the interface provide ultra-fast charge transfer and thereby enabling fabrication of efficient devices. [11,12]

Among various aspects application of TMDCs layered material for optoelectronics application is quite promising due to possibility of integrating with various other semiconductors. It has been demonstrated that different TMDCs layers can be combined in lateral or vertical structures to develop a novel heterojunction-based device due to unique band structure at the interfaces, realising ultrafast charge transfer and executional optoelectronic properties. [13-19] The heterostructure of MoS_2 and GaN also provides an opportunity to develop photoresponsive device beyond the ultraviolet (UV) wavelength

and extending to visible light. [20,21] The lattice matched MoS_2-GaN heterojunction can be practically applicable technology for optoelectronics devices such as photodetector, sensors, and light emission device applications. [21,23] Recently, growth of MoS_2 layers on GaN and their interface characteristics have been explored to develop a novel heterojunction device. [21-25]

Previously, several reports demonstrated growth MoS_2 layer on SiO_2 (300 nm) coated silicon substrate by CVD, where the electrically insulating SiO_2 layer help to determine the electrical transport properties of as-synthesized MoS_2 crystals without a transfer process. It has been observed that the MoS_2 domains on such substrates are randomly oriented, due to which line-defects in the grain boundaries are normally observed in a continuous film. [26, 27] To avoid the detrimental effect on electrical and mechanical properties of the grown films it is necessary to control the crystallographic orientation of the crystals grown on a substrate. Similarly, two dimensional (2D) MoS_2 layer has been synthesized on bulk semiconductors (silicon, GaAs etc.) to fabricate heterojunction photoresponsive devices. Among various semiconducting substrates, GaN with the least lattice mismatch of ~0.62% for MoS_2 monolayer can be significant to deposited unidirectional crystals and large area-continuous film. [28-34] The GaN is mechanically and thermally stable wide bandgap semiconductor (3.4 eV) material having wurtzite crystal structure. [27,28,30,32-35] This also paves the way to build a MoS_2/GaN heterojunction device for photodetector, light emitting devices (LEDs) as well as for various chemical sensor applications. [33,36]

In contrast to previous reports, I demonstrate growth of the large-area MoS_2 layers on free-standing GaN semiconductor and obtaining a photovoltaic photoresponsivity in the MoS_2/GaN vertical heterojunction. The growth and fabrication of a lattice matched

MoS_2/GaN free-standing heterojunction device and the origin of a photovoltaic photoresponsivity are elucidated.

Additionally, I demonstrate the suitability of a gallium (Ga)-polar GaN bulk wafer as a substrate for the of unidirectional MoS_2 crystal growth by CVD process III using the ammonium tetrathiomolybdate (ATM) as a precursor. The growth process of MoS_2 crystals on the Ga-polar GaN wafer and their interface properties, can be significant for heterojunction device applications.

4.2 Synthesis of MoS_2 layer using CVD process II

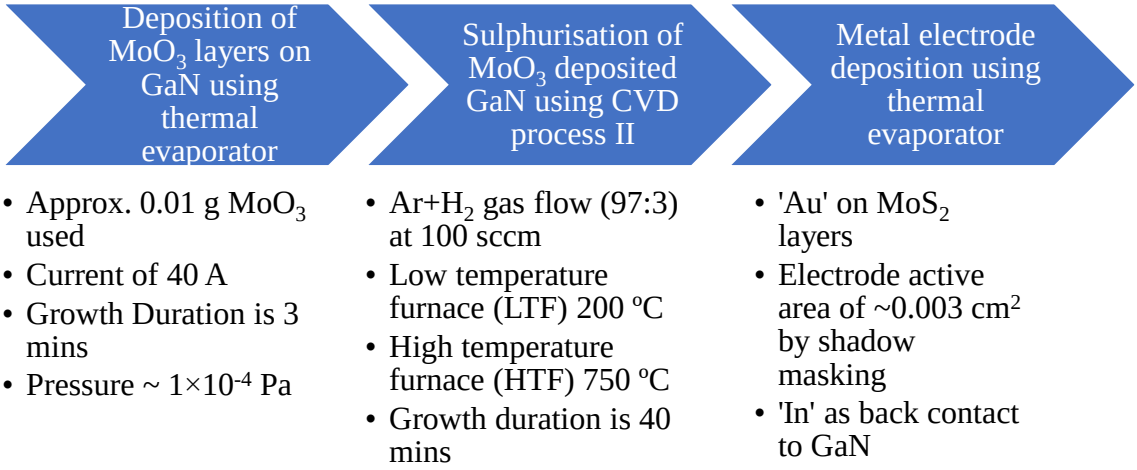

Diagram 4.1: Flow diagram of experimental procedure for the synthesis of MoS_2 on GaN substrate and device fabrication (CVD details in section 2.4)

In this study, I used the liquid phase grown germanium doped free-standing GaN with a doping level of $\leqq 1\times10^{18}$ cm^{-3}. A smooth top surface of GaN was obtained by reactive ion etching (RIE) and used for the growth of the MoS_2 layers. The GaN samples were cleaned using acetone and iso-propyl alcohol for 10 min each by sonication.

The synthesis of MoS_2 layer on GaN surface was performed in two steps. First, ten milligrams of molybdenum oxide, MoO_3 (99.9% Pure) was deposited on the surface of GaN substrate using the thermal evaporation technique. The duration of evaporation was kept 3 minutes and at 40 A of current under ~ 1×10^{-4} Pa vacuum condition. A thin layer of MoO_3 was obtained on the GaN substrates. Subsequently, MoS_2 layer was synthesized by sulphurisation process at high temperature and in the $Ar+H_2$ atmosphere. The sulphurisation process is performed in a quartz tube and in Ar and H_2 gas mixture (97:3) at 100 sccm of gas flow. 1 gram of sulphur powder (98.0%, FUJIFILM Wako Pure) was placed ~25 cm upstream of the MoO_3-deposited-GaN substrate. The low temperature furnace (LTF) is kept at 200 ºC for sulphur evaporation and high temperature furnace (HTF) is kept at 750 ºC for sulphur reaction with MoO_3. A growth period of 40 minutes was established, during which sulphur evaporated in LTF reacts with the MoO_3 to form MoS_2 layers on the GaN substrates. Metal electrodes were deposited on the synthesized MoS_2 layer and GaN substrates to fabricate the heterojunction devices. A shadow mask was placed above the substrate and MoS_2 layer. Gold (Au) on MoS_2 layers with electrode area of ~0.003 cm^2 and Indium (In) as back contact to GaN were deposited to complete the device structure.

4.2.1 Characterization of thermally evaporated MoO_3 film on GaN substrate

The thermally evaporated MoO_3 film on GaN substrate was investigated with scanning electron microscopy (SEM) and X-ray photoelectron spectroscopy. **Figure 4.1** (a) and (b) shows the SEM images of MoO_3 film at the centre part and edge part on the GaN. A uniform MoO_3 film was obtained at a constant evaporation rate of the MoO_3 powder.

The deposited MoO_3 film was also investigated by XPS analysis as shown in the **Figure**

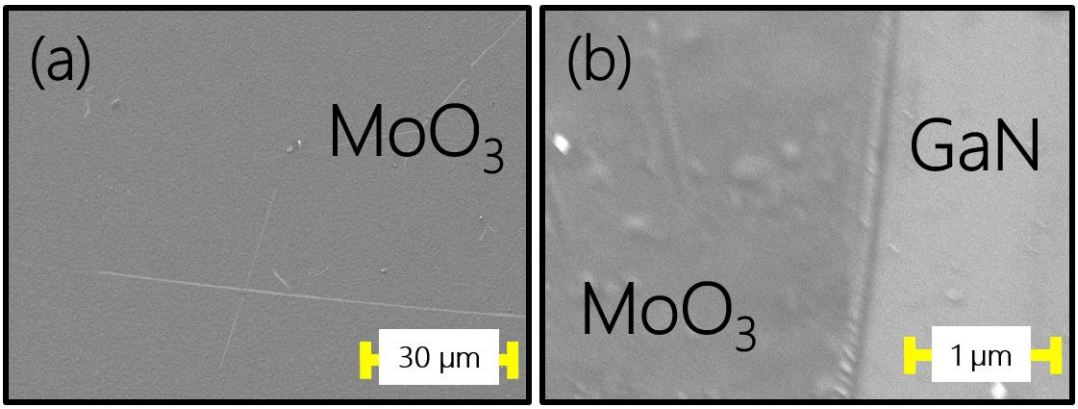

Figure 4.1: (a) and (b) FE-SEM images of MoO_3 surface at different location, deposited on GaN substrate

4.2 (a) showed the Mo3d related peaks with peak centres at 233 and 236.2 eV, corresponding to $3d_{5/2}$ and $3d_{3/2}$ transition of MoO_3, respectively. Also, there is no peak detected around 227 eV for the MoO_3 film, which is observed for MoS_2 film corresponding to the S-Mo bonding structure. I observed a strong O1s related peak at 530.9 eV as shown in **Figure 4.2** (b), corresponding to chemical structure of MoO_3 film on GaN. As the deposited MoO_3 film was very thin, the Ga3d peak for GaN substrate was also observed with a peak centre at 22.1 eV as shown in **Figure 4.2** (c).

4.2.2 Characterisations of synthesized MoS_2 layers on GaN substrate

Fabricated samples were characterized by Raman spectroscopy, scanning electron microscopy (SEM), ultraviolet-visible (UV-vis) absorption spectroscopy and photoelectron spectroscopy (PS). Raman analysis was performed using the NRS 3300 laser Raman spectrometer with a laser excitation wavelength of 532.08 nm. UV-Vis absorption spectroscopy analysis was performed with a JASCO V-670K spectrophotometer. SEM study was done using JEOL JSM 5600 with an accelerating

voltage of 20 kV. Photoelectron spectroscopy characterization was performed with the

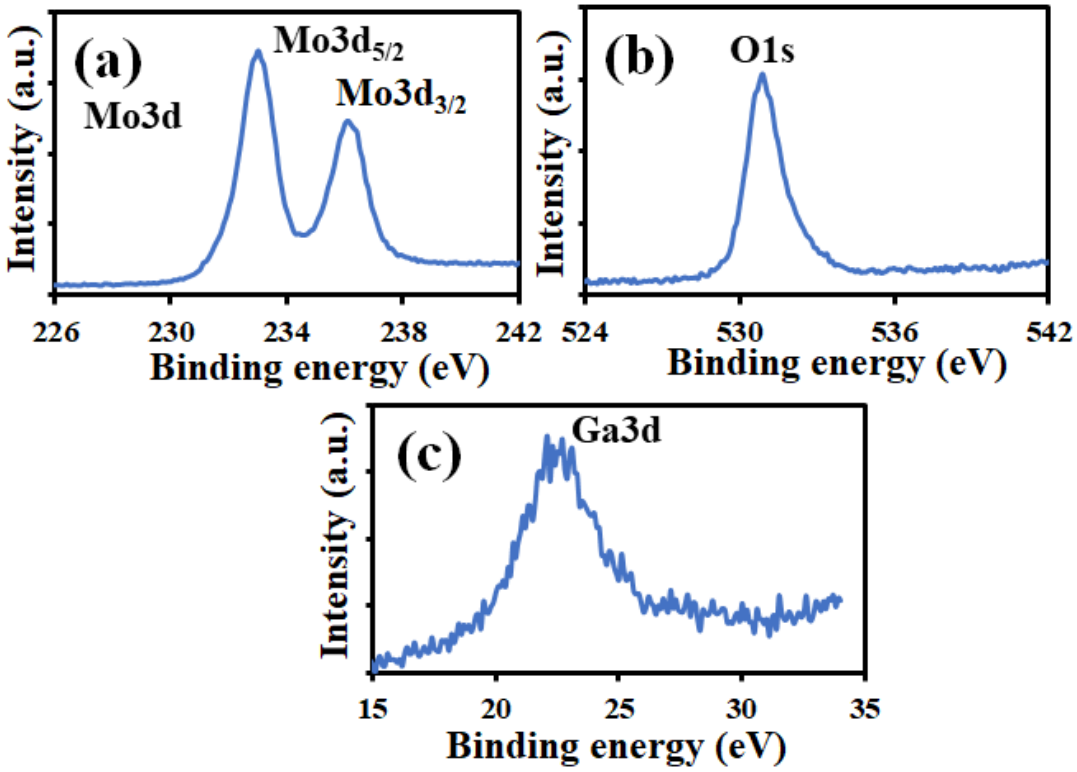

Figure 4.2: XPS spectra for (a) Mo3d with peak centres at 233 and 236.2 eV, corresponding to $3d_{5/2}$ and $3d_{3/2}$ transition of MoO_3, (b) O1s peak (c) Ga3d peak for the GaN substrate.

PHI 5000 VersaProbe using monochromated Al Kα excitation source (1486.6 eV). Current density-voltage (J-V) characteristic measurements were performed at room temperature using two probes system and a Keithley 2401 SourceMeter.

Figure 2.3 shows the ball and stick diagram of MoS_2 layers atop of GaN. Each molybdenum (Mo) atom is surrounded by six sulphur (S) atom forming a trigonal prismatic coordination sphere. The bulk MoS_2 consist of several layers like graphite, where the S-Mo-S configuration forms a monolayer. The GaN bulk single crystal is a wurtzite structure with one Ga atom has three nearest neighbours connected by a covalent

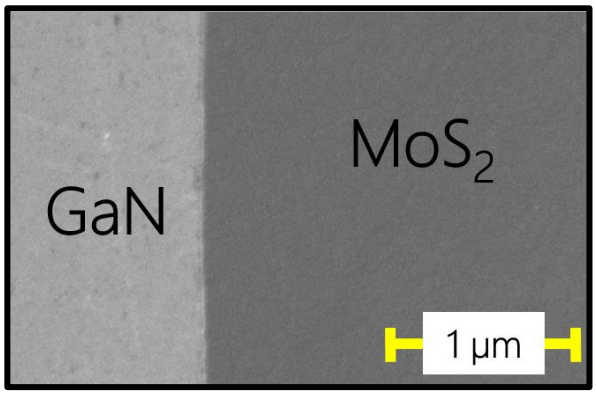

Figure 4.3: SEM image of MoS_2 layer atop GaN substrate

bond. In this study, the growth of MoS_2 layers on GaN was carried out at 750 °C, considering the in-place lattice mismatch is only 0.3% at this growth temperature. This also signify that the MoS_2 layers on GaN will not be in a compress state with a small positive lattice mismatch. Figure 4.4 (b) shows a SEM image of the MoS_2 layer synthesized by sulphurisation process of MoO_3 on GaN surface without effecting the GaN surface morphology. The image shows a uniform film formation of MoS_2 layer on the

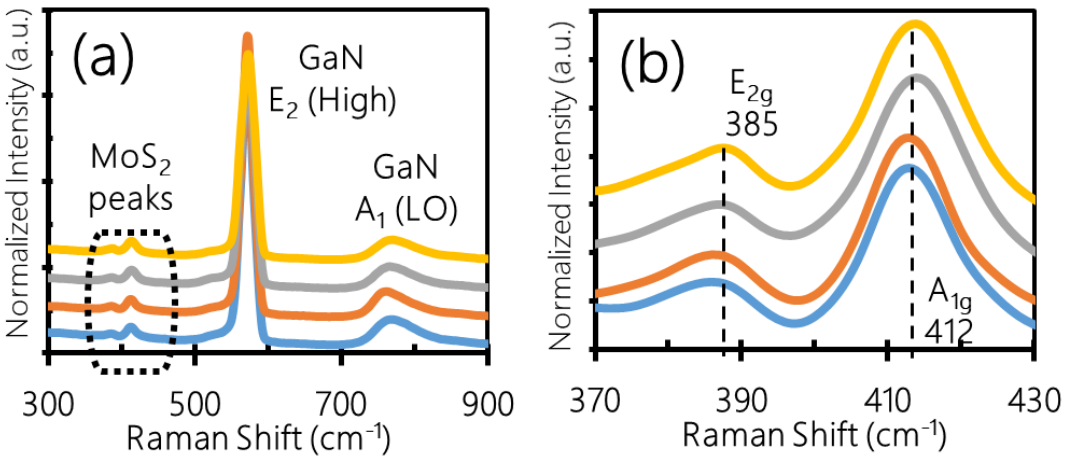

Figure 4.4: Raman spectra of (a) MoS_2/GaN heterostructure at 4 different sampling points and (b) corresponding to MoS_2 peaks at 4 different sampling points

GaN substrate due to the suitability of GaN substrate for MoS_2 layer growth. Further, I

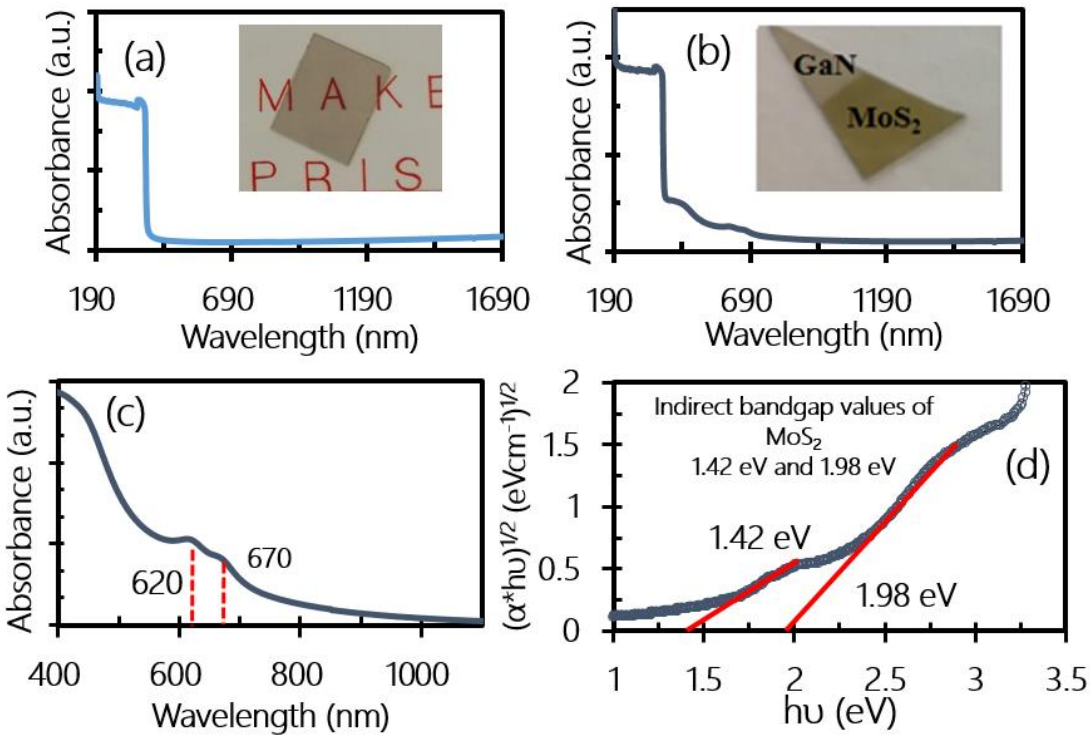

Figure 4.5: (a) UV-Vis absorption spectra for pristine GaN substrate (inset shows the transparency of the sample) (b) UV-Vis absorption spectroscopy spectra of MoS_2 layer deposited GaN (inset shows the transparency of free-standing MoS_2-GaN heterostructure) and (c) Absorption spectra of only MoS_2 layers and (d) Tauc plot for MoS_2 layers at room temperature

carried out Raman spectroscopic analysis of the synthesized MoS_2 layers on GaN. Figure 4.4 (c) shows a Raman spectrum for the MoS_2-GaN heterostructure at four different sampling position. The mean E_2 (High) and A_1 (LO) peaks corresponding to GaN layer were observed at 570 and 749 cm^{-1}, respectively. Additional small intensity peaks were observed at lower wavenumber as shown by the blue circle corresponding to the MoS_2 layer. Figure 4.4 (d) shows the mean E_{2g} and A_{1g} peaks of MoS_2 layer at 385 and 412 cm^{-1} at four different sampling position, respectively with a separation of 27 cm^{-1}

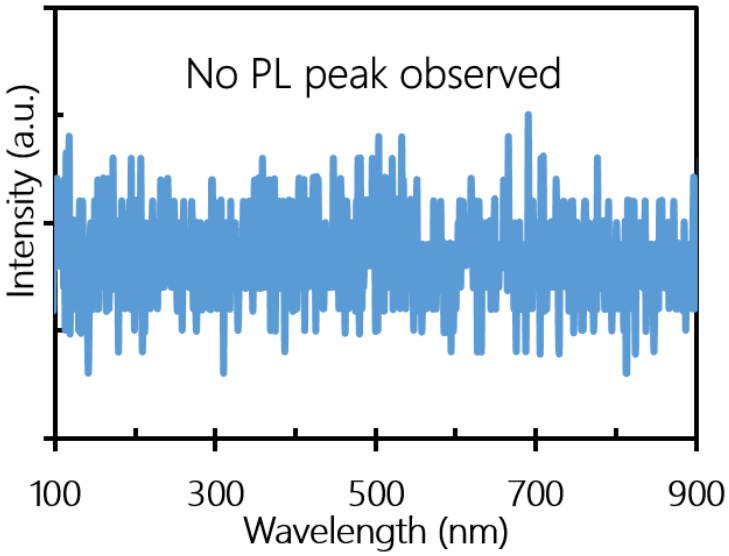

Figure 4.6: PL spectrum of the thin MoS_2 layer measured by 532 nm laser as excitation source (Thickness ~6.5 nm)

corresponding to few-layers MoS_2. [37,38] It is worth to note that the Raman spectra was uniform thought out the continuous film of MoS_2 on GaN. Thus, the microscopy and spectroscopy studies confirmed the formation of a uniform MoS_2 layer on GaN and their heterostructure.

Figure 4.5 (a) shows the UV-Vis absorption spectrum for pristine GaN substrate. The absorption edge was found to be at 367 nm of wavelength corresponding to the wide bandgap (~3.38 eV) of GaN. Inset of the **Figure 4.5** (a) shows the highly visible light transparent free-standing GaN substrate. **Figure 4.5** (b) shows the UV-Vis absorption spectrum for the MoS_2-GaN heterostructure. Absorption can be overbred in the wavelength range of 367-700 nm, corresponding to the MoS_2 layers. Inset of the figure shows the visible light semi-transparent MoS_2-GaN heterostructure. **Figure 4.5** (c) shows the signature absorption peaks of MoS_2 layers at 620 and 670 nm for the MoS_2-GaN heterostructure sample. **Figure 4.5** (d) shows the Tauc plot for the absorption spectrum of MoS_2 layers and an optical band gap of 1.42 eV is estimated. This agrees with reported

bandgap value for few-layers MoS_2. [39] Subsequently, the heterostructure of MoS_2 and GaN was investigated by fabricating a two-terminal diode structure under dark and monochromatic light illumination.

The absence of any PL peak signifies the synthesis of few layer characteristics of MoS_2 deposition.

4.2.3 Band Offset calculation for the heterostructure

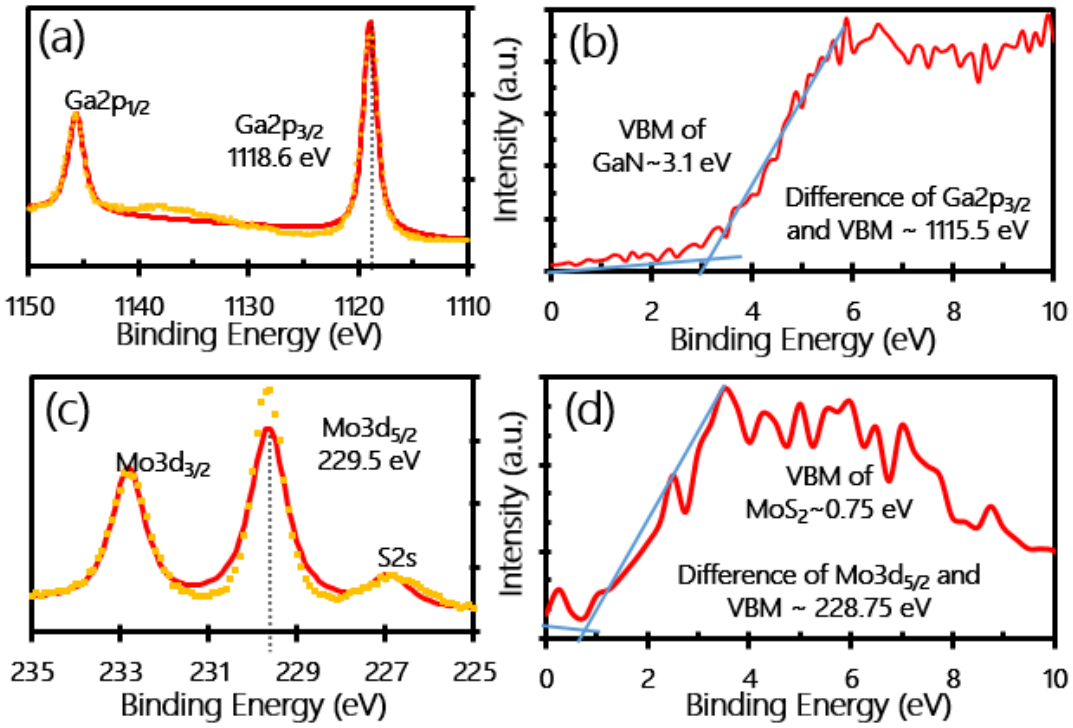

Figure 4.7: XPS (a) Ga2p peaks ($2p_{3/2}$ – 1118.6 eV and $2p_{1/2}$ – 1145.7 eV) (b) VBM spectra of GaN (c) Mo3d peak ($3d_{5/2}$ – 229.5 eV and $3d_{3/2}$ – 232.6 eV) and (d) VBM spectra for as-synthesized MoS_2 few-layers

The band alignment of the fabricated heterostructure was evaluated by photoelectron spectroscopy studies of the samples. Figure 4.7 (a) shows the Ga2p peaks with peak centres at 1118.6 and 1145.7 eV corresponding to $2p_{3/2}$ –and $2p_{1/2}$, respectively. Figure 4.7 (b) shows the VBM spectrum for GaN, which was found to be 3.1 eV. Figure 4.7 (c)

shows the XPS peaks for Mo3d were observed at 229.5 and 232.6 eV, corresponding to $3d_{5/2}$ and $3d_{3/2}$ transition, respectively. The peak at 227 eV corresponds to the S2s core-level which indicates S-Mo bonding. [12] Figure 4.7 (d) shows the VBM spectrum of MoS_2, which was found to be 0.75 eV. Further, these measured values were used to determine the band alignment of MoS_2-GaN heterojunction devices. The valence band offset (VBO) of MoS_2/GaN heterointerface was determined by calculating the energy difference between the Ga and Mo core levels from the MoS_2/GaN heterojunction sample and the individual energy of core levels of Ga and Mo relative to the respective valence band maximum of the GaN and MoS_2 layer. The valence band offset (VBO) for MoS_2-GaN heterojunction can be calculated by the method provided by Tangi and Kraut et al., [40,41] expressed as

$$\Delta E_v = \left(\Delta E^{GaN/MoS_2}_{Ga2p_{3/2}-Mo3d_{5/2}}\right) + \left(\Delta E^{MoS_2}_{Mo3d_{5/2}-VBM}\right) - \left(\Delta E^{GaN}_{Ga2p_{3/2}-VBM}\right) \ldots (1)$$

Here, the first term refers to the energy core level difference of Ga2p and Mo3d resulting from the heterostructure of MoS_2 and GaN. VBM of MoS_2 and GaN are observed to 0.75 and 3.1 eV, respectively. The energy difference $\left[\Delta E^{GaN/MoS_2}_{Ga2p_{3/2}-Mo3d_{5/2}} = \left(E^{MoS_2}_{Mo3d_{5/2}} - E^{GaN}_{Ga2p_{3/2}}\right)\right]$ between $Mo3d_{5/2}$ and $Ga2p_{3/2}$ core-levels is observed to be 889.1 eV calculated using Figure 4.7 (a) and Figure 4.7 (c). The second term on right side of Eq. (1) is the core level energy of $Mo3d_{5/2}$ determined with respect to the valence band maximum for MoS_2. The energy difference $\left[\Delta E^{MoS_2}_{Mo3d_{5/2}-VBM} = \left(E^{MoS_2}_{Mo3d_{5/2}} - E^{MoS_2}_{VBM}\right)\right]$ between Mo $3d_{5/2}$ core-level and the VBM is observed to be 228.75 eV as depicted in Figure 4.7 (c) and Figure 4.7 (d). The third term on right side of Equation (1) is the core level energy of $Ga3d_{5/2}$ determined with respect to the valence band maximum for GaN. The energy

difference $\left[\Delta E^{GaN}_{Ga2p_{3/2}-VBM} = \left(E^{GaN}_{Ga2p_{3/2}} - E^{GaN}_{VBM}\right)\right]$ between Ga $3p_{3/2}$ core-level and the valence band maximum is observed to be 1115.5 eV. Thus, substituting the estimated three terms in equation (1), the valence band offset (VBO) ΔE_{v} value is calculated to be 2.35 eV.

$$\Delta E_C = \Delta E_{\mathrm{v}} + E_g^{MoS_2} - E_g^{GaN} \quad \ldots (2).$$

Further, the conduction band offset (CBO) ΔE_C value is calculated by substituting the bandgap (E_g) of MoS_2 and GaN and the obtained ΔE_{v} in eq. 2. Hence, the measured CBO (ΔE_C) is obtained to be approximately 0.44 eV. Previously, VBO and CBO of the monolayer MoS_2 and GaN heterojunction has been reported to be around 1.86 and 0.56 eV, respectively with type II band alignment.[40] Now, the behaviour of photo-excited electrons and holes in the MoS_2-GaN heterojunction were explained considering the VBO and CBO values in a type II band alignment.

4.3 Synthesis of MoS_2 using CVD process III

In these experiments, I used liquid phase grown germanium doped free-standing Ga-terminated GaN wafer with a doping level of $\leqq 1 \times 10^{18}$ cm^{-3}. The GaN wafer samples were cleaned using standard Piranha solution (H_2SO_4/ H_2O_2 ~7/3) for 10 mins and then later with acetone and iso-propyl alcohol for 10 min each by sonication. Subsequently, the ammonium tetrathiomolybdate $[(NH_4)_2MoS_4]$ precursor was dissolved in N,N-Dimethylformamide (DMF) solution (1mg/1ml or approximately 0.1 wt. % solution). this solution was then spin-coated onto the surfaces of GaN wafer at 2000 rpm for 60 sec. Later the substrates were kept in quartz tube of length 80 cm, along with sulphur powder in two different temperature furnaces, separately. A low pressure of nearly 2 pa in the

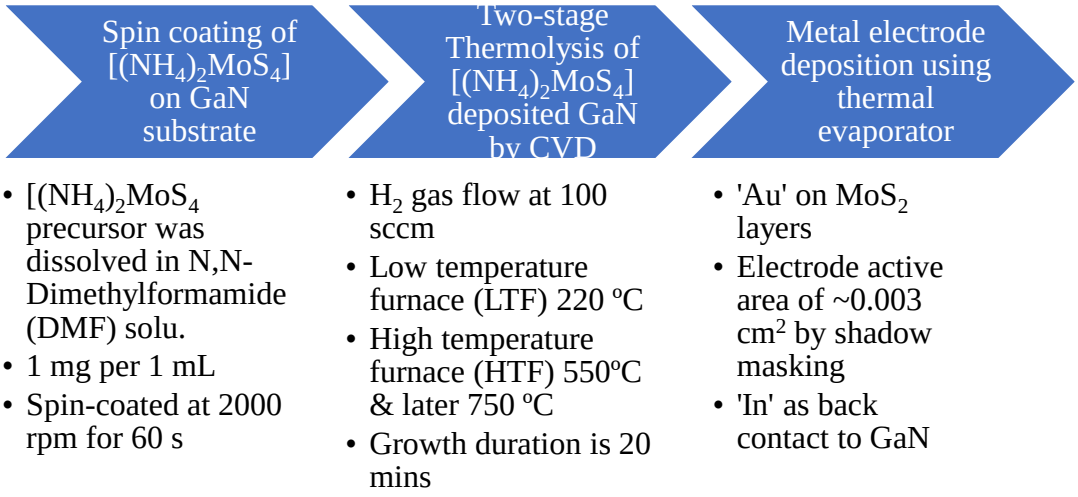

Diagram 4.2: Flow diagram of experimental procedure for the synthesis of MoS_2 on GaN substrate and device fabrication (CVD details in section 2.5)

quartz tube chamber was maintained at the initial stage. Following, 100 sccm of hydrogen (H_2) gas was introduced into the quartz tube growth chamber. Then, the temperature of high temperature furnace (HTF) containing the GaN substrate was raised to 750° C and low temperature furnace (HTF) containing sulphur was raised to 220° C. The pressure in the quartz tube, was kept at around 1 atm as sulphur powder start evaporating. A growth period of 20 minutes was established. Following the growth period, the CVD system was cooled to room-temperature.

The synthesized samples were analysed by scanning electron microscope (SEM), Raman spectroscopy and X-ray photoelectron spectroscopy (XPS) and photoluminescence (PL) analysis. The Raman analysis was done using the NRS 3300 laser Raman spectrometer with a laser excitation wavelength of 532.08 nm. SEM study was performed using JEOL JSM 5600 with an accelerating voltage of 20 kV. XPS analysis was performed using Versa Probe using the monochromated Al Kα excitation source (1486.6 eV). PL analysis

was performed with a confocal scanning (NX-3DFLIM-N03, Tokyo Instruments, Japan) equipped with a Nd:YVO_4 diode laser.

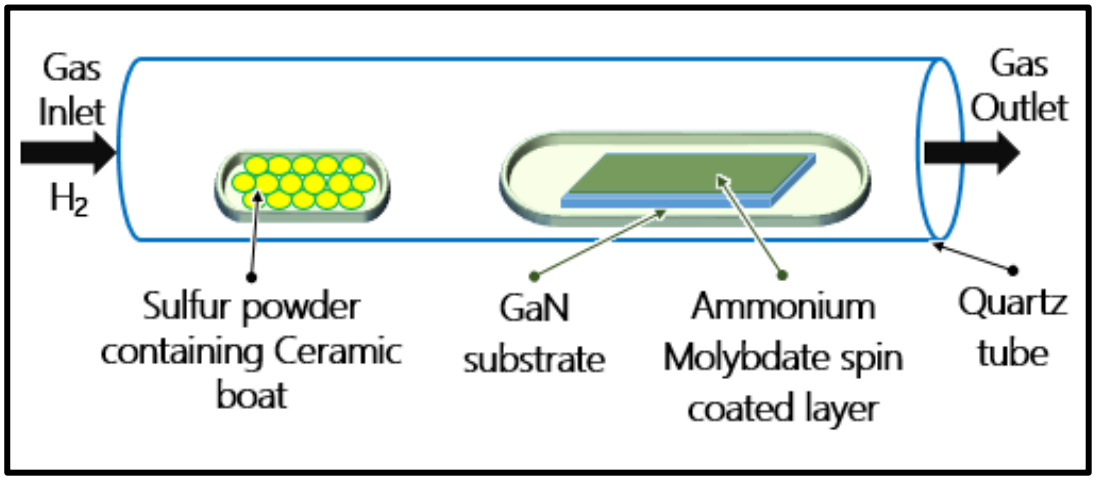

Figure 4.8: Schematic diagram of experimental process deployed in synthesis of MoS_2

4.3.1 Characterisations of synthesized lattice matched MoS_2 crystal and layer

Figure 2.19 (a) shows the schematic of the ATM precursor molecules along with the synthesis process. The ATM precursor is free from oxygen and containing an ammonium component, which decompose to for MoS_2 layer. In absence of oxygen and presence of the ammonium component can provide better coordination for growth of MoS_2 layer on the GaN substrate. **Figure 2.19** (b) schematic diagram of the side and cross view of MoS_2 monolayer crystals on lattice matched GaN substrate. The top-view clearly shows the two monolayer MoS_2 crystals with a relative rotation angle of $\theta = 60°$, where the edges are

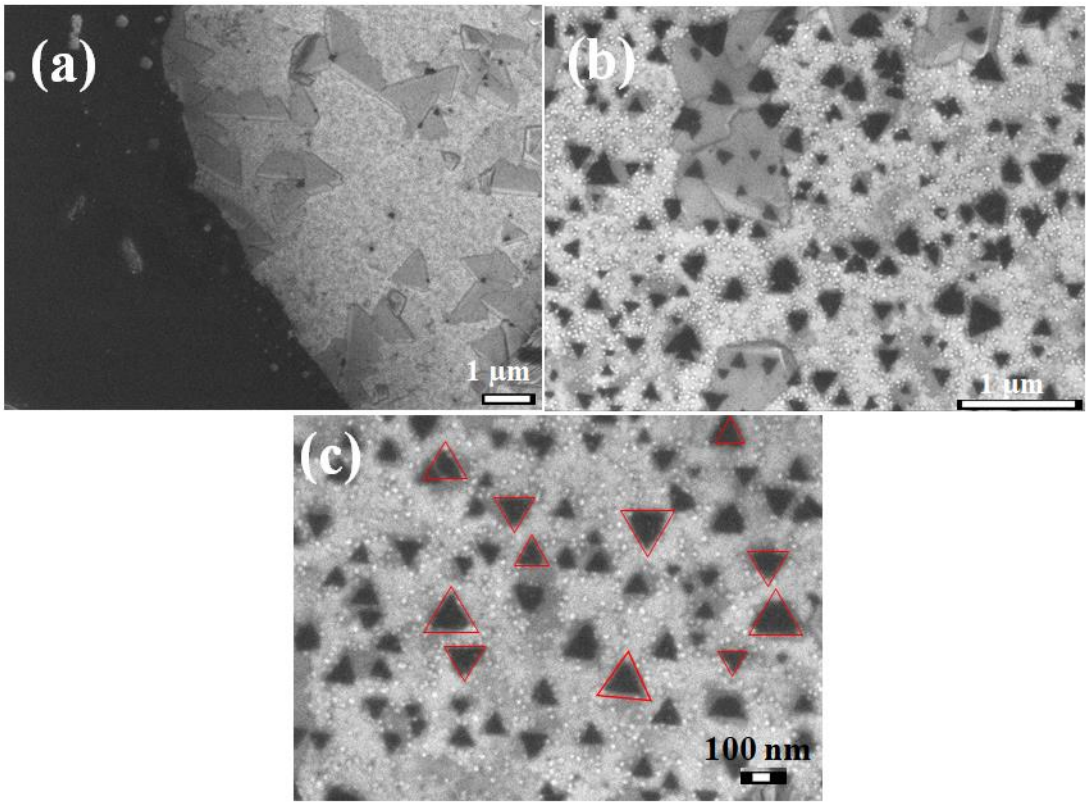

Figure 4.9: (a) SEM image of unidirectional and oppositely oriented grown triangular MoS_2 crystals on GaN. (b) Continuous MoS_2 film obtained on the GaN substrate

parallel to each other. In the growth process, the ATM precursor solution was spin coated on the GaN substrate to obtain uniform distribution of the precursor on the substrate surface. Now, the growth was performed in sulphur enriched environment, such that the decomposing ATM precursor laterally growth with the Mo and sulphur atom coordination. **Figure 4.9** (a) shows the SEM image of MoS_2 crystals on the GaN wafer, presenting the epitaxial growth of individual crystals. The synthesized MoS_2 crystals islands synthesized have dimensions of 100-300 nm, where the edge orientation of the crystals is almost uniform. This signifies the possibility of using oxygen free ATM precursor use for growth of epitaxial MoS_2 crystals on a GaN substrate. Previously, Ruzmetov et al. [41] has

presented epitaxial growth of triangular MoS_2 crystal on GaN film on sapphire substrate with similar domain size using MoO_3 as precursors. However, synthesis of a continuous film on the GaN can be more significant to fabricate practical heterojunction devices. **Figure 4.9** (b) shows an edge area on GaN, where a continuous film of MoS_2 was obtained. The nucleated triangular MoS_2 crystals merged to form a continuous film. In this study, I obtained that the Ga-polar surface of GaN is more suitable for nucleation of the MoS_2 crystals, which may be due to better thermally stability of Ga-face GaN. The synthesized MoS_2 crystals were further analysed by Raman and PL analysis.

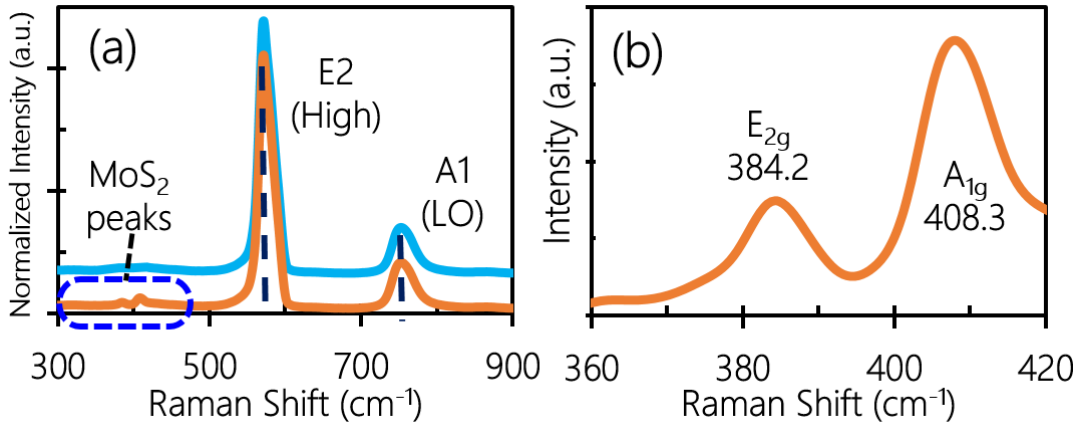

Figure 4.10: Raman spectra of (a) bare GaN wafer before and after growth of MoS_2 crystals. (b) E_{2g} and A_{1g} peaks of MoS_2 crystal on GaN substrate. (c) PL spectra of MoS_2

Figure 4.10 (a) shows Raman spectra of bare GaN and as-synthesized MoS_2 crystals on GaN wafer. I observe E2 (high) and A1 (LO) peaks at 570.0 and 754.3 cm^{-1}, respectively. Raman spectra of MoS_2-GaN structure is depicted in orange line. The peaks E2 (high) and A1 (LO) were observed for the heterojunction, corresponding to GaN, at 570.0 and 749.1 cm^{-1}, respectively. Low intensity peaks corresponding to MoS_2 is encircled in **Figure 4.10** (a) is analysed to confirm the quality of the crystals. **Figure 4.10** (b) shows

the E_{2g} and A_{1g} peaks at 385.4 and 408.1 cm^{-1}, respectively, with a peak

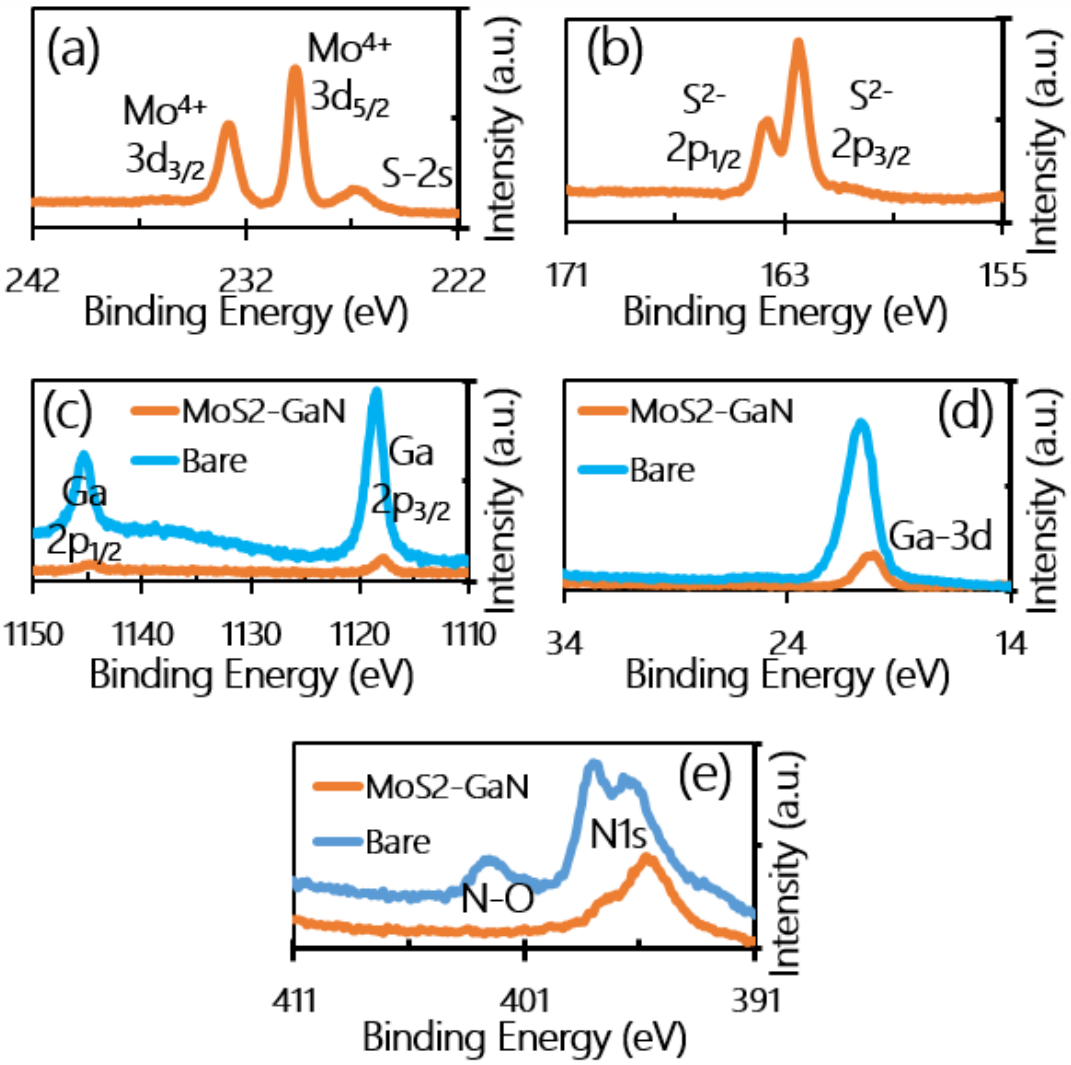

Figure 4.11: XPS spectra of (a) Mo $3d_{5/2}$ (229.7 eV) and $3d_{3/2}$ (232.8 eV) (b) S $2p_{3/2}$ (162.5 eV) and $2p_{1/2}$ (163.6 eV) for the synthesized MoS_2 layer on GaN wafer. (c) $Ga2p_{3/2}$ (1145.4 eV) and $2p_{1/2}$ (1144.8 eV) (d) Ga3d (20.6 eV) (e) N1s peaks for the synthesized MoS_2-GaN heterostructure in comparison to bare GaN wafer

difference of 22.7 cm^{-1}. **Figure 4.12** shows the PL spectrum for the triangular MoS_2 crystals on GaN substrate with a sharp peak at wavelength of 666 nm, corresponding to

1.86 eV. The Raman and PL study shows formation of monolayer triangular crystal on bulk GaN wafer. This showed the effectiveness of the oxygen free TMA precursor for growth of 2D MoS_2 crystals on GaN substrate.

XPS analysis was performed to characterize the synthesized MoS_2-GaN heterostructure. **Figure 4.11** (a) shows the XPS spectra for bare GaN and MoS_2-GaN heterostructure. The Mo3d was observed two splitted peak at 232.8 and 229.7 eV, corresponding to $3d_{3/2}$ and $3d_{5/2}$ peaks, respectively. A small intensity S2s peak is also observed at around 227.0 eV, attributing to the formation of MoS_2 layer. **Figure 4.11** (b) shows the S2p spectrum for the synthesized MoS_2 layer on GaN. The two splitted peaks were observed at 162.5 and 163.6 eV, corresponding to $2p_{3/2}$ and $2p_{1/2}$, respectively. The Mo and S XPS peaks can be correlated with previous reported results confirming the formation of MoS_2 layer structure on GaN wafer. **Figure 4.11** (c) shows the Ga2p for the MoS_2-GaN heterostructure in comparison of bare GaN. The Ga $2p_{1/2}$ and $Ga2p_{3/2}$ peaks were observed at around 1145.4 and 1144.8 eV for the MoS_2-GaN heterostructure as well as for bare GaN without significant change. **Figure 4.11** (d) shows the Ga3d peak was observed at around 20.7 eV for bare GaN and 20.1 eV for MoS_2-GaN heterostructure, the shift in the Ga3d peak may be due to electronic interaction at the interface. **Figure 4.11** (e) shows the XPS spectra for N1s of GaN for the for MoS_2-GaN heterostructure in comparison of bare GaN wafer. The N1s XPS analysis showed a nitrogen and oxygen bonded peak at around 41.5 eV. This indicates the native oxide impurities on the GaN surface. There was no such nitrogen and oxygen bonded peak after the growth of MoS_2 layer by the developed process. This indicate that the interface of MoS_2 and GaN is stable with less amount of impurities as well as without distortion of the GaN structure. In this context, I obtained that the Ga-polar surface of GaN wafer is suitable for nucleation and growth of MoS_2 crystals for

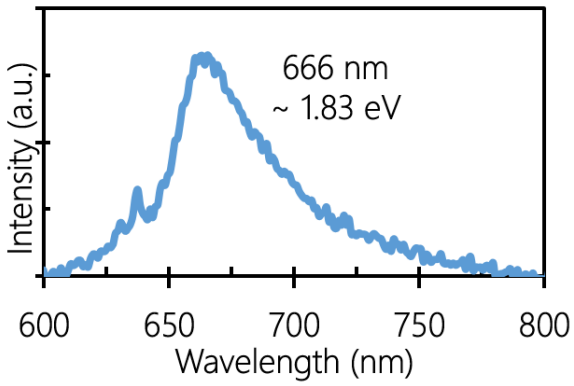

Figure 4.12: PL spectra of MoS_2

fabrication of an effective heterostructure. My studies confirmed the formation of a thin heterostructure of the synthesized MoS_2 film on Ga-polar GaN, with a stable chemical structure. [42-47]

4.4 Device fabrication and performance using CVD II

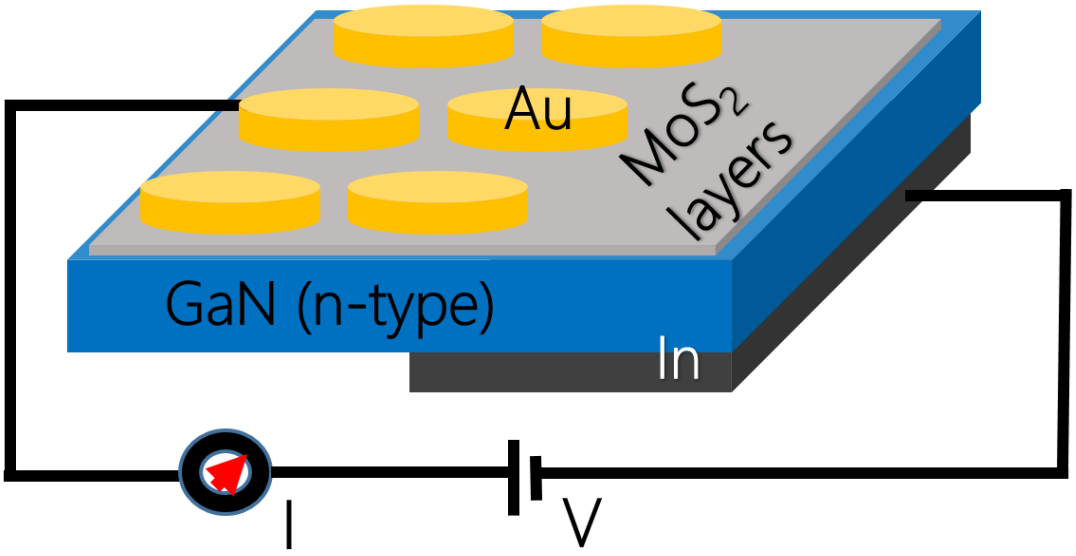

Figure 4.13: Schematic diagram of the MoS_2-GaN heterojunction device with 'Au' contact on MoS_2 layers

Figure 4.14 (a) shows a schematic diagram for the fabricated heterojunction device with

a device structure of Au/MoS_2/GaN/In. Figure 4.14 (b) shows J-V characteristics curve

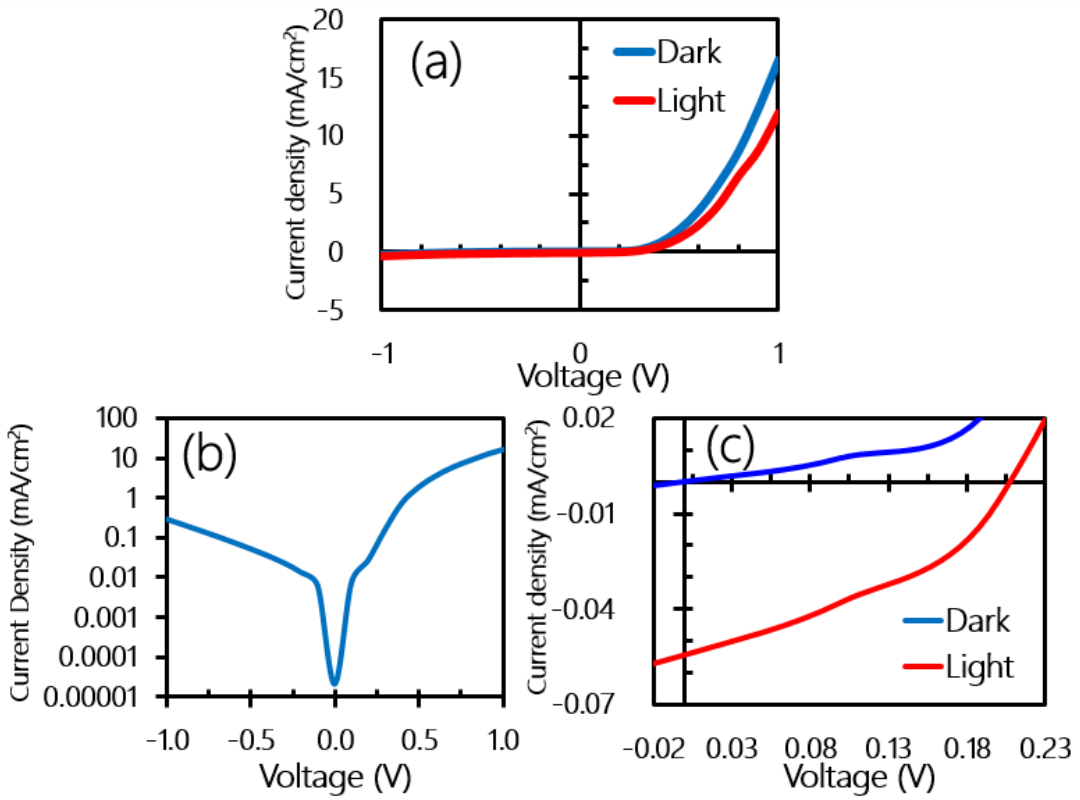

Figure 4.14: (a) J-V characteristics without light illumination for the fabricated device (b) Log plot of corresponding J-V characteristics and (c) High magnification J-V characteristics, with and without light illumination for the device, showing the photovoltaic photoresponsivity

without light illumination. A nonlinear rectifying J-V characteristic was observed, with a suitable diode characteristic and low reverse saturation current. The turn-on voltage is obtained to be 0.35 V in forward bias condition. Figure 4.14 (c) shows the Log plot of J-V characteristics corresponding to Figure 4.14 (b), where the rectification ratio is in order of 10^2. The calculated ideality factor from thermionic emission equation is found to be 2.5.

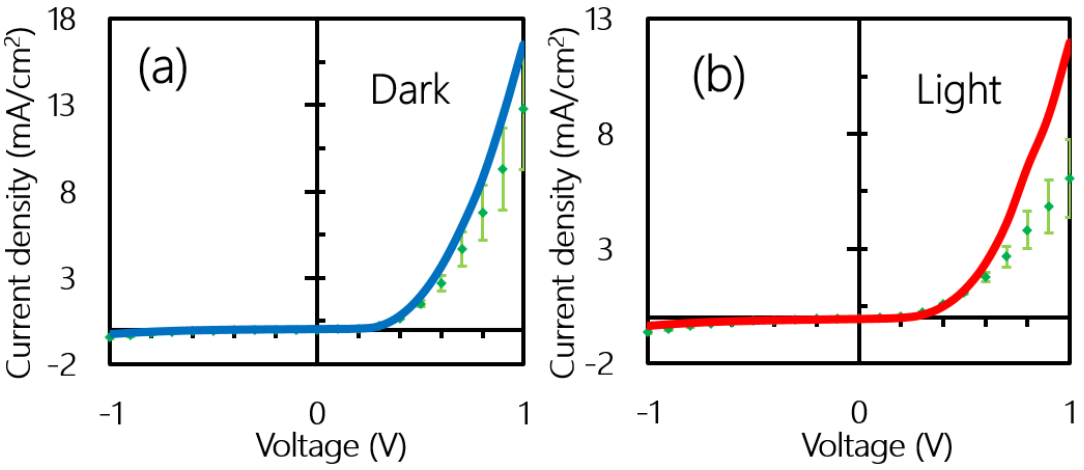

Figure 4.15: J-V characteristics for device (Au/MoS_2/GaN/In) showing an excellent diode characteristic with average current density and standard deviation under (a) dark (N=3) and (b) light illumination (N=4) condition

Figure 4.14 (d) shows the J-V characteristics without (in blue line) and with (in red line) light illumination for the device with structure Au/MoS_2/GaN/In. The device showed similar excellent rectification behaviour under light illumination and a photoresponsive photovoltaic action was obtained. The open circuit voltage (V_{oc}) and short circuit current density (J_{sc}) were obtained as 0.2 V and 0.054 mA/cm^2, respectively for the MoS_2-GaN heterojunction device. Previously, photoresponsivity without photovoltaic action in the undoped MoS_2 layer and n-type GaN horizontal device has been obtained under a biased voltage condition as reported by Moun et al.[33] Again, a photovoltaic action in the MoS_2 few-layers and p-type GaN based heterojunction as reported by Zhuo et al.[38] In contrast to previous reported results, a photovoltaic action was observed in the undoped MoS_2 layers and n-type GaN vertical heterojunction in this study. This suggest that the recombination of the photo-induced generated carriers is low due to which a V_{oc} can be observed in the device. The observed photovoltaic photoresponsivity in the fabricated device was investigated from the band configuration of MoS_2 few-layers and GaN

substrate. The band alignment is analysed by photoelectron spectroscopy to find out the conduction and valence band offset values.

Figure 4.15 shows the measurement of standard deviation of current density-voltage (J-V) for the fabricated device. Photovoltaic action was obtained in all the measured J-V spectra under light.

4.4.1 Energy band diagram

Figure 4.16 shows the energy band diagram of MoS_2/GaN layer in equilibrium condition. The bandgap values of MoS_2 and GaN are depicted as per the measured values from the optical absorption studies. The band diagram is estimated from the measured VBO (~2.35 eV) and CBO (~0.44 eV) values for the MoS_2-GaN heterointerface. It can be observed that the few-layers MoS_2 and the freestanding GaN formed a type II band alignment in presence of large VBO value. The formation of such band alignment can be significant to develop an effective photoresponsive device. The behaviour of photoexcited electrons and holes at the heterointerface is demonstrated in the **Figure 4.16** (b). As it can be observed, photoexcited electrons can effectively move across the junction toward GaN, where movement of holes is restricted. The large VBO will prevent movement of holes toward the GaN as a result the photoexcited electrons and holes can be separated effectively with low recombination loss. In the fabricated MoS_2/GaN heterojunction a suitable photovoltage (0.2 V) and photocurrent was obtained due to type II band alignment with suitable VBO and CBO values. Thus, my study revealed that the MoS_2 and GaN are two promising materials to develop efficient lattice match heterojunction photoresponsive devices. This also signifies possibility of implementing the MoS_2/GaN

heterostructure for sensors and light emission device applications.

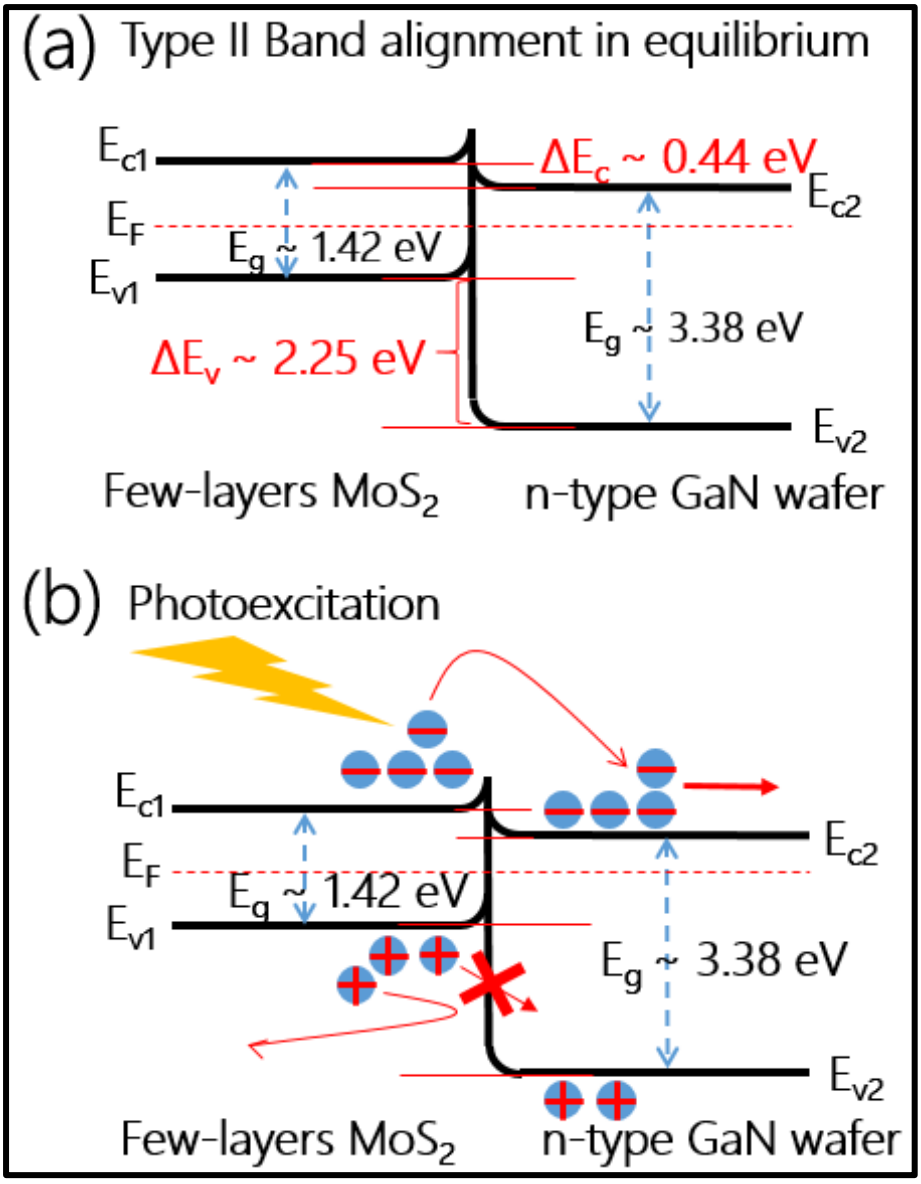

Figure 4.16: (a) Formation of type II band alignment for the few-layers MoS_2 and GaN in equilibrium, presenting the CBO and VBO at the heterointerface (b) Photoexcitation process for the MoS_2-GaN heterojunction. Electrons effectively moves across the junction toward GaN, where movement of holes is restricted due to large VBO

4.5 Device fabrication and performance using CVD III

Figure 4.17 shows schematic of the fabricated device with a device structure of

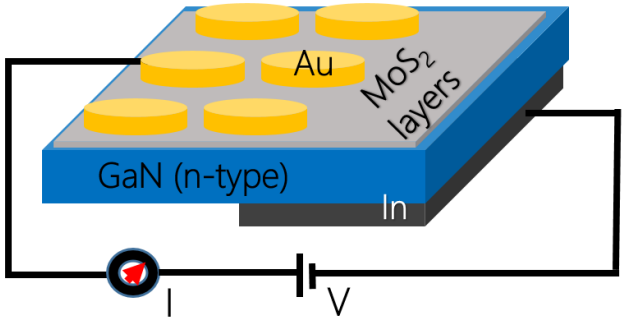

Figure 4.17: Schematic of fabricated device structure

Au/MoS_2/GaN/In. The J-V characteristics of the fabricated device was analysed for with and without monochromatic light illumination. **Figure 4.18** (a) and (b) show the J-V characteristics in dark condition and corresponding logarithmic plot for bias voltage of +2 to -2 V. The J-V characteristics fort the MoS_2-GaN heterojunction showed excellent diode characteristic with a leakage current density of 1.37×10^{-6} A/cm^2 at -2V, where the rectification ratio is obtained as 5×10^7 and the diode ideality factor was analysed by using the thermionic emission equation which is found to be 2.1. The diode ideality factor is much better than many other reported GaN based heterojunction devices. [30,32,33] The excellent rectification of the MoS_2-GaN heterojunction can be explained by formation of an excellent heterojunction interface as observed from the XPS analysis.

Figure 4.18 (c) shows the J-V characteristic under monochromatic light (300-1100 nm). The diode rectification under light illumination is almost unchanged and photoresponse was observed for the heterojunction device. **Figure 4.18** (d) shows J-V characteristic for applied bias voltage of -0.06 to 0.24 V, presenting a photovoltaic action with short circuit current of 9.8 $\times10^{-5}$ mA/cm^2 and open circuit voltage of 0.208 V. At present the photovoltaic action is not significantly high for self-powered photosensor applications.

However, the excellent rectification and low reverse saturation current can be important for application of the developed MoS_2-GaN heterojunction photosensors, gas, chemical

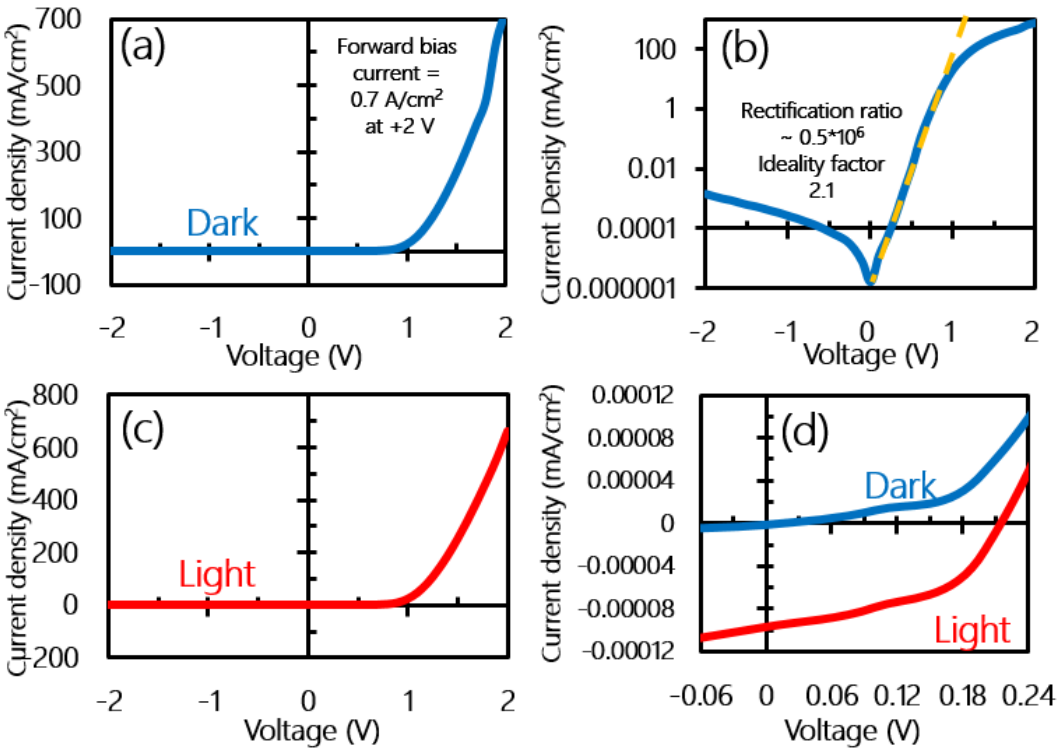

Figure 4.18: Schematic of fabricated device structure, (b) J-V characteristics without light illumination, (c) Logarithmic plot of J-V characteristics without light illumination, (d) J-V characteristics of under monochromatic white light and (e) J-V characteristics with and without light illumination for photovoltaic action

and other sensor device applications. Rectification behaviour of the same GaN sample with only metal contacts (Au/GaN/In) is shown in **Figure 4.19** (b) and it has been compared with rectification of the heterostructure. Here I observed that the turn-on voltage is smaller for metal schottky junction device (Au/GaN/In) than that of the

Au/MoS_2/GaN/In device. Further, the rectification ratio is lower for the Au/GaN/In device.

We compare the device performance of the two device Au/MoS_2/GaN/In. As seen in **Figure 4.14** and **Figure 4.18**, we can comment on the differences arising in their performances. In the device where MoS_2 was synthesised using CVD III showed lesser rectification with that of MoS_2 using CVD II. This is attribute to the lesser number of synthesised layers on the substrate. Whereas the photovoltaic photoresponsivity was higher in device CVD II MoS_2. The reason for which is the differences in the metal electrode 'Au' deposited on MoS_2/GaN using thermal evaporator.

Additional device study of metal only contact was carried out. The J-V characteristics are shown **Figure 4.19**. The results of this is compared with the heterostructure device as

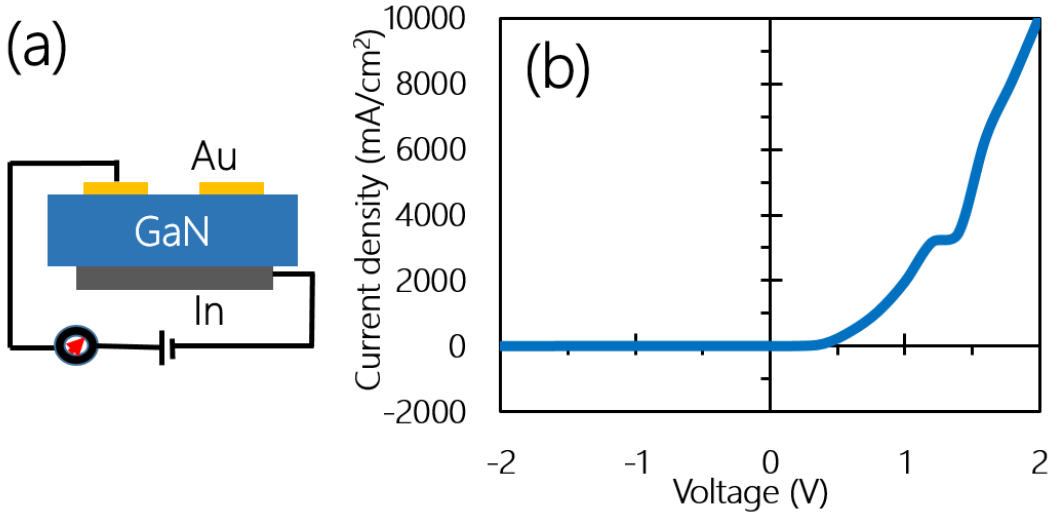

Figure 4.19: (a) Schematics of the schottky device (b) J-V characteristics of Au/GaN/In device without light illumination

shown in **Table 4.1**. With this we can deduce that the excellent rectification of the heterostructure device i.e. Au/MoS_2/GaN/In is majorly due to the heterojunction behaviour between the MoS_2 and GaN material.

Table 4.1: Comparison of rectification behaviours of heterostructure with that of the metal contacts on GaN substrate

Device	**Onset voltage**	**Rectification ratio**	**Current density at +2 V**
Au/MoS_2/GaN/In	1.0 V	0.5×10^6	0.70 A/cm^2
Au/GaN/In	0.4 V	10^3	10.04 A/cm^2

4.6 Conclusion and key findings of the study

In conclusion, I have demonstrated the growth of uniform few-layers MoS_2 film on free-standing GaN wafer by sulphurisation process of MoO_3 thin layer, labelled as CVD process II. SEM study showed a uniformly continuous MoS_2 film formation on the GaN surface without effecting the GaN morphology. As well as I successfully have grown MoS_2 triangular crystals on a Ga-polar GaN free-standing substrate using ammonium containing ATM precursor, labelled as CVD process III.

Raman spectra for the MoS_2/GaN heterostructure synthesized using second process showed constant GaN related peaks indicating no effect on the host substrate after the growth. The MoS_2 related E_{2g} and A_{1g} peaks at 385 and 412 cm^{-1}, respectively, are also consistent at different points with almost same separation (~27 cm^{-1}) corresponding to few-layers film formation. A photovoltaic photoresponsivity was obtained in the MoS_2/GaN heterojunction with vertical current flow across the junction. The VBO and CBO values were found to be 2.35 and 0.44 eV, respectively, corresponding to type II band alignment for the fabricated heterojunction. In such a band configuration, the photoexcited electron effectively moved across the junction, where the movement of holes toward GaN is restricted due to large VBO. This signify that the photoexcited

electron and holes can be effectively separated with low recombination loss, due to which a photovoltage appeared across the MoS_2-GaN heterojunction. The demonstrated CVD process II can be significant to develop MoS_2/GaN heterostructure based photodiode and for other optoelectronics device application.

In the third CVD process the synthesis was performed in sulphur enriched environment to achieve better coordination of the sulphur atom and molybdenum atoms from decomposed ATM precursor, using ammonium tetrathiomolybdate. The SEM, Raman and PL analysis showed growth of unidirectional triangular MoS_2 crystals as well as continuous film attributing to the lattice matched GaN substrate. XPS studies showed a good interface quality of the synthesized MoS_2 layer and GaN, where the surface oxygen at the interface was significantly less than that of the bulk GaN wafer. The Ga-polar GaN is a suitable substrate for nucleation of the MoS_2 crystals, which may be due to better thermally stability of Ga-face GaN. A fabricated MoS_2-GaN heterojunction diode showed significantly low reverse saturation current density of 1.37×10^{-6} A/cm^2 at -2 V, where the rectification ratio is obtained as 5×10^7. A photovoltaic action was also observed under illumination of monochromatic light, which can be important for photosensing applications. Thus, my study revealed the suitably of Ga-polar GaN wafer for growth of MoS_2 crystals with excellent interface quality using the oxygen-free and ammonium containing organic molecule as precursor using CVD process III.

Comparing the semiconducting performances of the device in which MoS_2 were synthesised on GaN we observe the photovoltaic photoresponsivity and rectification difference arising due to the number of layers of MoS_2 and the thickness/opacity of the deposited metal electrode.

4.7 Bibliography

[1] R. F. Davis, "III-V Nitrides for Electronic and Optoelectronic Applications," *Proc. IEEE*, vol. 79, no. 5, pp. 702–712, 1991, doi: 10.1109/5.90133.

[2] T. Egawa, T. Jimbo, and M. Umeno, "Characteristics of InGaN/AlGaN light-emitting diodes on sapphire substrates," *J. Appl. Phys.*, vol. 82, no. 11, pp. 5816–5821, Dec. 1997, doi: 10.1063/1.366450.

[3] J. Millan, P. Godignon, X. Perpina, A. Perez-Tomas, and J. Rebollo, "A survey of wide bandgap power semiconductor devices," *IEEE Trans. Power Electron.*, vol. 29, no. 5, pp. 2155–2163, May 2014, doi: 10.1109/TPEL.2013.2268900.

[4] J. K. Kim *et al.*, "Light-extraction enhancement of GaInN light-emitting diodes by graded-refractive-index indium tin oxide anti-reflection contact," *Adv. Mater.*, vol. 20, no. 4, pp. 801–804, Feb. 2008, doi: 10.1002/adma.200701015.

[5] G. Kalita, M. Dzulsyahmi Shaarin, B. Paudel, R. Mahyavanshi, and M. Tanemura, "Temperature dependent diode and photovoltaic characteristics of graphene-GaN heterojunction," *Appl. Phys. Lett.*, vol. 111, no. 1, p. 013504, Jul. 2017, doi: 10.1063/1.4992114.

[6] P. Gupta *et al.*, "Layered transition metal dichalcogenides: promising near-lattice-matched substrates for GaN growth," *Sci. Rep.*, vol. 6, no. 1, pp. 1–8, Jul. 2016, doi: 10.1038/srep23708.

[7] T. P. O'Regan *et al.*, "Structural and electrical analysis of epitaxial 2D/3D vertical heterojunctions of monolayer MoS_2 on GaN," *Appl. Phys. Lett.*, vol. 111, no. 5, p. 051602, Jul. 2017, doi: 10.1063/1.4997188.

[8] P. Yan *et al.*, "Epitaxial growth and interfacial property of monolayer MoS_2 on gallium nitride," *RSC Adv.*, vol. 8, no. 58, pp. 33193–33197, Jul. 2018, doi: 10.1039/c8ra04821e.

[9] J. Wang, H. Shu, P. Liang, N. Wang, D. Cao, and X. Chen, "Thickness-Dependent Phase Stability and Electronic Properties of GaN Nanosheets and MoS_2/GaN van der Waals Heterostructures," *J. Phys. Chem. C*, vol. 123, no. 6, pp. 3861–3867, Feb. 2019, doi: 10.1021/acs.jpcc.8b10915.

[10] D. Ruzmetov *et al.*, "Vertical 2D/3D Semiconductor Heterostructures Based on Epitaxial Molybdenum Disulfide and Gallium Nitride," *ACS Nano*, vol. 10, no. 3, pp. 3580–3588, Mar. 2016, doi: 10.1021/acsnano.5b08008.

[11] B. Peng *et al.*, "Ultrafast charge transfer in MoS_2/WSe_2 p-n Heterojunction," *2D Mater.*, vol. 3, no. 2, p. 025020, May 2016, doi: 10.1088/2053-1583/3/2/025020.

[12] R. D. Mahyavanshi, P. Desai, A. Ranade, M. Tanemura, and G. Kalita, "Observing Charge Transfer Interaction in CuI and MoS_2 Heterojunction for Photoresponsive Device Application," *ACS Appl. Electron. Mater.*, vol. 1, no. 3, pp. 302–310, Mar. 2019, doi: 10.1021/acsaelm.8b00069.

[13] X. Duan *et al.*, "Lateral epitaxial growth of two-dimensional layered semiconductor heterojunctions," *Nat. Nanotechnol.*, vol. 9, no. 12, pp. 1024–1030, Jan. 2014, doi: 10.1038/nnano.2014.222.

[14] G. Gao *et al.*, "Artificially stacked atomic layers: Toward new van der waals solids," *Nano Lett.*, vol. 12, no. 7, pp. 3518–3525, Jul. 2012, doi: 10.1021/nl301061b.

[15] M. M. Furchi, A. Pospischil, F. Libisch, J. Burgdörfer, and T. Mueller, "Photovoltaic effect in an electrically tunable Van der Waals heterojunction," *Nano Lett.*, vol. 14, no. 8, pp. 4785–4791, Aug. 2014, doi: 10.1021/nl501962c.

[16] S. K. Pradhan, B. Xiao, and A. K. Pradhan, "Enhanced photo-response in p-Si/MoS_2 heterojunction-based solar cells," *Sol. Energy Mater. Sol. Cells*, vol. 144, pp. 117–127, Jan. 2016, doi: 10.1016/j.solmat.2015.08.021.

[17] A. Pospischil, M. M. Furchi, and T. Mueller, "Solar-energy conversion and light emission in an atomic monolayer p-n diode," *Nat. Nanotechnol.*, vol. 9, no. 4, pp. 257–261, Mar. 2014, doi: 10.1038/nnano.2014.14.

[18] M. Y. Li *et al.*, "Epitaxial growth of a monolayer WSe_2-MoS_2 lateral p-n junction with an atomically sharp interface," *Science (80)*, vol. 349, no. 6247, pp. 524–528, Jul. 2015, doi: 10.1126/science.aab4097.

[19] R. Cheng *et al.*, "Electroluminescence and photocurrent generation from atomically sharp WSe_2/MoS_2 heterojunction p-n diodes," *Nano Lett.*, vol. 14, no. 10, pp. 5590–5597, Oct. 2014, doi: 10.1021/nl502075n.

[20] M. Moun, M. Kumar, M. Garg, R. Pathak, and R. Singh, "Understanding of MoS_2/GaN Heterojunction Diode and its Photodetection Properties," *Sci. Rep.*, vol. 8, no. 1, p. 11799, Dec. 2018, doi: 10.1038/s41598-018-30237-8.

[21] K. Zhang *et al.*, "Large scale 2D/3D hybrids based on gallium nitride and transition metal dichalcogenides," *Nanoscale*, vol. 10, no. 1, pp. 336–341, Jan. 2018, doi: 10.1039/c7nr07586c.

[22] D. Ruzmetov *et al.*, "Van der Waals interfaces in epitaxial vertical metal/2D/3D semiconductor heterojunctions of monolayer MoS_2 and GaN," *2D Mater.*, vol. 5, no. 4, p. 045016, Aug. 2018, doi: 10.1088/2053-1583/aad1b7.

[23] E. W. Lee *et al.*, "Layer-transferred MoS_2/GaN PN diodes," *Appl. Phys. Lett.*, vol. 107, no. 10, p. 103505, Sep. 2015, doi: 10.1063/1.4930234.

[24] S. Krishnamoorthy *et al.*, "High current density 2D/3D MoS_2/GaN Esaki tunnel diodes," *Appl. Phys. Lett.*, vol. 109, no. 18, p. 183505, Oct. 2016, doi: 10.1063/1.4966283.

[25] R. Zhuo *et al.*, "High-performance self-powered deep ultraviolet photodetector based on MoS_2/GaN p-n heterojunction," *J. Mater. Chem. C*, vol. 6, no. 2, pp. 299–303, Jan. 2018, doi: 10.1039/c7tc04754a.

[26] S. Najmaei *et al.*, "Electrical transport properties of polycrystalline monolayer molybdenum disulfide," *ACS Nano*, vol. 8, no. 8, pp. 7930–7937, 2014, doi: 10.1021/nn501701a.

[27] O. V. Yazyev and Y. P. Chen, "Polycrystalline graphene and other two-dimensional materials," *Nature Nanotechnology*, vol. 9, no. 10. Nature Publishing Group, pp. 755–767, Jan. 01, 2014, doi: 10.1038/nnano.2014.166.

[28] M. Tangi *et al.*, "Determination of band offsets at GaN/single-layer MoS_2 heterojunction," *Appl. Phys. Lett.*, vol. 109, no. 3, p. 032104, Jul. 2016, doi: 10.1063/1.4959254.

[29] I. Popov, G. Seifert, and D. Tománek, "Designing electrical contacts to MoS_2 Monolayers: A computational study," *Phys. Rev. Lett.*, vol. 108, no. 15, p. 156802, Apr. 2012, doi: 10.1103/PhysRevLett.108.156802.

[30] P. Yan *et al.*, "Epitaxial growth and interfacial property of monolayer MoS_2 on gallium nitride," *RSC Adv.*, vol. 8, no. 58, pp. 33193–33197, Jul. 2018, doi: 10.1039/c8ra04821e.

[31] A. J. Mughal, T. N. Walter, K. A. Cooley, A. Bertuch, and S. E. Mohney, "Effect of substrate on the growth and properties of MoS_2 thin films grown by plasma-enhanced atomic layer deposition," *J. Vac. Sci. Technol. A*, vol. 37, no. 1, p. 010907, Jan. 2019, doi: 10.1116/1.5074201.

[32] P. Gupta *et al.*, "Layered transition metal dichalcogenides: promising near-lattice-matched substrates for GaN growth," *Sci. Rep.*, vol. 6, no. 1, pp. 1–8, Jul. 2016, doi: 10.1038/srep23708.

[33] T. P. O'Regan *et al.*, "Structural and electrical analysis of epitaxial 2D/3D vertical heterojunctions of monolayer MoS_2 on GaN," *Appl. Phys. Lett.*, vol. 111, no. 5, p. 051602, Jul. 2017, doi: 10.1063/1.4997188.

[34] A. Yamada, K. P. Ho, T. Akaogi, T. Maruyama, and K. Akimoto, "Layered compound substrates for GaN growth," *J. Cryst. Growth*, vol. 201, pp. 332–335, May 1999, doi: 10.1016/S0022-0248(98)01342-6.

[35] Z. I. Alferov, “The history and future of semiconductor heterostructures,” *Semiconductors*, vol. 32, no. 1. American Institute of Physics Inc., pp. 1–14, 1998, doi: 10.1134/1.1187350.

[36] W. Wu *et al.*, “Piezoelectricity of single-atomic-layer MoS_2 for energy conversion and piezotronics,” *Nature*, vol. 514, no. 7253, pp. 470–474, Oct. 2014, doi: 10.1038/nature13792.

[37] S. Xiao *et al.*, “Atomic-layer soft plasma etching of MoS_2,” *Sci. Rep.*, vol. 6, no. 1, pp. 1–8, Jan. 2016, doi: 10.1038/srep19945.

[38] A. J. Mughal, T. N. Walter, K. A. Cooley, A. Bertuch, and S. E. Mohney, “Effect of substrate on the growth and properties of MoS_2 thin films grown by plasma-enhanced atomic layer deposition,” *J. Vac. Sci. Technol. A*, vol. 37, no. 1, p. 010907, Jan. 2019, doi: 10.1116/1.5074201.

[39] J. K. Ellis, M. J. Lucero, and G. E. Scuseria, “The indirect to direct band gap transition in multilayered MoS_2 as predicted by screened hybrid density functional theory,” *Appl. Phys. Lett.*, vol. 99, no. 26, p. 261908, Dec. 2011, doi: 10.1063/1.3672219.

[40] M. Tangi *et al.*, “Determination of band offsets at GaN/single-layer MoS_2 heterojunction,” *Appl. Phys. Lett.*, vol. 109, no. 3, p. 032104, Jul. 2016, doi: 10.1063/1.4959254.

[41] E. A. Kraut, R. W. Grant, J. R. Waldrop, and S. P. Kowalczyk, “Precise determination of the valence-band edge in X-Ray photoemission spectra: Application to measurement of semiconductor interface potentials,” *Phys. Rev. Lett.*, vol. 44, no. 24, pp. 1620–1623, Jun. 1980, doi: 10.1103/PhysRevLett.44.1620.

[41] D. Ruzmetov *et al.*, “Vertical 2D/3D Semiconductor Heterostructures Based on Epitaxial Molybdenum Disulfide and Gallium Nitride,” *ACS Nano*, vol. 10, no. 3, pp. 3580–3588, Mar. 2016, doi: 10.1021/acsnano.5b08008.

[42] H. Yang, A. Giri, S. Moon, S. Shin, J. M. Myoung, and U. Jeong, “Highly Scalable Synthesis of MoS_2 Thin Films with Precise Thickness Control via Polymer-Assisted Deposition,” *Chem. Mater.*, vol. 29, no. 14, pp. 5772–5776, Jul. 2017, doi: 10.1021/acs.chemmater.7b01605.

[43] J. Yang *et al.*, “Wafer-scale synthesis of thickness-controllable MoS_2 films via solution-processing using a dimethylformamide/n-butylamine/2-aminoethanol solvent system,” *Nanoscale*, vol. 7, no. 20, pp. 9311–9319, May 2015, doi: 10.1039/c5nr01486g.

[44] K. K. Liu *et al.*, "Growth of large-area and highly crystalline MoS_2 thin layers on insulating substrates," *Nano Lett.*, vol. 12, no. 3, pp. 1538–1544, Mar. 2012, doi: 10.1021/nl2043612.

[45] S. Najmaei *et al.*, "Vapour phase growth and grain boundary structure of molybdenum disulphide atomic layers," *Nat. Mater.*, vol. 12, no. 8, pp. 754–759, Jun. 2013, doi: 10.1038/nmat3673.

[46] A. M. Van Der Zande *et al.*, "Grains and grain boundaries in highly crystalline monolayer molybdenum disulphide," *Nat. Mater.*, vol. 12, no. 6, pp. 554–561, Jun. 2013, doi: 10.1038/nmat3633.

[47] G. H. Han *et al.*, "Seeded growth of highly crystalline molybdenum disulphide monolayers at controlled locations," *Nat. Commun.*, vol. 6, no. 1, pp. 1–6, Jan. 2015, doi: 10.1038/ncomms7128.

CHAPTER 5

5 Summary and future scope of work

5.1 Summary

In this research work, high quality of MoS_2 crystals, layers were synthesized using CVD techniques. Various experimental parameters of the developed CVD process were optimized to synthesize MoS_2 layered structure.

Chapter 1 is an attempt to broadly describe the 2D-TMDCs, thus MoS_2 as a promising candidate for electronics, electrical and material applications. Basic key properties of MoS_2 in general has been outlined, with addition of properties which are very relevant to the further study been carried out. Especially in this chapter, the results of other researchers are cited acknowledging their work.

In Chapter 2, I have shown the various processes and techniques used in CVD for the MoS_2 growth and the characterization techniques used for the synthesized MoS_2 layers/crystals in brief.

CVD process I, as detailed in chapter 2 was divided in to two techniques.

In the first technique, the crystal synthesised were bigger in domain size of nearly 50 µm. Though this technique resulted in lesser number of successful results during laboratory experimentation. This is due to the crucial growth parameters in play for synthesis of

MoS_2 triangular crystals. In technique 2, a uniform layer of MoO_3 was deposited and was used as a precursor. This enabled availability of uniform precursor for the growth. The repeated results of this resulted in crystals of sizes 30 µm in almost all the experiments conducted especially on Ga-polar GaN and p-type Silicon substrate.

For crystal growth we find relation of CVD high furnace temperature, the quantity of sulphur and MoO_3, the position of the substrate with respect to the precursor, gas composition etc. plays an important role in crystal morphology and nucleation. By optimizing these growth parameters, domain size of 50 µm were synthesized successfully. Later the various characterization methods were used to ascertain the chemical composition, structure, photoluminescence etc.

CVD processes II was used for synthesis of MoS_2 few-layer growth with varying thicknesses on different substrates for the study of electronic performance of heterostructure devices and to study the heterojunction properties at the interface.

In Chapter 3, I studied the influence of molybdenum sulphide (MoS_2) and p-type silicon (Si) interface states on spectral photoresponse characteristics.

It was observed that due to an effective field effect across the heterojunction the spectral photoresponse of the device improved substantially with an applied bias voltage than that of a photovoltaic mode. The MoS_2 layers deposited on the p-type Si wafer showed a photovoltaic action and a photoresponsivity of 139 mA/W in a bias voltage of -5V. The spectral photoresponse (mA/W) of the device was enhanced with applied bias voltage than that of photovoltaic mode. Another key finding was observed in increase in photoresponsivity at a higher wavelength (>600 nm) is significant than that of lower wavelength (<500 nm) at the bias voltage of -5V.

In chapter 4, I have demonstrated the growth of uniform few-layers MoS_2 film on free-standing GaN wafer by sulphurisation process of MoO_3 thin layer, using CVD process labelled II. A photovoltaic photoresponsivity was obtained in this heterojunction with vertical current flow across the junction. This signify that the photoexcited electron and holes can be effectively separated with low recombination loss, due to which a photovoltage appeared across the heterojunction. Additionally, I present the growth of MoS_2 crystals on the lattice matched Ga-polar GaN wafer using ammonium tetrathiomolybdate (ATM) as a precursor in a CVD process III. I obtained a unidirectional triangular MoS_2 crystals and continuous film on free-standing Ga-polar GaN substrate. In my study I revealed the suitability of bulk Ga-polar GaN wafer for MoS_2 crystals growth using the ammonia containing ATM precursor. The semiconducting behaviour of the device showed photovoltaic photoresponsivity and rectification difference arising due to the differences in number of layers of MoS_2 and the thickness/opacity of the deposited metal electrode.

Chapter 5 summarizes the whole thesis and mention here as well as the future prospect of this study.

Above-mentioned new findings will help in better understanding the nature and properties of heterostructures of MoS_2, and alternative growth of MoS_2 crystals using the ammonia containing ATM precursor in the CVD process and were published in international journals potential worth for PhD thesis.

5.2 Future scope of work

5.2.1 Prospects in MoS_2/Si heterojunction study

My study can be extended further by understanding the interface quality and its performance on photocarriers in the interface states at the MoS_2/Si heterojunction. Fundamental understanding in efficacy improvement in photodetection of the heterostructure can be carried out. Numerous experimental studies have been carried out, though the theoretical findings for electrical and optical behaviour can probe deeper into this. One such research question that could be investigated is spectral responsivity and its relationship with junction properties.

5.2.2 Prospects in MoS_2/GaN heterojunction study

Taking the research further, understanding the relation of growth parameters with the quality of layer and crystals growth can be addressed. In the various laboratory experiments in MoS_2 growth on GaN that I conducted, only a part resulted in assured epitaxial growth of crystals. Understanding the epitaxial growth in relations with growth parameters can further take my study deeper into a potential heterostructures fabrication. Layer dependent study of the catalytic behaviour can address the relation between the bandgap modulations of MoS_2 and it the catalytic potentials.

5.2.3 Prospects in fabrication of heterostructures using CVD

I studied the growth of MoS_2 crystals on the lattice matched Ga-polar GaN wafer using ammonium tetrathiomolybdate (ATM) as a precursor in a CVD process. Further, optimizing growth parameters for the synthesis of MoS_2 can be carried out with for synthesizing larger crystals or uniform layer on various substrates.

In the experimental section I have come across the methodology of spin coating the precursor on to the GaN substrate. Below a critical concentration of this precursor, we observe that the spin coated layer gets transformed into a triangular crystal which are epitaxial in orientation. Such a method of synthesis could be classified under top-down approach for obtaining 2D MoS_2. This mechanism can be explored further and critical questions pertaining to the synthesis can be answered.

List of Research Contributions

(A) Original papers published in international journals with a corresponding authorship

while in candidature for degree at NITech;

Influence of MoS_2-Silicon Interface States on Spectral Photoresponse Characteristics

---

Journal:	Physica Status Solidi (A), Applications and Materials Science
Authors:	Pradeep Desai,* Ajinkya K. Ranade, Rakesh Mahyavanshi, Masaki Tanemura, Golap Kalita
Article DOI:	10.1002/pssa.201900349
Date of Acceptance:	2019 June 17

Growth of uniform MoS_2 layers on free-standing GaN semiconductor for vertical heterojunction device application

---

Journal:	Journal of Materials Science: Materials in Electronics
Authors:	Pradeep Desai,* Ajinkya K. Ranade, Mandar Shinde, Bhagyashri Todankar, Rakesh D. Mahyavanshi, Masaki Tanemura, Golap Kalita
Article DOI:	10.1007/s10854-019-02723-w
Date of Acceptance:	2019 December 08

Synthesis of MoS_2 Layers on GaN using Ammonium Tetrathiomolybdate for Heterojunction Device Applications

---

Journal:	Crystal Research and Technology

Authors: Pradeep Desai,* Bhagyashri Todankar, Ajinkya K. Ranade, Masaharu Kondo, Takehisa Dewa, Masaki Tanemura, Golap Kalita

Article DOI: 10.1002/crat.202000198

Date of Acceptance: 2021 January 14

(B) Co-author publications

- "Ultraviolet radiation-induced photovoltaic action in γ-CuI/β-Ga_2O_3 heterojunction"; Muhammed Emre Ayhan, Pradeep Desai, Masaki Tanemura, Golap Kalita et al., Mater. Lett., Nov 2019
- "Formation of Effective CuI‐GaN Heterojunction with Excellent Ultraviolet Photoresponsive Photovoltage"; Ajinkya K. Ranade, Pradeep Desai, Masaki Tanemura, Golap Kalita et al., Phys. Status Solidi (a), Jun 2019
- "Ultraviolet light induced electrical hysteresis effect in graphene-GaN heterojunction"; Ajinkya K. Ranade, Pradeep Desai, Masaki Tanemura, Golap Kalita et al., Appl . Phys. Lett., Mar 2019
- "Observing Charge Transfer Interaction in CuI and MoS_2 Heterojunction for Photoresponsive Device Application"; Rakesh D. Mahyavanshi, Pradeep Desai, Masaki Tanemura, Golap Kalita et al., ACS Appl. Mater. Interfaces, Feb 2019
- "Photovoltaic action with broad band photoresponsivity in germanium-MoS_2 ultrathin heterojunction"; Rakesh D. Mahyavanshi, Golap Kalita, Pradeep Desai, Masaki Tanemura et al., IEEE T. Electron Dev., Aug 2018
- "Photovoltaic action in graphene-Ga_2O_3 heterojunction with deep-ultraviolet irradiation"; Golap Kalita, Rakesh D. Mahyavanshi, Pradeep Desai, Masaki Tanemura et al. Phys. Status Solidi Rapid Res. Lett., May 2018

(C) Conferences presented with Institute's affiliation

- "Epitaxial growth of triangular MoS_2 crystals on freestanding GaN wafer by spin coating precursor"; Pradeep Desai, Masaki Tanemura, Golap Kalita et al., **2nd International Conference on Smart Materials for Sustainable Technology,** Feb. 22 – 25, 2020, Bogmollo, Goa, INDIA (ORAL)

- "Growth of MoS_2 crystals on 4H-SiC substrate for photocatalytic application"; Pradeep Desai, Masaki Tanemura, Golap Kalita et al., **32nd International Microprocesses and Nanotechnology Conference**, Oct. 28 – 31, 2019, International Conference Center Hiroshima, Hiroshima, JAPAN (POSTER).

- "Fabrication of heterostructure with MoS_2 layers and GaN for photoresponsive device application"; Pradeep Desai, Masaki Tanemura, Golap Kalita et al. **The 80th JSAP Autumn Meeting**, Sept. 18 – 21, 2019, Hokkaido University, Sapporo, JAPAN (ORAL).

- "Deposition of MoS_2 layer on GaN semiconductor for photoresponsive device application"; Pradeep Desai, Masaki Tanemura, Golap Kalita et al., **The 57th Fullerenes-Nanotubes-Graphene General Symposium**, Sept. 3 – 5, 2019, Nagoya University, Nagoya, JAPAN (POSTER)

- "Fabrication of MoS_2 layers on free standing GaN for heterojunction photoresponsive device applications"; Pradeep Desai, Masaki Tanemura, Golap Kalita et al., **2019 International Conference on Solid State Device and Materials**, Sept. 2 – 5, 2019, Nagoya University, Nagoya, JAPAN (POSTER)

- "Influence of MoS_2/Silicon Interface States on Bias Dependent Photoresponse"; Pradeep Desai, Masaki Tanemura, Golap Kalita et al. **The 66th JSAP Spring Meeting**, March 9 – 12, 2019, Tokyo Institute of Technology, Tokyo, JAPAN (ORAL)

List of Figures

List of Diagrams

List of Tables

ABBREVIATIONS

TMDC	Transition metal Dichalcogenides
MoS_2	Molybdenum disulphide /disulfide
ML	Mono layer
SiO_2	Silicon dioxide
GaN	Gallium nitride
SiC	Silicon carbide
MoO_3	Molybdenum dioxide
$(NH_4)_2MoS_4$	Ammonium thiomolybdate
S	Sulphur/Sulfur
VdW	Van der waals
2H	Hexagonal phase
1T	Octahedral phase
CVD	Chemical vapour deposition
LTF	Low temperature furnace
HTF	High temperature furnace
FET	Field effect transistor
DFT	Density functional theory
VBM	Valence band maxima
CBM	Conduction band minima
UV	Ultraviolet
E_{2g}	In-plane vibrations of Raman mode
A_{1g}	Out of-plane vibrations of Raman mode
OM	Optical microscopy
FE-SEM	Field emission scanning electron microscopy
PL	Photoluminescence spectra
XPS	X-ray photoelectron spectroscopy
AFM	Atomic force microscopy
TEM	Transmission electron microscopy

Acknowledgement

In my endeavour for doctoral degree, I had steady faithful support, belief, and blessings of my native family in Goa-India. My families' contributions cannot be netted in words.

Despite typical struggles, stresses of living in a foreign land, my maverick nature, despite 'blue relationships' I had in Japan, despite unpredicted behaviour of ongoing worldwide Covid19 pandemic[1], despite having to undergo a major gastrectomy surgery, and following the admission until recovery, and despite my ongoing health treatment of metastasis carcinoma, I was able to see this day.

Thank you to all well-wishers and believers.

Choosing & living in Japan has made the journey remarkable & memorable for me. Specifically, to mention, it was the experience of the systematic & mannerly culture of Japan, the unique weather & landscapes, 'arubaito' working in a hospital. These are and will be remembered by me when I think of my time as a PhD candidate.

Financial benefits that I received while in Japan was the foremost reason for a successful completion of degree in due course of time.

[1] Pixabay Licensed

I am grateful for the research assistant fund I received while in my first year in Kalita Laboratory from '*Frontier Research Institutes, Inc.*' of NITECH.

Also, to '*Nagoya East Medical Centre*' hospital in imaike where I did 'Arubaito'.

My sincere thanks to '*NGK Insulator Ltd.*' company, Nagoya (**日本ガイシ株式会社、日本ガイシ留学生基金**), for considering me deemed candidate to be awarded with scholarship during my second and third year. I am pleased for continual support from **Mrs. Yacko Tasaki San, Ms. Atsuko Sato San** and likewise to other members from *NGK Insulator Ltd.*

Frontier Research Institutes

名古屋市立 東部医療センター
Nagoya City East Medical Center

NGK INSULATORS

I extend my gratification to 'International student office' of NITECH and its staff members. Especially, **Ms. Izumi Yamamoto, Mrs. Kazumi Yamashita, Ms. Yuriko Yamamoto, Mrs. Yui Shirai, Mrs. Ai Shimizu, Mrs. Kim Eunju, Ms. Mana Baba, Mr. Toshiya Ozawa, Ms. Yuka Murase,** and people attached to this office those I did not mentioned.

I am thankful to **(Dr.) Golap Kalita** explicitly for the finger-pointed instructions for carrying out research which enabled for the publication of three research articles. It has certainly helped me in fulfilling the requirements of doctoral degree.

My many thanks to **(Dr./Prof.) Masaki Tanemura** for the inspiration & encouragement I received. Ultimately, I was able to successfully defend my PhD thesis under his blessed guidance.

I will be forever grateful to **Ms. Norimi Yamashita** for her diligence.

Many thanks to colleagues for their assistances with whom I worked in the laboratory and in NITECH. Namely, **Dr. Rakesh Mahyavanshi, Dr. Ajinkya Ranade, Mr. Shun Fukuaka, Mr. Yahata Takanori, Mr. Muhammad Dzulsyahmibin Shaarin, Mr. Abdul Aziz Arif Bin Mutalib, Mr. Krishna Rao, Ms. Bhagyashree Todankar, Mr. Shuhei Nakanishi, Mr. Daiki Terai, Mr. Kai Okazaki,** and people attached to the 'Kalita Laboratory' & 'Tanemura Laboratory' in past those that I did not mentioned. Further, I thank **Mr. Balsingh Chaudhary, and Dr. Debaleen Biswas** for their assistances in general matters. Lastly, I mention **Dr. Balaram Paudel,** whose uncorrupted & humbled nature was an inspiration and the assistance I derived will be forever admirable.